

**Università della Calabria**

Dipartimenti di Chimica e di Fisica

---

Dottorato di Ricerca in  
Scienze e Tecnologie delle Mesofasi e dei Materiali Molecolari  
XXII Ciclo

**Ph.D. Thesis**

**Photoconducting and Photorefractive  
Azo-Polymers**

**Settore disciplinare: CHIM02**

**Supervisore**  
**Prof. Attilio Golemme**

**Candidato**  
**Huawei Li**

**Coordinatore**  
**Prof. Carlo Versace**

---

Anno Accademico 2008-2009

To my parents and wife.



## **Acknowledgements**

I would like to express my deepest gratitude to my supervisor, Professor Attilio Golemme from University of Calabria, for his constant encouragement and guidance during my Ph.D. studies. In the preparation of the thesis, he has spent much time reading through each draft and provided me with inspiring advice. Without his illuminating instruction, insightful criticism and expert guidance, the completion of this thesis would not have been possible.

I thank Professor Loris Giorgini from University of Bologna, who supplied polymers for this research.

I thank Professor Carlo Versace from University of Calabria, the coordinator of this Ph.D. course, for his help in the academic affairs.

I thank Dr. Roberto Termine from University of Calabria, who has instructed and helped me a lot in the past three years.

I thank Dr. Nicolas Godbert from University of Calabria for his technical support during my Ph.D. studies.

I thank Madam Teresa Ting for her good suggestions about thesis writing.

I thank Professor Jean-Michel Nunzi for giving me the opportunity to work in his lab at Queen's University, Canada.

Finally, I greatly appreciate the support from my parents and wife.

# INDEX OF CONTENTS

<b>Introduction</b> .....	1
---------------------------	---

## **Chapter 1**

### **Photorefractivity: Principles and Requirements.**

1.1 Introduction.....	3
1.2 Fundamentals of photorefractivity.....	4
1.3 Properties of photorefractive polymers.....	8
1.3.1 Charge carriers photogeneration.....	9
1.3.2 Charge transport.....	11
1.3.3 Space-charge field formation.....	14
1.3.4 Refractive index modulation.....	17
1.3.4.1 Non-linear optical materials.....	17
1.3.4.2 Orientational enhancement effect.....	18
<b>Bibliography</b> .....	21

## **Chapter 2**

### **Photorefractive polymers.**

2.1 Introduction.....	24
2.2 Key components relevant to PR polymers.....	24
2.2.1 Sensitizers.....	24
2.2.2 Charge transporting moieties.....	27
2.2.3 Chromophores.....	28
2.2.4 Plasticizers.....	29
2.3 Guest-host polymers.....	30
2.4 Fully functionalized polymers.....	32
2.5 Low $T_g$ and high $T_g$ PR polymers.....	33

2.5.1 Low $T_g$ PR polymers.....	33
2.5.2 High $T_g$ PR polymers.....	34
<b><i>Bibliography</i></b> .....	35

## **Chapter 3**

### **Azo-polymers: Light-induced effects and applications.**

3.1 Brief history of azobenzene.....	39
3.2 Isomerization of the azo-aromatic group.....	40
3.3 Three classes of azo compounds.....	41
3.4 Photo-induced motions in azo-polymers.....	42
3.5 Azo group binding, local free volume and polymer matrix.....	45
3.6 Experimental methods for the photoorientation investigation.....	46
3.7 Properties and applications of azopolymers.....	47
3.7.1 Applications based on motions at the molecular level.....	47
3.7.2 Applications based on motions at the domain level.....	48
3.7.3 Applications based on massive macroscopic motions.....	49
<b><i>Bibliography</i></b> .....	52

## **Chapter 4**

### **Measurement techniques.**

4.1 Sample preparation.....	54
4.2 Absorption coefficient measurement.....	55
4.3 Photoconductivity.....	56
4.4 Charge carrier mobility.....	58
4.4.1 Time-of-flight.....	58
4.4.2 Space charge limited current.....	61
4.5 Two-beam coupling.....	65
4.6 Four-wave mixing experiment.....	71

4.7	Steady state ellipsometry.....	74
4.8	Transient ellipsometry.....	76
4.9	Moving grating technique for phase shift measurement.....	77
	<b><i>Bibliography</i></b> .....	80

## **Chapter 5**

### **Results: photoconductivity and mobility.**

5.1	Azo-polymers: structures and UV-Vis spectra.....	82
5.2	HOMO and LUMO levels of the polymers.....	86
5.3	Photoconductivity measurements.....	89
5.4	Photoconductivity of azo-polymers without carbazole.....	96
5.5	Hole mobility measurement.....	97
	<b><i>Bibliography</i></b> .....	107

## **Chapter 6**

### **Results: photorefractivity.**

6.1	Polymers and their functional groups.....	109
6.2	Light-induced birefringence.....	110
6.3	Light-induced surface relief grating.....	112
6.4	Effect of illumination with a single light beam.....	113
6.5	Light-induced absorption increase.....	114
6.6	Two-beam coupling (2BC) results.....	116
6.7	Inversion of energy exchange.....	117
6.8	Phase shift measurement.....	118
6.9	Improvement of PR dynamics.....	121
6.10	The roles of chromophore dipole moment and electric field.....	123
6.11	Photorefractivity with and without chiral groups.....	124
6.12	Photorefractivity in azo-polymers without carbazole groups.....	126

6.13 Refractive index modulation mechanism.....	127
6.14 PR effect without external electric field.....	128
6.15 Conclusions.....	131
<b><i>Bibliography</i></b> .....	133

## INTRODUCTION

As an important branch of optoelectronic media, organic materials have been extensively studied because of their technological relevance for a variety of applications. One of the crucial points of research in this field is the development of new light sensitive materials that exhibit properties such as high efficiency, high sensitivity, high speed, long working life and low cost. Materials which show non-linear optical properties are of particular relevance in this field, since they allow the manipulation and transformation of an optical signal: under proper conditions, several features of a signal, such as frequency, phase or direction of propagation can be controlled.

An important subset of non-linear optical materials are the materials showing photorefractive properties, which are of wide interest and among the most promising non-linear optical materials used in optoelectronic and photonic devices. Photorefractive materials are photoconductors in which the space redistribution of charges photogenerated by a non-uniform illumination creates a space-charge field. In turn, such a field affects the refractive index if the material exhibits non-linear optical properties and/or spontaneous (or field-induced) birefringence. There are many applications related to photorefractive effect, such as data storage, holography and image processing.

This research project was focused on the photoconducting and photorefractive characterization of azo-polymers. Polymers were initially characterized by DCS (to determine  $T_g$ ) and a protocol to prepare samples between conducting electrodes was established. The photoconducting properties of a series of different polymers containing the carbazole moiety were then investigated and a structure/property relationship was established, linking photoconduction to the nature of the linking group between the polymeric chain and the carbazole unit.

Photorefractive properties were characterized by Multi-Wave Mixing techniques. Room temperature photorefractivity without pre-poling was demonstrated in polymers and co-polymers with a glass transition temperature well above 100 °C. The compounds used are multifunctional side-chain polymers exhibiting chiral, semiconducting, photochromic and non-linear optical (azoaromatic moieties) properties. The photorefractive performance was linked to the reorientational effect of the photogenerated space-charge field, that well below the glass transition temperature can be active in the

presence of the conformational mobility achieved via the trans-cis light-induced isomerization. The grating build-up time, which was long at  $\lambda = 632.8$  nm (with a time constant  $\tau \sim 500$ - $1000$  s) decreases by two orders of magnitude at  $\lambda = 532$  nm, where absorption is higher.

Several other properties were also studied, in order to obtain a deeper insight into the mechanism of photorefractive behaviour for the polymers under investigation. In particular, studies of light and electric field-induced birefringence were carried out, as well as AC ellipsometric experiments. The results of such characterizations allowed separating the different roles of light and electric field in the photorefractive process.

Finally, a surprising result was the measurement of photoconductivity in an azo-polymer not containing carbazole units. In our knowledge, this is the first observation of such behaviour and photorefractive results seem to indicate that the conduction is due to electrons rather than holes.

This thesis is organized as follows:

- **Chapter 1** introduces the principles and requirements for photorefractivity.
- **Chapter 2** introduces the photorefractive polymers.
- **Chapter 3** introduces the light-induced effect in azo-polymers and their applications.
- **Chapter 4** introduces the relevant measurement techniques.
- **Chapter 5** introduces the photoconductivity and mobility results.
- **Chapter 6** introduces results relevant to photorefractivity.

## Chapter 1

### PHOTOREFRACTIVITY:

### PRINCIPLES AND REQUIREMENTS

#### 1.1 Introduction

For many years, considerable research efforts have been devoted to the study of the interaction between light and matter to replace the electronic devices with faster, more sensitive, and more reliable optical devices. To this aim, light sensitive materials with high optical quality, high efficiency, high sensitivity, long lifetime, low cost, and good processability have attracted much attention. Among light-sensitive media, photorefractive (PR) materials have recently been extensively studied for their various applications, such as data storage<sup>1-4</sup>, phase conjugation<sup>5-7</sup>, image amplification and processing<sup>8-10</sup>, holographic recording<sup>11-13</sup> and infrared imaging<sup>14</sup>.

The photorefractive effect is a spatial modulation of the refractive index due to charge redistribution in optically nonlinear materials. The effect arises when charge carriers, photogenerated by a spatially non-uniform light intensity, separate by drift and/or diffusion processes and become trapped to produce a non-uniform space-charge distribution. The effect was first observed in 1966<sup>15</sup> by Ashkin and co-workers. They found that intense laser radiation focused on ferroelectric LiNbO<sub>3</sub> and LiTaO<sub>3</sub> crystals induced a semi-permanent index change. This phenomenon was unwanted for their purposes, therefore they referred to it as an “optical damage”. However, the potential of this new effect for use in high density optical data storage was realized soon after by Chen and co-workers.<sup>16</sup> The effect later became known as PR effect and was first studied mainly on inorganic crystals. In more recent years, new classes of materials became candidates for PR applications, such as organic crystals, glasses, polymers<sup>17,18</sup> and liquid crystals.<sup>19-21</sup> The most important properties that a PR material must exhibit are photoconductivity (light dependent electrical conductivity) and an electric field dependent refractive index.<sup>22</sup>

Usually, high refractive index variations can be induced under low-power laser illumination in PR materials. In contrast to many grating formation mechanisms with thermal, electronic, or chemical origins, the unique characteristic of PR effect is the



nonlocal property arising from charge migration, which leads to a phase shift between the incident light intensity pattern and the refractive index modulation. This nonlocal response is a fingerprint of the photorefractive effect and enables energy transfer between two coherent laser beams.<sup>23</sup>

## 1.2 Fundamentals of photorefractivity

The photorefractive effect is based on a redistribution of charges photogenerated under a non-uniform illumination, leading to an internal electric field pattern that modulates the refractive index through the electro-optic effect.<sup>24</sup> Therefore, the PR effect can be observed in materials that are simultaneously photoconductive and electro-optic. A photoconductor is a material that is a good insulator in the dark and becomes conductive upon illumination. The electrical conductivity of the material is due to mobile charge carriers that are created by absorbed photons.

Photorefractivity can be described step by step with the help of Fig. 1.1. PR materials can be illuminated by two coherent laser beams with the same wavelength, as shown in Fig. 1.1(a). These beams interfere to produce a spatially modulated intensity distribution  $I(x)$ , given by<sup>25</sup>:

$$I(x) = I_0[1 + m \cos(2\pi x / \Lambda)] \quad (1.1)$$

where  $I_0 = I_1 + I_2$  is the total incident intensity, i.e., the sum of the intensities of the two beams,  $m = 2(I_1 I_2)^{1/2} / (I_1 + I_2)$  is the fringe visibility, and  $\Lambda$  is the period of the sinusoidal light distribution, which depends on the wavelength, on the refractive index  $n$  of the material and on the angle between the two beams inside the material, according to Eq.(1.2).  $\Lambda$  can vary generally from a fraction of a micrometer to a couple of tens of micrometers.

$$\Lambda = \frac{\lambda}{2n \sin(\Delta a_{\text{int}})} \quad (1.2)$$

In photoconductive materials, following a spatially periodic photoexcitation, more carriers are generated in the regions near the light maxima, as shown in Fig. 1.1(c), because the photogeneration rate can be assumed proportional to the local value of the light intensity. In the simplest model, one kind of carriers (electrons or holes) migrate from the positions of high intensity where they were generated and leave behind fixed charges of the opposite sign, as shown in Fig. 1.1 (d). The migration process is limited by

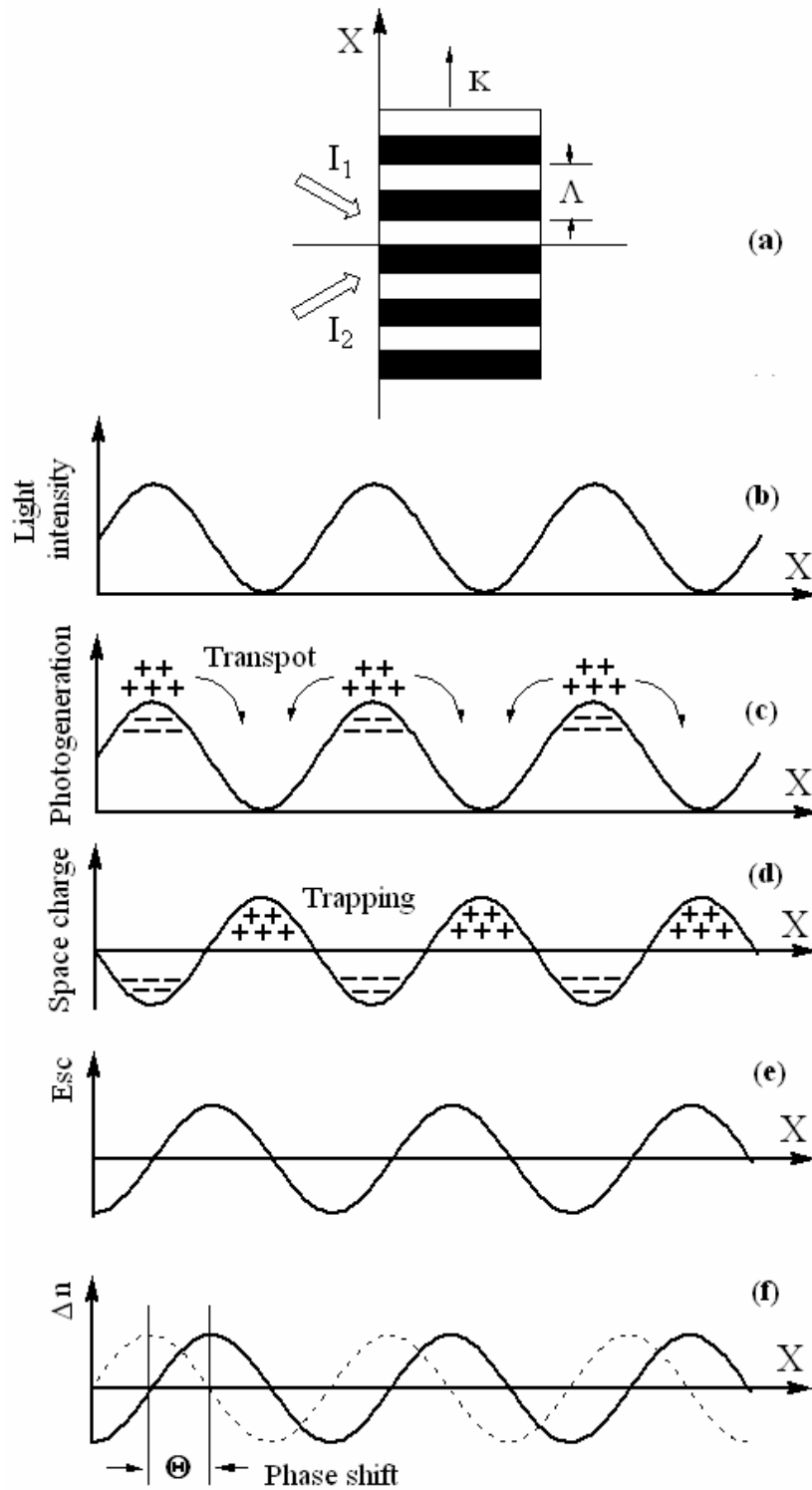


Fig. 1.1. Schematic representation of the steps for the build-up of a photorefractive grating.

traps present in the material under the form of impurities or more generally any structural modification of the local environment of a site that leads to a deformation of the local

potential and to a lower energy state for the carriers. During the transport process, the carriers can, to some extent, move away from the brighter regions (higher density regions) to the darker regions (lower density regions). The characteristic distance over which the carriers migrate in an efficient photorefractive material is in the micrometer range. The carriers trapped in the darker regions and the fixed charges of opposite sign, left behind in the brighter regions, give rise to an inhomogeneous space-charge distribution. The space-charge distribution is in phase with the light distribution if transport is governed by diffusion only, and can be phase shifted when drift in response to an applied field is present. If the light is removed, this space-charge distribution can remain in place for a period of time which can vary between nanoseconds and years depending on the photorefractive material class. For a one-dimensional light distribution described by Eq. (1.1), a space-charge distribution  $\rho(x)$ , in a material with a dielectric constant  $\epsilon$ , induces an internal space-charge field  $E_{sc}(x)$  described by Poisson's law (Eq.(1.3)):

$$\frac{dE_{sc}}{dx} = \frac{4\pi\rho}{\epsilon} \quad (1.3)$$

The last step in the build-up of a photorefractive grating is the modulation of the refractive index by this internal space-charge via the electro-optic effect which will be discussed in details in section 1.3.4 below. The refractive index modulation recorded in the material at the end of the process will have the same spatial periodicity. The spatial derivative that appears in Poisson's equation is of paramount importance since it is the origin of the non-local response of photorefractive materials, namely the phase shift between the refractive index modulation and the initial light distribution. This phase shift is unique to PR materials and can lead to energy transfer between two incident beams. In addition, "photorefractivity" is then more than a refractive index variation induced by light and the photorefractive effect is very different from many other mechanisms that can lead to grating formation, such as thermal, chemical, and electronic nonlinearities. In contrast to many processes studied in nonlinear optics, the photorefractive effect is very sensitive and can be observed using milliwatts of laser power. One of the important properties of photorefractive materials is the possibility of storing gratings combined with the possibility of erasing the grating at any time with a uniform light source. All these properties make photorefractive materials important for dynamic holographic recording/retrieval and for all the related applications.<sup>26</sup>

Photorefractive materials can be divided in two classes: inorganic crystals and

organic materials. The photorefractive effect has been first studied mainly in inorganic crystal,<sup>27</sup> including LiNbO<sub>3</sub>, BaTiO<sub>3</sub> and KNbO<sub>3</sub>, which belong to the class of ferroelectrics, Bi<sub>12</sub>SiO<sub>20</sub> and other sillenites, semiconductors such as GaAs, InP, CdTe,<sup>28</sup> and semiconductor multiquantum wells (MQW).<sup>29-35</sup> The basic physical model for photorefractivity in inorganic materials is based on the Kukhtarev model,<sup>36-40</sup> which gives the first-order component of the steady-state space-charge field created by a sinusoidal light distribution. The amplitude of the space-charge field  $E_{sc}$  is given by :

$$E_{sc} = m \left( \frac{E_0^2 + E_D^2}{\left(1 + E_D/E_q\right)^2 + \left(E_0/E_q\right)^2} \right)^{1/2} \quad (1.4)$$

where  $E_0$  is the component of the applied field along the grating vector. The diffusion field  $E_D$  is defined as:

$$E_D = \frac{K k_B T}{e} \quad (1.5)$$

where  $K = 2\pi/\Lambda$  is the grating vector,  $k_B$  is the Boltzmann constant,  $T$  is the temperature, and  $e$  is the elementary charge. In Eq. (1.4), the trap-limited field  $E_q$  is given by:

$$E_q = \frac{e N_T}{K \epsilon \epsilon_0} \quad (1.6)$$

where  $\epsilon$  is the dielectric constant,  $\epsilon_0$  the permittivity of free space, and  $N_T$  the density of photorefractive traps. The phase shift  $\Theta$  between the space-charge field and the light interference pattern resulting directly from transport is given by:

$$\Theta = \arctg \left[ \frac{E_D}{E_0} \left( 1 + \frac{E_D}{E_q} + \frac{E_0^2}{E_D E_q} \right) \right] \quad (1.7)$$

If transport is driven only by diffusion, the phase shift will be  $\pi/2$ , otherwise it will depend on the relative strength of the diffusion and drift processes, and will be smaller than  $\pi/2$ .

This model introduced by Kukhtarev and co-workers has provided a solid framework for the description of the formation of photorefractive gratings in inorganic crystals and agrees reasonably well with experiment results. However, in organic photorefractive materials, it is difficult to speculate on the validity of this model since it does not take into account several important aspects of charge generation, transport, trapping, and recombination that are intrinsic to organic materials. Furthermore, discovery

of the Orientational Enhancement Effect (which does not exist in PR inorganic materials and will be discussed in details in section 1.3.4.2) in 1994 by Moerner and coworkers<sup>41</sup> altered the picture of the electro-optical nonlinearity and led to an even more complicated description of the PR effect in organics. Overall, the process of PR grating formation in most organic materials can be viewed as a space-charge field formation followed by a non-instantaneous reorientation of chromophores in response to the total local field, which is the sum of the space-charge field and the applied dc field.<sup>42</sup> Nevertheless, the following basic physical trends can be extracted from the Kukhtarev model and applied to organic materials. Eq. (1.6) shows that the maximum value for the space-charge depends, for a given material, on the trap density  $N_T$  and on its low-frequency dielectric constant  $\epsilon$ . In most of the inorganic crystals, these two parameters are not very favorable to the buildup of a strong space-charge field. High doping levels are difficult to achieve in crystals because crystals have the tendency to be repellent to impurities. In addition, since in inorganic crystals the electro-optic properties are often driven by ionic polarizability, high electro-optic properties are accompanied by a high dielectric constant which limits the value of the space-charge field. In organics, the electronic origin of the nonlinearity leads to materials with high second-order nonlinear optical properties and simultaneously a low dielectric constant at low frequencies. Moreover, traps are not due to impurities but rather to structural defects or conformational disorder characteristic of non-crystalline materials. As a result, very high trap densities can be present and the space-charge field can reach saturation. Saturation occurs when the value of the internal space-charge field balances the external field. Polymers prepared in thin films can support very large electric fields, leading to significantly higher space-charge fields in polymers than in inorganic crystals. These considerations make organic materials and especially polymers very attractive for photorefractivity and have been the driving force in the early development of organic photorefractive materials.

### 1.3 Properties of photorefractive polymers

To be photorefractive, a material should combine photosensitivity to generate charge carriers and photoconductivity to separate them through transport, provide traps for them to store the space charge field, and possess a field-dependent refractive index such as through the electro-optic effect. In the following, the physical models currently

used to describe charge generation and transport in amorphous organic photoconductors will be described.

### 1.3.1 Charge carriers photogeneration

The photogeneration process consists in the creation of non-interacting charges of opposite signs through light absorption. A higher carrier photogeneration rate gives faster and better PR performance, but excessive absorption should be avoided because light must be transmitted through the medium if volume effects are to be observed. Materials with moderately low absorption coefficient but high photogeneration rate are thus ideal. Photogeneration can be followed by recombination, which limits the formation of free carriers that can participate in the transport process and is, therefore, a loss for the formation of the space-charge. In organic materials, owing to a low dielectric constant, the screening of the Coulomb interaction between the electron and hole is small, resulting in low photogeneration efficiency unless an electric field is applied to counteract recombination. The quantum efficiency for carriers generation is, therefore, strongly field dependent and increases with the applied field.

A model involving excitons<sup>43</sup> was proposed to understand the mechanism leading to separated charges induced by an absorbed photon. The exciton is an excited state in which the distance between charges is larger than in the ground state but with the two charges still coulombically interacting. Depending on experimental conditions, the excitons can dissociate completely to give separated charges or return to the ground state by geminate recombination, as shown in Fig. 1.2.

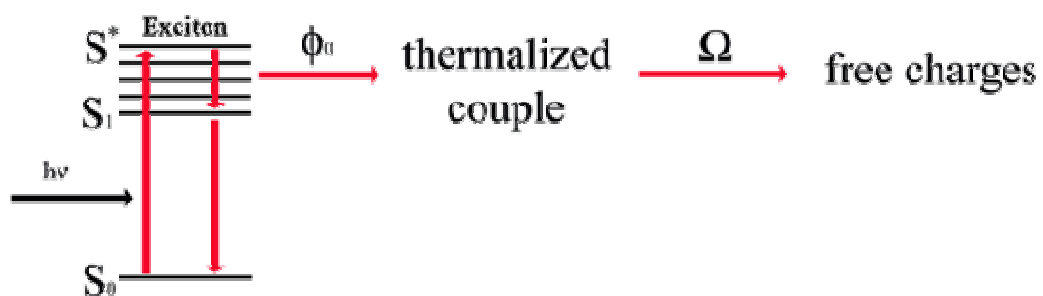


Fig. 1.2. Scheme of the photogeneration process.

Geminate recombination is usually described by the Onsager's theory for the dissociation of ion pairs in weak electrolytes.<sup>44,45</sup> This theory, derived by solving the

Smoluchowshi equations, describes the photogeneration process as obtained by exciton formation followed by the creation of an intermediate state in which the electron-hole pairs are thermalized (Fig. 1.2) at a typical distance  $r_0$ . At this state, thermal fluctuations can separate the charges if the thermal energy  $k_B T$  is comparable to the electrostatic binding energy of the pair. A Coulomb radius  $r_c$  is defined as the distance at which thermal and electrostatic energies are equal:

$$r_c = \frac{e^2}{\epsilon_{DC} k_B T} \quad (1.8)$$

where CGS units are used. Charge separation is efficient if  $r_0$  is not much shorter than  $r_c$ , otherwise its probability is low.

The two parameters describing the separation process are the primary quantum yield  $\phi_0$  and the escape probability  $\Omega$ .  $\phi_0$  represents the probability that an exciton becomes a thermalized couple, while  $\Omega$  is the probability that an excited charge moves beyond the Coulomb radius and avoids recombination. From Osanger's model it is possible to obtain the analytical expression for  $\Omega$ <sup>45</sup>:

$$\Omega(r, \theta, E) = e^{-A} e^{-B} \sum_{n=0}^{\infty} \sum_{m=0}^{\infty} \frac{A^m B^{m+n}}{m!(m+n)!} \quad (1.9)$$

where, in CGS units:

$$A = \frac{e^2}{\epsilon_{DC} k_B T r} \quad (1.10)$$

$$B = (1 + \cos \theta) \frac{e E r}{2 k_B T} \quad (1.11)$$

where  $E$  is the applied electric field,  $e$  is the elementary charge,  $\epsilon_{DC}$  is the static dielectric constant,  $k_B$  is the Boltzman constant,  $T$  is the temperature and  $\theta$  is the polar angle between applied field and the direction connecting the two charges.

Defining the quantum efficiency as  $\phi(E, r_0) = \phi_0 \Omega$ , it is interesting to derive the dependence of  $\phi$  on the applied field  $E$ . Under the assumption that the distribution of thermalized pairs is isotropic, Mozumder<sup>46</sup> integrated the product  $\phi_0 \Omega$  over space, and obtained a good numerical approximation to Onsager's quantum efficiency  $\phi(E)$  in terms of the infinite sum:

$$\phi(E) = \phi_0 \left( 1 - \xi^{-1} \sum_0^{\infty} A_n(\kappa) A_n(\xi) \right) \quad (1.12)$$

Where  $A_n(x)$  is a recursive formula given by:

$$A_n(x) = A_{n-1}(x) - \frac{x^n e^{-x}}{n!} \quad (1.13)$$

and  $A_0(x) = 1 - e^{-x}$ ,  $\kappa = \frac{r_c}{r_0}$ ,  $\xi = \frac{er_0 E}{k_B T}$ .

In Eq. (1.12),  $\phi_0$  is the primary quantum yield, i.e., the fraction of absorbed photons that results in bound thermalized electron-hole pairs. It is considered independent of the applied field. For the infinite sum in Eq. (1.12), good convergence is found for  $n=10$ . The convergence of Eq. (1.12) makes it possible to derive the dependence of photogeneration on  $r_0$  and electric field  $E$ . For example, if the thermalization radius  $r_0$  is within the 10-30 Å range, typical for organic materials, the photogeneration efficiency  $\phi$  varies strongly with the electric field and it can increase by several orders of magnitude by increasing the electric field from 10 to 100 V/ $\mu\text{m}$ , as shown in Fig. 1.3.

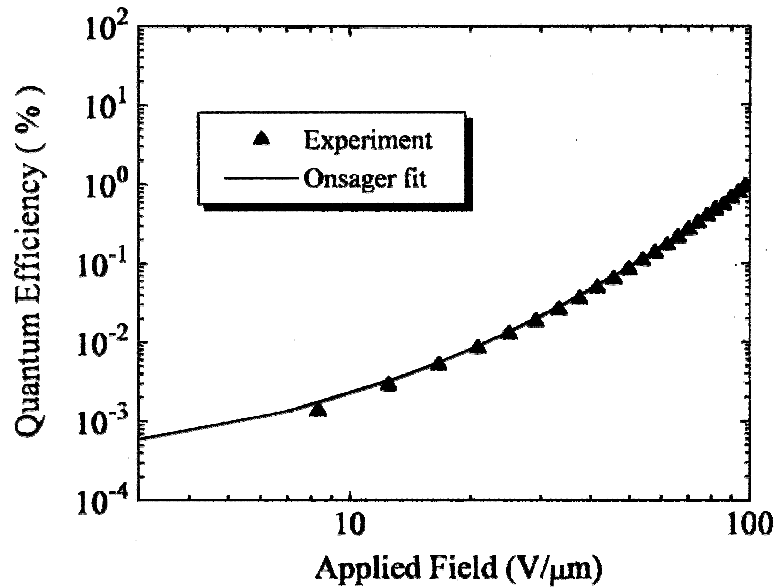


Fig. 1.3. Photogeneration efficiency measured as function of the applied field in a film of PVK/DR1/TNF.<sup>46</sup>

### 1.3.2 Charge transport

After photogeneration of free carriers, the next step in the buildup of a space-charge is their transport from brighter regions of the interference pattern (where they are generated), to other regions, where they get trapped. The transport mechanisms depend on the nature of materials. In crystals, because of the ordered structure, electronic band formation is allowed and consequently the photogenerated electrons can move easily.



In contrast to inorganic photorefractive crystals with a periodic structure, photorefractive polymers are nearly amorphous. The local energy level of each molecule/moiety is affected by its non-uniform environment. The disorder in amorphous photoconductors splits the conduction bands of molecular crystals into a distribution of localized electronic states. As a result, photogenerated charges must “hop” between localized levels with a transport mechanism that should be considered not as a continuous process but rather as a series of discrete events. The hopping mechanism for the case of hole transport is schematically described in Fig. 1.4. A sensitizer (electron acceptor to generate a hole) with density  $N_A$  is excited, a free hole is injected into the transport manifold, hopping between transport sites until it either becomes trapped or recombines with ionized acceptors with a rate  $\gamma$ .

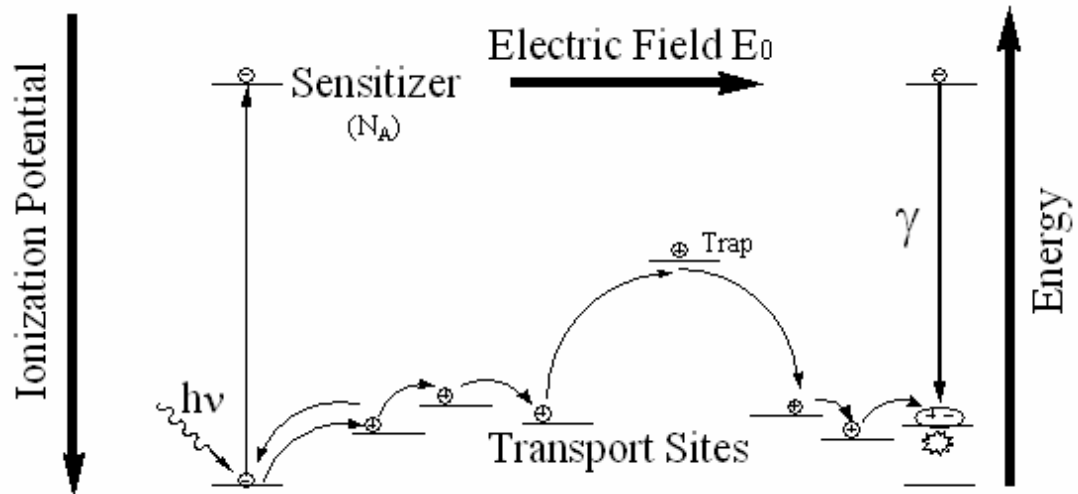


Fig. 1.4. Schematic representation of hole transport and trapping model.

The parameter that typically describes the transport process is the drift mobility  $\mu$  defined by Eq.(1.14):

$$\vec{v} = \mu \vec{E} \quad (1.14)$$

where  $\vec{v}$  is the drift velocity of charges moving under the influence of the applied electric field  $\vec{E}$ .

In organics, due to the nature of the trapping and detrapping processes, drift mobility can be analyzed in terms of its Poole-Frenkel dependence on electric field<sup>47-49</sup>:

$$\mu = \mu_0 \exp\left(-\frac{F_0 - \beta E^{1/2}}{k_B T_{\text{eff}}}\right) \quad (1.15)$$

where:

$$T_{\text{eff}} = \left(\frac{1}{T} - \frac{1}{T_0}\right)^{-1} \quad (1.16)$$

and  $\beta$  is a constant coefficient depending on the transport system,  $F_0$  is the zero-field activation energy,  $E$  is the applied electric field,  $\mu_0$  is a parameter depending on the material and  $T_0$  is a particular temperature value at which the curves  $\mu$  vs.  $T$  intersect for all applied fields. Although this is one of the most used empirical relations to fit experimental data<sup>50</sup>, it overestimates drift mobility by several orders of magnitude because it considers a trap free transport mechanism.<sup>51</sup> Further enhancements were necessary in order to improve the correlation between theoretical and experimental data.

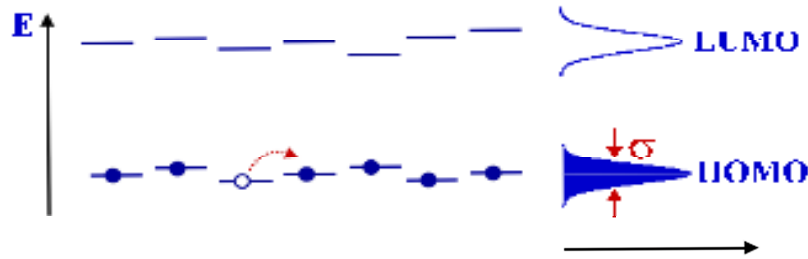


Fig. 1.5. Energetic disorder in transporting levels.

A fundamental work in the field of intermolecular hopping transport is due to Scher and Montroll<sup>52</sup>, who explained this hopping-type transport by a continuous time random walk model (CTRW) in which the charge carriers are hopping between equally spaced lattice sites. Other models based on multiple trapping/detrapping have also been proposed.<sup>53</sup> However, discrepancies from these simple models have been found experimentally<sup>54</sup> and more elaborate models that include the effects of disorder between the different sites have been developed.<sup>55</sup> Among the most recent ones, the so-called disorder formalism is already widely used, which assumed a Gaussian distribution of the positions<sup>56</sup> and of the hopping sites energies<sup>57,58</sup> (Fig. 1.5) and in addition that:

- 1) electrons and phonons do not interact;
- 2) no correlation exists between successive hops;

- 3) the hopping rates  $v_{AB}$  between states A and B with energies  $\varepsilon_A$ ,  $\varepsilon_B$  and position  $R_A$  and  $R_B$  can be expressed in the Miller-Abrahamas form:

$$v_{AB} = v_0 \exp(-2\gamma|R_A - R_B|) \cdot \Theta \quad (1.17)$$

where:

$$\begin{aligned} \Theta &= \exp\left(-\frac{\varepsilon_A - \varepsilon_B}{k_B T}\right) && \text{if } \varepsilon_A > \varepsilon_B \\ \text{or} &&& \\ \Theta &= 1 && \text{if } \varepsilon_A < \varepsilon_B \end{aligned}$$

In Eq. (1.17)  $v_0$  is a frequency prefactor and  $\gamma$  is an inverse wavefunction decay length<sup>58</sup>. It is possible to observe that the probabilities of hopping to higher and lower energy sites are different. According to the disorder formalism model, if  $\sigma$  and  $\Sigma$  are the standard deviations of the Gaussian distributions for energy and position, respectively, the drift mobility  $\mu$  is given by:

$$\mu = \mu_0 \exp\left[-\left(\frac{2}{3} \frac{\sigma}{k_B T}\right)^2\right] \exp\left[C\sqrt{E}\left(\frac{\sigma^2}{k_B^2 T^2} - \Sigma^2\right)\right] \quad (1.18)$$

where  $C$  is an empirical constant.

### 1.3.3 Space-charge field formation

At some point the photogeneration and transport processes reach equilibrium and give a steady state of charge density and electric field. Several models were developed for the description of space-charge field formation. First we will discuss a simple band theory developed for inorganic crystals, often referred to as the Kukhtarev model<sup>59</sup>, and then the specific models developed for organics. It is important to analyze Kukhtarev's model because it has a relative simple form, and it is often used to interpret PR data in organics. In addition, most of the models developed for organic materials can be considered as its extensions.

Usually, holes are the higher mobility carriers in photorefractive materials, although in some photorefractive materials the carriers are electrons.<sup>60-62</sup> For this reason, the Kukhtarev model for hole transport will be described (differences when electrons are considered are minimal, *vide infra*). In the model, an analytic form for the space-charge field is obtained by solving an appropriate set of electrodynamic and continuity equations. For the process to occur, the presence of a population of electron acceptors that provides holes to the transport process is necessary. By defining  $N_A$  as the total acceptors

concentration,  $N_A^-$  as the ionized acceptors concentration,  $N_D^+$  as the donors concentration and  $n_H$  as the holes concentration, the rate equation for holes formation is expressed by:

$$\frac{\partial n_H}{\partial t} = \frac{\partial N_A^-}{\partial t} - \frac{\nabla \cdot \vec{j}_H}{e} \quad (1.19)$$

where  $\vec{j}_H$  is the hole current and  $e$  is the elementary charge. It is also possible to write the following equation:

$$\frac{\partial N_A^-}{\partial t} = (vI(x) + \beta)(N_A^- - N_A) - n_H \gamma^- N_A \quad (1.20)$$

where  $v$  and  $\beta$  are the photogeneration and thermal generation rates of holes, respectively, and  $\gamma$  is the recombination rate. In addition, the current due to holes is:

$$\vec{j}_H = n_H \mu_H e \vec{E} - T \mu_H k_B \nabla n \quad (1.21)$$

where  $\mu_H$  is the hole mobility,  $\vec{E}$  the electric field,  $T$  the temperature and  $k_B$  the Boltzman constant. The electric field associated with the charge distribution can be expressed by Poisson's equation:

$$\epsilon_{DC} \nabla \cdot \vec{E} = 4\pi(n_H + N_D^+ - N_A^-)e \quad (1.22)$$

Expanding in series the unknown quantities  $n_H$ ,  $N_A^-$ ,  $\vec{E}$  and  $\vec{j}_H$ , it is possible to linearize the equation system and obtain the solution for the component of the electric field varying in space,  $E_1$ :

$$E_1 = -m \frac{(E_0 - iE_D)E_q}{E_q + E_D + iE_0} \quad (1.23)$$

where  $E_D$  and  $E_q$  are the so called diffusion and the trap limited fields, respectively:

$$E_D = \frac{Kk_B T}{e} \quad E_q = \frac{4\pi e}{\epsilon_{DC} K} N_{\text{eff}} \quad (1.24)$$

where  $K = 2\pi/\Lambda$  is the grating vector and  $N_{\text{eff}}$  an effective trap density. The phase  $\phi_{\text{hole}}$  between the light pattern and the internal electric field  $E_{\text{sc}}$  is:

$$\phi_{\text{hole}} = \tan^{-1} \frac{\text{Im}(E_1)}{\text{Re}(E_1)} = \tan^{-1} \left[ -\frac{E_D}{E_0} \left( 1 + \frac{E_D}{E_q} + \frac{E_0^2}{E_D E_q} \right) \right] \quad (1.25)$$

The space-charge field  $E_{\text{sc}}$  can then be expressed as:

$$E_{sc} = |E_1| \cos(Kx + \phi_{hole}) \quad (1.26)$$

The same solution can be obtained in the case of electron transport, with the only difference in the sign of the imaginary part of  $E_{sc}$ . This leaves unaltered the amplitude of  $E_{sc}$  but the sign of the phase in Eq. (1.26) is opposite:  $\phi_{hole} = -\phi_{electrons}$ .

Models to analyze the specific properties of organic photorefractive materials have also been developed. Twarowski<sup>63</sup> first introduced “organic features” within Kukhtarev model and took into account the electric field dependence of the photogeneration efficiency. Schildkraut and Buettner<sup>64,65</sup> went a bit further because they also considered the rate equations of trap density in the system of PR dynamical equations and took into account the electric field dependence of both photogeneration efficiency and carrier mobility. The importance of this work lies in the presented evidence that the dynamics of the trapping-detrapping process must be taken into account in order to obtain a good agreement between theoretical and experimental data. Further studies were then developed by considering mostly the role of traps. Cui<sup>66</sup> was able to study the dynamics of the space-charge field erasure by considering, in addition to the no traps and deep traps cases, other two different kinds of traps: optically active traps, from which the charges can be extracted by illumination, and shallow traps from which the charges can be thermally and optically removed.

The PR model was further developed by Ostroverkhova and Singer<sup>67</sup> who considered two kinds of traps, shallow and deep. In this study, the term “deep” meant that the rate of thermal detrapping for these traps was at least one order of magnitude smaller than that of the shallow traps, but still having a nonzero probability for detrapping. The main focus of this study was to develop an understanding of trapping and recombination processes as well as to determine various photoelectric rates from photocurrent dynamics to predict the time evolution of the space-charge field. The simulated results showed good agreement with experimental data for several PVK based materials. These studies also point out that the preillumination history of the sample plays an important role on photorefractive dynamic properties, as already experimentally observed in several systems<sup>68-71</sup>.

Although understanding of the photoconductive properties of PR organic materials has significantly improved over the past years, there are still a lot of open issues and some effects have not yet been considered in the models. For example, the effect of the contact

electrodes, the role of ionic and electronic dark currents and the effect of the non-uniform illumination across the sample due to absorption.

### 1.3.4 Refractive index modulation

The last step in PR grating formation is the refractive index change in response to the space-charge field. Depending on the material, an electric field can induce refractive index variations through several mechanisms which can roughly be classified in two different categories: non-linear optical effects (NLO) and orientational enhancement effects (OE).

#### 1.3.4.1 Non-linear optical materials

The refractive index modulation can be achieved through the linear electro-optic effect (Pockels effect) and less frequently through the quadratic electro-optic effect (Kerr effect). It is possible to express the electric polarization  $\vec{P}$  for linear media as<sup>72</sup>:

$$\vec{P} = \chi \vec{E} \quad (1.27)$$

where  $\chi$  is the electric susceptibility. In non-linear optical materials, the polarization is instead given by:

$$\vec{P} = \chi^{(1)} \vec{E} + \chi^{(2)} \vec{E} \vec{E} + \chi^{(3)} \vec{E} \vec{E} \vec{E} \dots \quad (1.28)$$

Since the intensity of light, in CGS units, is given by:

$$E_0^2 = \frac{8\pi}{cn} \quad (1.29)$$

where  $c$  is the speed of light in vacuum, and considering the following relations:

$$\varepsilon = 1 + 4\pi\chi \quad (1.30)$$

$$n^2 = \varepsilon \quad (1.31)$$

the refractive index is given by:

$$n = n_0 + \frac{4\pi\chi^{(2)}}{n_0} E(x) + \frac{6\pi\chi^{(3)}}{n_0} E^2(x) + \frac{12\pi\chi^{(3)}}{cn_0^2} I \quad (1.32)$$

where  $I$  is the light intensity.

The above relation can be rewritten for convenience as:

$$n = n_0 + n_1 E + n_2 E^2 + n_3 I \quad (1.33)$$

and the values of  $n_1$ ,  $n_2$  and  $n_3$  can be obtained by comparing Eq. (1.32) and (1.33). The  $n_1$  term, proportional to the electro-optic tensor  $\chi^{(2)}$ , describes the Pockels effect, while  $n_2$  describes the quadratic or Kerr effect. The variation of the refractive index induced by the Pockels effect ( $\Delta n$ ) can be deduced by using the following relations:

$$\Delta n = n_0 - n = n_0 - n_0 - \frac{4\pi\chi^{(2)}}{n_0} E_{sc} = -\frac{4\pi\chi^{(2)}}{n_0} E_{se} \quad (1.34)$$

where it is clear that the variation of the refractive index is linear with the electric field. From Eq. (1.33) and (1.34) it is also evident that, for symmetry reasons,  $n_1$  must vanish in centrosymmetric materials while  $n_2$  may not. In anisotropic substances  $\chi^{(2)}$  is obviously a tensor and the observed  $\Delta n$  can be related to the symmetry of the system.

Pockels effect can be observed only in non-centrosymmetric materials. As amorphous materials are essentially centrosymmetric, in this case centrosymmetry can be removed by adding to the material particular molecules with high dipole moment, called chromophores, that can be oriented by an external electric field.

### 1.3.4.2 Orientational enhancement effect

The Pockels effect plays an important role to modulate the refractive index. However, some materials show an index modulation which is too high to be attributed to the Pockels effect by itself.<sup>41</sup> A study by Moerner and co-workers revealed an additional mechanism participating in the PR grating formation in organic materials.<sup>41</sup> The essence of this mechanism called ‘‘orientation enhancement’’ (OE) is that in a material with glass transition temperature ( $T_g$ ) lower than or near the operating temperature, the NLO chromophores, which are necessary constituents of a PR polymer composite or glass, can be aligned not only by the externally applied electric field  $E_0$  but also in situ by the sinusoidally varying space-charge field  $E_{sc}$  during grating formation.

The OE effect is illustrated schematically in Fig. 1.6. When no electric field is applied to the sample, the molecules are randomly oriented (Fig. 1.6 (a)). As an external field  $E_0$  is applied to the sample, the molecules reorient and align along the electric field (Fig. 1.6 (b)). In the PR experiment, the interfering light beams 1 and 2 produce a sinusoidally varying space-charge field  $E_{sc}$  by the mechanisms described in section 1.2. The uniform external field  $E_0$  will vectorially add to  $E_{sc}$  to produce a total local field  $E$ . Because the NLO chromophores have orientational mobility which depends on their  $T_g$

and on their molecular size, a spatially periodic orientational pattern is produced as the electric field orients the molecules by virtue of their ground-state dipole moment ( $\mu_g$ ). Fig. 1.6 (c) illustrates the local order for the total field consisting of  $E_{sc} + E_0$  (the order shown is exaggerated for illustration purposes).

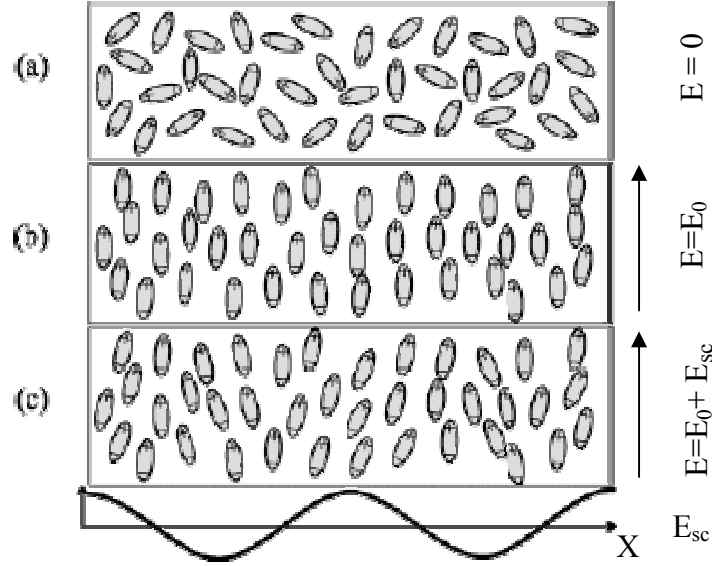


Fig. 1.6. Chromophore orientation in the electric field: (a) no electric field; (b) electric field  $E_0$  is applied; (c) spatially modulated space-charge field  $E_{sc}$  is added to the applied field.

In PR materials exhibiting the OE effect, it can be briefly summarized that the refractive index change ( $\Delta n$ ) in response to the total electric field ( $E=E_{sc} + E_0$ ) is a sum of the birefringent ( $\Delta n_{BR}$ ) and electro-optic ( $\Delta n_{EO}$ ) contributions ( $\Delta n = \Delta n_{BR} + \Delta n_{EO}$ ) given by

$$\Delta n_{BR} \approx \frac{1}{2} n \Delta \chi^{(1)} \approx \frac{1}{2} n C_{BR} E^2 \quad (1.35)$$

$$\Delta n_{EO} \approx \frac{1}{2} n \Delta \chi^{(2)} E \approx \frac{1}{2} n C_{EO} E^2 \quad (1.36)$$

$$C_{BR} = \frac{2Nf_{\infty}\Delta\alpha}{45} \left( \frac{\mu}{k_B T} \right)^2 \quad (1.37)$$

$$C_{EO} = \frac{Nf_0 f_{\infty}^2 \mu_g \beta}{5 k_B T} \quad (1.38)$$



where  $N$  is the dipole concentration,  $f_0$  and  $f_\infty$  are the local field factors,  $k_B$  is the Boltzmann constant,  $T$  is the temperature,  $\Delta\alpha$  is the polarizability anisotropy, and  $\beta$  is the only nonvanishing component of the hyperpolarizability tensor  $\beta_{ijk}$  (in the case of an ideal molecule with cylindrical symmetry).

Due to the importance of the OE effect, the design of chromophores for photorefractivity has diverged from the strategy of the early 1990s, in which only hyperpolarizability was emphasized. Thus, rather than seeking chromophores with large first hyperpolarizability, it is often more important to select chromophores with a large linear polarizability anisotropy.

In overall PR performance, the OE effect leads to enhanced steady-state properties (larger gain and diffraction efficiencies than expected due to the simple electro-optic effect) as well as more complicated dynamics determined not only by the rate of space-charge field formation, but also by the ability of the NLO chromophores to dynamically orient during the grating formation. Therefore, an additional factor that could limit the speed of hologram growth, rotational mobility of the chromophores in the polymer composite, is introduced. Molecular orientation times can range from picoseconds (observed in liquids<sup>73</sup>) to extremely long times of years or more observed in permanently poled polymers,<sup>74</sup> depending upon the viscosity of the material, the size of the chromophore, the presence of plasticizing agents, temperature relative to  $T_g$ , and other factors.<sup>75-79</sup>

To summarize, space-charge field formation in PR organic materials is a complicated process that requires further theoretical modelling supported by experimental results. The OE effect brings the advantage of higher diffraction efficiencies and gain coefficients. However, because chromophore orientation does not proceed instantaneously, the analysis of the PR dynamics is challenging, especially when the rate of space-charge field formation is of the same order of magnitude as the reorientation speed. To assess the factors that limit PR speed in every material, it may be helpful to separately measure the orientational mobility.

## BIBLIOGRAPHY

1. P. M. Lundquist, C. Poga, R. G. DeVoe, Y. Jia, W. E. Moerner, M. P. Bernal, H. Coufal, R. K. Grygier, J. A. Hoffnagle, C. M. Jefferson, R. M. Macfarlane, R. M. Shelby, G. T. Sincerbox. *Opt. Lett.*, **1996**, 21, 890.
2. N. Cheng, B. Swedek, P. N. Prasad. *Appl. Phys. Lett.*, **1997**, 71, 1828.
3. S. J. Strutz, L. M. Hayden. *Appl. Phys. Lett.*, **1999**, 74, 2749.
4. K. D. Harris, R. Ayachitula, S. J. Strutz, L. M. Hayden, R. J. Twieg. *Appl. Opt.*, **2001**, 40, 2895.
5. J. Feinberg, K. R. Macdonald. *Top. Appl. Phys.*, **1989**, 62, 151.
6. A. E. Chiou, *Proc. IEEE*, **1999**, 87, 2074.
7. K. Matsushita, P. P. Banerjee, S. Ozaki, D. Miyazaki. *Opt. Lett.*, **1999**, 24, 593.
8. A. Goonesekera, D. Wright, W. E. Moerner. *Appl. Phys. Lett.*, **2000**, 76, 3358.
9. A. Grunnet-Jepsen, C. L. Thompson, W. E. Moerner. *Science*, **1997**, 277, 549.
10. E. Mecher, F. Gallego-Gomez, H. Tillmann, H. H. Horhold, J. C. Hummelen, K. Meerholz. *Nature*, **2002**, 418, 959.
11. J. L. Maldonado, G. Ramos-Ortiz, O. Barbosa-García, M. A. Meneses-Nava, L. Márquez, M. Olmos-López. *Int. J. Mod. Phys. B.*, **2007**, 21, 2625.
12. F. Gallego-Gómez, F. D. Monte, K. Meerholz. *Nature Materials*, **2008**, 7, 490.
13. S. Tay, P. A. Blanche, R. Voorakaranam, A. V. Tunc, W. Lin, S. Rokutanda, T. Gu, D. Flores, P. Wang, G. Li, P. St Hilaire, J. Thomas, R. A. Norwood, M. Yamamoto, N. Peyghambarian. *Nature*, **2008**, 451, 694.
14. B. Kippelen, S. R. Marder, E. Hendrickx, J. L. Maldonado, G. Guillemet, B. L. Volodin, D. D. Steele, Y. Enami, Sandalphon, Y. J. Yao, J. F. Wang, H. Röckel, L. Erskine, N. Peyghambarian. *Science*, **1998**, 279, 54.
15. A. Ashkin, G. D. Boyd, J. M. Dziedzic, R. G. Smith, A. A. Ballmann, J. J. Levinstein, K. Nassau. *Appl. Phys. Lett.*, **1966**, 9, 72.
16. F. S. Chen, J. T. LaMacchia, D. B. Fraser. *Appl. Phys. Lett.* **1966**, 13, 223.
17. K. Sutter, J. Hullinger, P. Günter. *Solid State Commun.*, **1990**, 74, 867.
18. K. Sutter, P. Günter. *J. Opt. Soc. Am. E*, **1990**, 7, 2274.
19. E. V. Rudenko, A. V. Sukhov. *JETP Lett.*, **1994**, 59, 142.
20. I. C. Khoo, H. Li, Y. Liang. *Opt. Lett.*, **1994**, 19, 1723.
21. G. P. Wiederecht, B. A. Yoon, M. R. Wasielewski. *Science*, **1995**, 270, 1974.
22. P. Günter, J. P. Huignard. *Photorefractive materials and their applications*, Berlin: Springer-Verlag; **1988**.
23. D. L. Staebler, J. J. Amodei. *J. Appl. Phys.*, **1972**, 43, 1042.
24. P. Yeh. *Introduction to Photorefractive Nonlinear Optics*, John Wiley & Sons, New York, **1993**.
25. H. J. Eichler, P. Günter, D. W. Pohl. *Laser-Induced Dynamic Gratings*, Springer-Verlag, Berlin, **1986**.
26. A. Marrakchi, K. Rastani. in *Photonic Switching and Interconnects*, A. Marrakchi, Ed, Marcel Dekker, New York, **1994**.
27. P. Günter. *Phys. Rep.*, **1982**, 93, 199.
28. G. Roosen. *Int. J. Optoelectronics*, 1989, 4, 459.
29. A. M. Glass, D. D. Nolte, D. H. Olson, G. E. Doran, D. S. Chemla, W. H. Knox. *Opt. Lett.*, **1990**, 15, 264.
30. D. D. Nolte, D. H. Olson, G. E. Doran, W. H. Knox, A. M. Glass. *J. Opt. Soc. Am. B*, **1990**, 7, 2217.

31. D. D. Nolte, Q. Wang, M. R. Melloch. *App. Phys. Lett.*, **1991**, 58, 2067.
32. Q. Wang, D. D. Nolte, M. R. Melloch. *App. Phys. Lett.*, **1991**, 59, 256.
33. Q. Wang, R. M. Brubaker, D. D. Nolte, N. R. Melloch. *J. Opt. Soc. Am. B*, **1992**, 9, 1626.
34. A. Partovi, A. M. Glass, D. H. Olson, G. J. Zydik, K. T. Short, R. D. Feldman, R. F. Austin. *Appl. Phys. Lett.*, **1992**, 59, 1832.
35. A. Partovi, A. M. Glass, D. H. Olson, G. J. Zydik, H. M. O'Bryan, T. H. Chin, W. H. Knox. *Appl. Phys. Lett.*, **1993**, 62, 464.
36. N. V. Kukharev, *Pis'ma Zh. Tekh. Fiz.* **1976**, 2, 114 (*Sov. Tech. Phys. Lett.*, **1976**, 2, 438).
37. N. V. Kukharev, V. B. Markov, S. G. Odulov. *Opt. Commun.*, **1977**, 23, 338.
38. N. V. Kukharev, V. B. Markov, S. G. Odulov, M. S., V. L. Vinetskii. *Ferroelectrics*, **1979**, 22, 949.
39. V. L. Vinetskii, N. V. Kukharev, *Fiz. Tverd. Tela (Leningrad)*, **1975**, 16, 3714 (*Sov. Phys. Solid State*, **1975**, 16, 2414).
40. V. L. Vinetskii, N. V. Kukharev, *Kvant. Elektron. (Moscow)*, **1978**, 5, 405 (*Sov. J. Quantum Electron.*, **1978**, 8, 231).
41. W. E. Moerner, S. M. Silence, F. Hache, G. C. Bjorklund. *J. Opt. Soc. Am. B*, **1994**, 11, 320.
42. O. Ostroverkhova, W. E. Moerner. *Chem. Rev.*, **2004**, 104(7), 3267.
43. P. M. Borsenberger, D. S. Weiss: '*Organic Photoreceptors for Xerography*', Dekker Inc., New York, **1998**.
44. L. Onsager. *J. Chem. Phys.*, **1934**, 2, 599.
45. L. Onsager. *Phys. Rev.*, **1938**, 54, 554.
46. B. Kippelen, K. Meehrholz, N. Peyghambarian: '*An Introduction to Photorefractive Polymers*' in '*Nonlinear Optics of Organic Molecules and Polymers*', H. S. Nalwa and S. Miyata Eds., CRC Press Inc., London, (1997).
47. J. Frenkel. *Phys. Rev.*, **1938**, 54, 647.
48. D. M. Pai. *J. Chem. Phys.*, **1970**, **52**, 2285.
49. W. D. Gill. *J. Appl. Phys.*, **1972**, 43, 5033.
50. D. H. Dunlap. *Phys. Rev. B.*, **1995**, 52, 939.
51. M. Fujino, H. Mikawa, M. Yokoyama. *J. Non-Cryst. Solids*, **1984**, 64, 163.
52. H. Scher, E. W. Montroll. *Phys. Rev. B*, **1975**, 12, 2455.
53. S. W. Schmidlin. *Phys. Rev. B*, **1977**, 16, 2362.
54. D. Haarer. in *Frontiers of Polymer Research*, P. N. Prasad, J. K. Eds. Nigam, Plenum Press, New York, **1991**, 297.
55. M. Van der Auweraer, F. C. de Schryver, P. M. Borsenberger, H. Bässler. *Adv. Mater.* **1994**, 6, 199.
56. H. Bässler. *Phil. Mag. B*, **1984**, 50, 347.
57. H. Bässler. *Adv. Mater.*, **1993**, 5, 662.
58. H. Bässler. *Phys. Stat. Sol. B*, **1993**, 175, 15.
59. N. V. Kukhtarev, V. B. Markov, S. G. Odulov, M. S. Soskin, V. L. Vinetskii. *Ferroelectrics*, **1979**, 22, 949.
60. K. Okamoto, T. Nomura, S. H. Park, K. Ogino, H. Sato. *Chem. Mater.*, **1999**, 11, 3279.
61. L. M. Wang, M. K. Yu, L. P. Ng. *Phys. Rev. B*, **2000**, 62, 4973.
62. J. Sohn, J. Hwang, S. Y. Park, Y. Y. Noh, J. J. Kim. *Appl. Phys. Lett.*, **2002**, 81, 190.
63. A. Twarowski. *J. Appl. Phys.*, **1989**, 65, 2833.

64. J. S. Schildkraut, A. V. Buettner. *J. Appl. Phys.*, **1992**, 72, 1888.
65. J. S. Schildkraut, Y. P. Cui. *J. Appl. Phys.*, **1992**, 72, 5055.
66. Y. P. Cui, B. Swedek, N. Cheng, J. Zieba, P. N. Prasad. *J. Appl. Phys.*, **1999**, 85, 38.
67. O. Ostroverkhova, K. D. Singer. *J. Appl. Phys.*, **2002**, 92, 1727.
68. E. Hendrickx, Y. D. Zhang, K. B. Ferrio, J. A. Herlocker, J. Anderson, N. R. Armstrong, E. A. Mash, A. P. Persoons, N. Peyghambarian, B. Kippelen. *J. Mater. Chem.*, **1999**, 9, 2251.
69. J. A. Herlocker, C. Fuentes-Hernandez, K. B. Ferrio, E. Hendrickx, P. A. Blanche, N. Peyghambarian, B. Kippelen, Y. Zhang, J. F. Wang, S. R. Marder. *Appl. Phys. Lett.*, **2000**, 77, 2292.
70. E. Mecher, R. Bittner, C. Brauchle, K. Meerholz. *Synth. Met.*, **1999**, 102, 993.
71. E. Mecher, F. Gallego-Gomez, H. Tillmann, H. H. Horhold, J. C. Hummelen, K. Meerholz. *Nature*, **2002**, 418, 959.
72. P. Prasad, D. J. Williams: '*Introduction to Non Linear Optical Effects in Molecules and Polymers*', Wiley, New York, **1991**.
73. J. S. Baskin, A. H. Zewail. *J. Phys. Chem. A*, **2001**, 105, 3680.
74. M. Stahelin, D. M. Burland, M. Ebert, R. D. Miller, B. A. Smith, R. J. Twieg, W. Volksen, C. A. Walsh. *Appl. Phys. Lett.*, **1992**, 61, 1626.
75. O. Ostroverkhova, W. E. Moerner, M. He, R. J. Twieg. *Chem. Phys. Chem.*, **2003**, 4, 732.
76. R. D. Dureiko, D. E. Schuele, K. D. Singer. *J. Opt. Soc. Am. B*, **1998**, 15, 338.
77. D. B. Hall, A. Dhinojwala, J. Torkelson. *Phys. Rev. Lett.*, **1997**, 79, 103.
78. P. Pretre, U. Meier, U. Stalder, C. Bosshard, P. Günter, P. Kaatz, C. Weder, P. Neuenchwander, U. W. Suter. *Macromolecules*, **1998**, 31, 1947.
79. J. C. Ribierre, L. Mager, A. Fort, S. Mery. *Macromolecules*, **2003**, 36, 2516.

## Chapter 2

# PHOTOREFRACTIVE POLYMERS

### 2.1 Introduction

Since the photorefractive (PR) effect was first observed in 1966<sup>1</sup> in an inorganic crystal of LiNbO<sub>3</sub>, more and more inorganic crystals such as BaTiO<sub>3</sub>, KNbO<sub>3</sub> and GaAs have been found to exhibit PR properties. However, the difficulty in crystal growing and sample preparation have limited the applications of inorganic PR crystals. Compared to inorganic PR crystals, organic materials are superior due to their versatility, lower cost and easier fabrication, and they are becoming promising candidates for PR applications.<sup>2</sup> Within organic photorefractive materials, polymers are among the most studied because of their low cost, ease of material processing, high electro-optic coefficients accompanied by low dc dielectric constants, ease of doping and tailorable properties.<sup>3</sup> The first observation of the photorefractive effect in a polymer was carried out in 1991 in a co-polymer of methylmethacrylate (PMMAPNA) doped with diethylamino-benzaldehyde diphenylhydrazone (DEH) which acted as the transport agent.<sup>4</sup> The grating in the composite was built up in about one second with a diffraction efficiency of the order of 10<sup>-5</sup>. Ever since then, this new phenomenon prompted an enormous development in photorefractive polymers.

As we will see in the following, there are some important functional components relevant to photorefractivity, such as sensitizers, photoconductors, chromophores, plasticizers, etc. In addition, we will discuss how photorefractive polymers can be classified either into guest-host polymer composites<sup>5,6</sup> and fully functionalized polymers<sup>7,8</sup>, or into low T<sub>g</sub> and high T<sub>g</sub> PR polymers, on the basis of their glass transition temperature.

### 2.2 Key components relevant to PR polymers

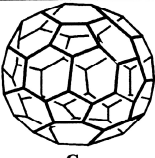
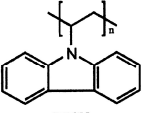
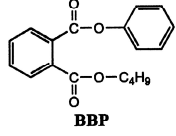
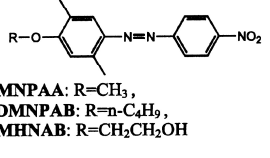
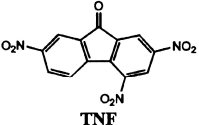
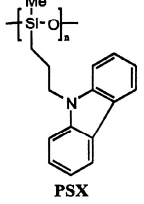
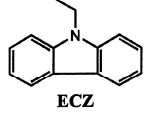
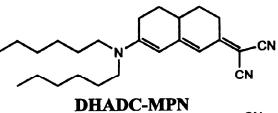
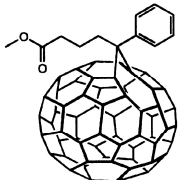
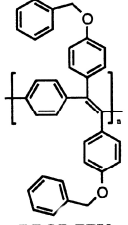
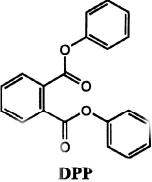
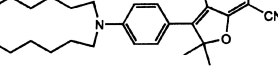
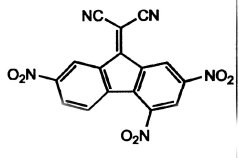
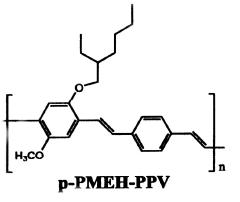
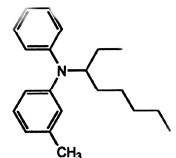
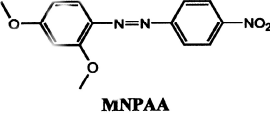
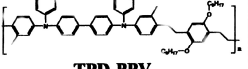
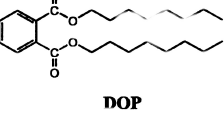
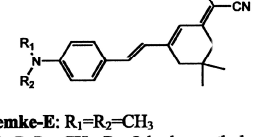
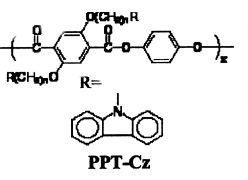
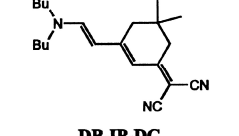
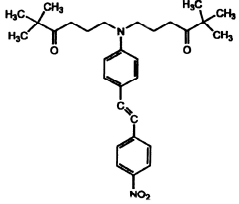
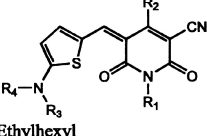
#### 2.2.1 Sensitizers

The sensitizer is usually added to the PR materials to assist in charge photogeneration. The properties of the sensitizer are very important for overall PR

performance, because the sensitizer determines the spectral response<sup>9</sup> of the PR composites and an efficient charge transfer between the sensitizer and the charge transporting matrix is necessary for good PR performance.<sup>10</sup> In addition, the PR speed may depend strongly on the photogeneration efficiency, therefore, optimization of the sensitizer is important for improving dynamic performance. Moreover, the sensitizer plays a major role in the steady-state properties of a PR material as it may also be linked to charge trapping, one of the crucial processes in PR grating formation.<sup>11</sup> To choose a sensitizer, wavelength sensitivity is important, and matching with the transport molecules should be considered. There are several classes of sensitizers. For example, semiconductor nanoparticles (NPs), including CdSe<sup>12-16</sup>, CdS<sup>17,18</sup>, LiNbO<sub>3</sub><sup>19</sup>, PbS<sup>20,21</sup>, PbSe<sup>22</sup>, Cu<sub>2</sub>S<sup>23</sup>, HgS<sup>24</sup> and CdSe/ZnS<sup>25,26</sup> have been utilized as sensitizers in PR polymers, and organic molecules and pigments have been utilized as sensitizers in organic photoconductors, including phthalocyanines, squaraines, perylene dyes and thiapyrylium salts. There are also some new approaches, such as incorporating various transition metal complexes into fully functionalized polymers and glasses,<sup>7,27-29</sup> and exploring semiconductor quantum dots like CdS and CdSe as sensitizers in hybrid organic-inorganic composites.<sup>30-35</sup> The most successful class of sensitizers are the charge transfer (CT) complexes formed between a donor-like and an acceptor-like molecule or moiety. The interaction between the donor D and the acceptor A leads to a new absorption band that does not appear in the spectrum of either component alone. Hence, spectral sensitivity in the visible and the near-infrared part of the spectrum can be achieved with CT complexes. Thus far, C<sub>60</sub>, TNF and TNFM are the most commonly used sensitizers that readily form CT complexes with donor-like molecules.<sup>11</sup>

Usually, an addition of up to 1% of a sensitizer leads to a significant improvement of both PR dynamics and steady-state properties. However, an excess of sensitizer may be detrimental to performance. For example, in a PVK-based material, it was observed<sup>36</sup> that as the concentration of the sensitizer (in this case TNFM) increased above 1.5%, the refractive index modulation decreased and the build-up time increased due to an excessively high trap density. In addition, an increased concentration of the sensitizer leads to an undesirable increase in absorption, thus an optimal concentration of commonly used sensitizers is below or around 1%.<sup>11</sup>

Table 2.1 Chemical structures of common PR sensitizers, photoconducting polymers, plasticizers, and chromophores (from reference 11).

Sensitizers	Polymers	Plasticizers	NLO chromophores
 C <sub>60</sub>	 PVK	 BBP	 DMNPAA: R=CH <sub>3</sub> , BDMNPAB: R=n-C <sub>4</sub> H <sub>9</sub> , DMHNAB: R=CH <sub>2</sub> CH <sub>2</sub> OH
 TNF	 PSX	 ECZ	 DHADC-MPN
 [6,6]PCBM	 DBOP-PPV	 DPP	 DCDHF-6
 TNFM	 p-PMEH-PPV	 EHMPA	 MNPA
	 TPD-PPV	 DOP	 Lemke-E: R <sub>1</sub> =R <sub>2</sub> =CH <sub>3</sub> , Ch C: R <sub>1</sub> =CH <sub>3</sub> , R <sub>2</sub> =2-hydroxyethyl
	 PPT-Cz		 DB-IP-DC
			 Stilbene A
			 R <sub>1</sub> =2-Ethylhexyl R <sub>2</sub> =Me R <sub>3</sub> -R <sub>4</sub> =Et ATOP-3

### 2.2.2 Charge transporting moieties

As we discussed in section 1.2, the charge transporting properties of a given photorefractive material are important since they control the build-up of the internal space-charge field that is responsible for the refractive index modulation through the electro-optic effect. There are several types of charge transporting moieties that have been utilized in PR materials such as charge transporting polymers (e.g., PVK, PSX, PPV),<sup>34,37-41</sup> inert polymer hosts (e.g., PS, PC, polysiloxane) doped with charge transporting molecules,<sup>29,42-45</sup> photoconductive low molecular weight glasses, etc. Although several electron-transporting and bipolar organic materials have been explored, most photoconductors currently used in PR composites are unipolar (hole) conductors.<sup>11</sup> Over the past years, the host polymer PVK, characterized by carrier mobilities  $\mu \sim 10^{-8}$ - $10^{-6}$  cm<sup>2</sup>/Vs (depending on electric field),<sup>46</sup> was the most widely utilized in PR polymer composites. The charge transporting property of PVK is based on carbazole group. As one of the most important fundamental structures in the field of organic electrical and optical materials,<sup>47</sup> carbazole compounds attract wide interest due to their applications in areas such as xerography, optical data storage and information processing in organic PR devices.<sup>4,34,40,48-53</sup> Carbazole-based compounds are attractive as photoconductors or charge-transporting materials for the following reasons:<sup>54</sup>

- Carbazolyl groups easily form relatively stable radical cations (holes),
- Some carbazole-containing compounds exhibit relatively high charge carrier mobilities,
- Different substituents can be easily introduced into the carbazole ring,
- Carbazole-containing compounds exhibit high thermal and photochemical stability,
- Carbazole is an inexpensive raw material readily available from coal-tar distillation.

Carbazole photoconductivity is based on the easy oxidability of the nitrogen atom and its ability to transport positive charge centers via the radical cation species.<sup>55</sup> The charge carrier transport process is schematically described in Fig. 2.1.



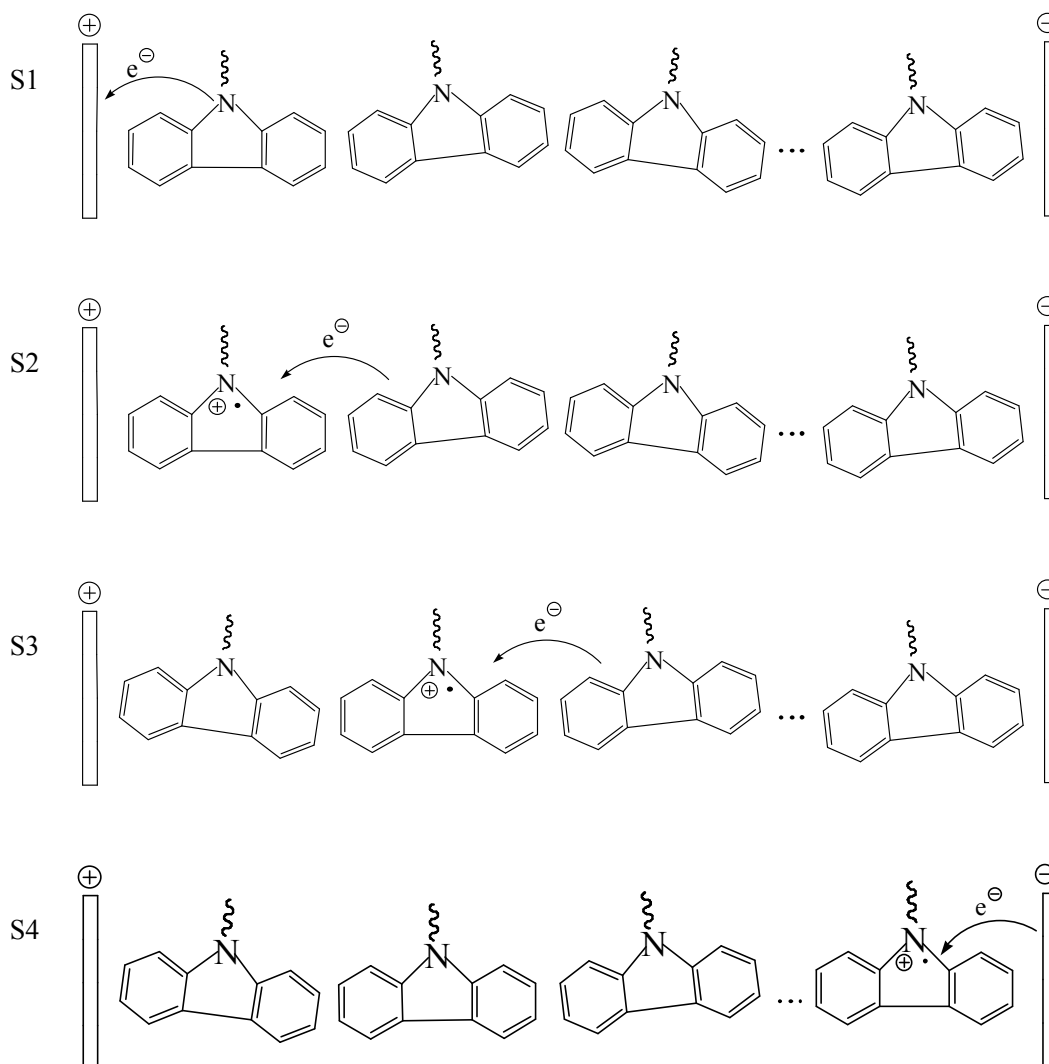


Fig. 2.1. Principles of charge carrier transport.

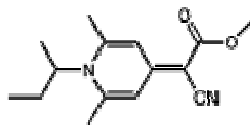
### 2.2.3 Chromophores

The NLO chromophore in PR polymer composites is mainly used to provide a functionality leading to a refractive index modulation in response to an electric field. As discussed in section 1.3.4.2 on the Orientational Enhancement Effect, several molecular parameters such as ground-state dipole moment ( $\mu_g$ ), polarizability anisotropy ( $\Delta\alpha$ ), and the first hyperpolarizability ( $\beta$ ) are of importance for the electric field-induced refractive index change. It was shown that a certain combination of these parameters, or chromophore figure-of merit (FOM), adequately describes the electro-optic nonlinearity important for the PR performance.<sup>56-58</sup> The FOM is defined as:<sup>59</sup>

$$FOM = \frac{1}{M} \left[ 9\mu_g \beta + \frac{2\mu_g^2 \Delta \alpha}{k_B T} \right] \quad (2.1)$$

where  $M$  is the molar mass,  $k_B$  is the Boltzmann constant, and  $T$  is the temperature.

The most successful NLO chromophores utilized in PR polymer composites<sup>58</sup> are azo dyes (e.g., DMNPAA), oxopyridone derivatives (e.g., ATOP-3), dicyanostyrene derivatives (e.g., AODCST), dicyanomethylenedihydrofuran derivatives (e.g., DCDHF-6), pyridone derivatives (e.g., 2BNCM), rigidized polyene derivatives (e.g., DHADC-MPN), etc. In addition to the NLO properties, many chromophores also exhibit charge-transporting properties, such as DHADC-MPN, DCDHF-6, etc.



**2BNCM**

Fig. 2.2 Chemical structure of 2BNCM.

The NLO chromophores also have other various additional properties that need to be taken into account for the PR performance. For example, although a high concentration of NLO chromophores is desirable to maximize electric field-induced birefringence, an excess of chromophores can cause PR composites to undergo phase separation, which affects optical clarity and reduces the shelf life of the PR device.<sup>60-62</sup> Furthermore, in PR composites with high chromophore concentration, dimer and aggregate formation, which may influence the electro-optic response, has been demonstrated by spectroscopic evidences.<sup>63,64</sup> Moreover, highly polar chromophore that possess high FOM may reduce the charge carrier mobility in the composite.<sup>65</sup> Finally, the chromophore ionization potential ( $I_p$ ) needs to be optimized with respect to that of the sensitizer and charge transport molecule because chromophores can participate in photogeneration, transport, and trapping processes.<sup>66-69</sup> As a result, the PR performance is highly influenced by relative  $I_p$  values of all constituents of the composites.

## 2.2.4 Plasticizers

Plasticizers are commonly added to a PR composite to lower the  $T_g$  and increase the polymer's flexibility, thus enhancing the OE effect, i.e., chromophore reorientation by

the space-charge field. The addition of a plasticizer generally causes a reduction in the cohesive intermolecular forces along the polymer chains. The chains can then move more freely relative to one another, and the stiffness of the polymer is reduced. There are two primary means of plasticization: internal and external. Internal plasticization involves the chemical alteration of a polymer or its monomer. This can be done either by random copolymerization or side chain grafting. The former tends to increase the flexibility by randomizing local environments: a more ordered copolymerization would imbue a higher degree of crystallinity thereby giving the opposite effect. The latter reduces crystallinity by disrupting interactions between the chains. The external plasticization is what we normally think of when we talk about a plasticized polymer, and involves the addition of an organic chemical during compounding (after polymerization). This chemical interacts with the polymer only physically, via its solvent capabilities. This type of plasticization is usually performed at elevated temperatures.

Plasticizers are usually inert organic materials with high boiling points and low vapor pressures. Although the inert plasticizer is more effective in lowering the  $T_g$ , it also dilutes the charge transporting moieties and at concentrations above 10% lowers mobility and reduces the PR phase shift. Functional plasticizers which have a direct functionality contributing to the PR performance are attractive.<sup>11</sup> For example, ECZ can act as both a plasticizer and a charge transporting molecule, and a tricyanopyrroline (TCP)-based NLO chromophore has demonstrated an important role in controlling  $T_g$  and NLO activity in the near-infrared (NIR) range.<sup>70</sup> Some commonly used plasticizers are shown in Table 2.1.

### 2.3 Guest-host polymers

Guest-host polymers are made by mixing low molecular weight molecules with the desired properties into a polymer matrix. This so-called guest-host approach provides enormous possibilities to obtain a PR polymer. In the guest-host composites, part of the functionalities are provided by one or more dopants and the polymeric chain can either be an inert matrix or provide some functions, such as carrier transport. The main advantage of this approach is the possibility to easily explore the influence of different dopants without complicated and time-consuming synthetic procedures. The choice of the host polymer as an inert matrix without any functionality is usually less favourable, because a

major part of the material would be inactive. Therefore, in most cases the host polymers provide some functionalities, for example, photoconductivity and EO properties. A typical guest-host PR material consists of 40-60 wt% of a photoconductor, 25-35 wt% of non-linear chromophores, 15-30 wt% of a plasticizer which is necessary in order to decrease the  $T_g$  of the material and allow chromophore reorientation and 1% or less of a photosensitizer.<sup>11</sup>

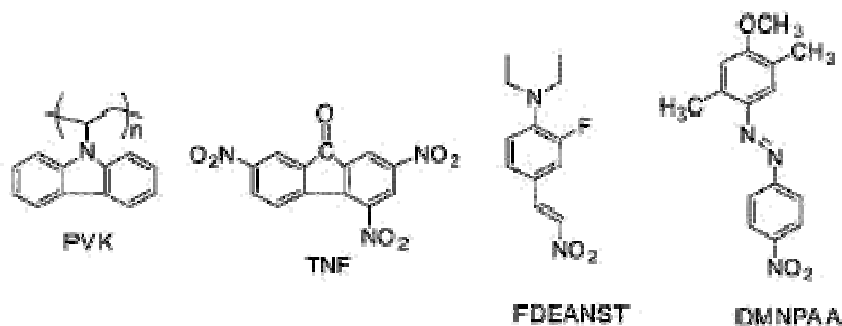


Fig. 2.3. Chemical structures of molecules in the guest-host PR polymers.

The first observation of PR properties in a guest-host polymer appeared in 1993<sup>71</sup> in a system consisting of a well-known photoconductive polymer poly(N-vinylcarbazole) (PVK), doped with a nonlinear optical (NLO) chromophore named as 3-fluoro-4-N,N-diethylamino-β-nitrostyrene (FDEANST). In this polymer a diffraction efficiency of 1% could be measured in 125- $\mu\text{m}$ -thick films at an applied field of 40V/ $\mu\text{m}$  and a grating growth time of 100 ms for a writing intensity of 1 W/ $\text{cm}^2$ . Compared to previous materials, the improvement in diffraction efficiency was two orders of magnitude. The photorefractive effect was confirmed by asymmetric two-beam coupling experiments and, for the first time, it was observed in a polymer that the PR gain exceeded the absorption coefficient of the sample. After a few months, a new polymer was reported which was based on the PVK:TNF charge-transfer complex but doped with the chromophore 2,5-dimethyl-4-(p-phenylazo)anisole (DMNPAA) with higher doping level and also doped with a photoconducting plasticizer (N-ethylcarbazole) in order to facilitate the poling process at room temperature.<sup>72</sup> In these samples, a diffraction efficiency close to the maximum value of 100% at an applied field of 61 V/ $\mu\text{m}$  was reported<sup>73</sup> and a net two-beam coupling gain coefficient of more than 200  $\text{cm}^{-1}$  was observed at 90 V/ $\mu\text{m}$ . This value is very high compared with the gain coefficient of BaTiO<sub>3</sub> which is of the order of

$30 \text{ cm}^{-1}$ . These high values were very encouraging for the development of guest-host polymers and, since then, several other polymeric matrices have been used to obtain materials with high diffraction efficiency.<sup>37,38,42,74,75</sup>

One important issue is that guest-host polymeric materials have been used not only in the visible region, but also in the near IR with the help of some sensitizers such as TNFM. For example, the composite PVK/DHADC-MPN/ECZ/TNFM showed at 830 nm an external diffraction efficiency  $\eta = 74\%$  at  $E = 59 \text{ V}/\mu\text{m}$ .<sup>23</sup> This expansion of the wavelength spectrum between 700 and 900 nm is very important because such spectral range is technologically interesting: biological tissues are not absorbing in this range and these materials are promising for bio-imaging applications.<sup>66,76</sup>

Although there are many advantages of guest-host photorefractive composites, they often exhibit problems related to phase separation, associated with thermodynamic instability. The dopants, which are usually small molecules, tend to crystallize or aggregate because of their incompatibility with macromolecules. These aggregates may cause severe optical scattering and may completely ruin the optical properties of the composites.<sup>77</sup>

## 2.4 Fully functionalized polymers

Considering the disadvantages of guest-host photorefractive composites, fully functionalized polymers, which incorporate all necessary functional species covalently within a single polymer in the backbone or side-chains, have attracted attention because they eliminate the problems of phase separation and crystallization and therefore could lead to a better thermal stability and longer shelf life for potential devices.<sup>11</sup> The first fully functionalized photorefractive polymer was reported in 1992. It consisted of a multifunctional polyurethane upon which charge generator, charge transporter, and NLO moieties were incorporated as side chains.<sup>78</sup> Although the 2BC gain coefficient of this material was only  $2.3 \text{ cm}^{-1}$ , it was encouraging and much progress has been made in the development of high-performance fully functionalized PR polymers.<sup>27,43,79-86</sup> The first fully functionalized PR polymer showing good net gain efficiency was the prepoled conjugated polymer containing Ru photogenerator complexes that was introduced into the polymer backbone, as shown in Fig. 2.4 (a). In this polymer a gain coefficient  $\Gamma = 200 \text{ cm}^{-1}$  was obtained, but the response time was long, on the order of several hundreds of seconds.<sup>28</sup> Soon after, a very good improvement in response time was achieved in

oligothiophenes<sup>87</sup> with covalently attached chromophores and the response time was about 40 ms. Polymethacrylates with attached charge transporting carbazole and NLO moieties (e.g., Fig. 2.4 (b), P6), sensitized with 1% TNFM, exhibited 100% internal diffraction efficiencies.<sup>82</sup>

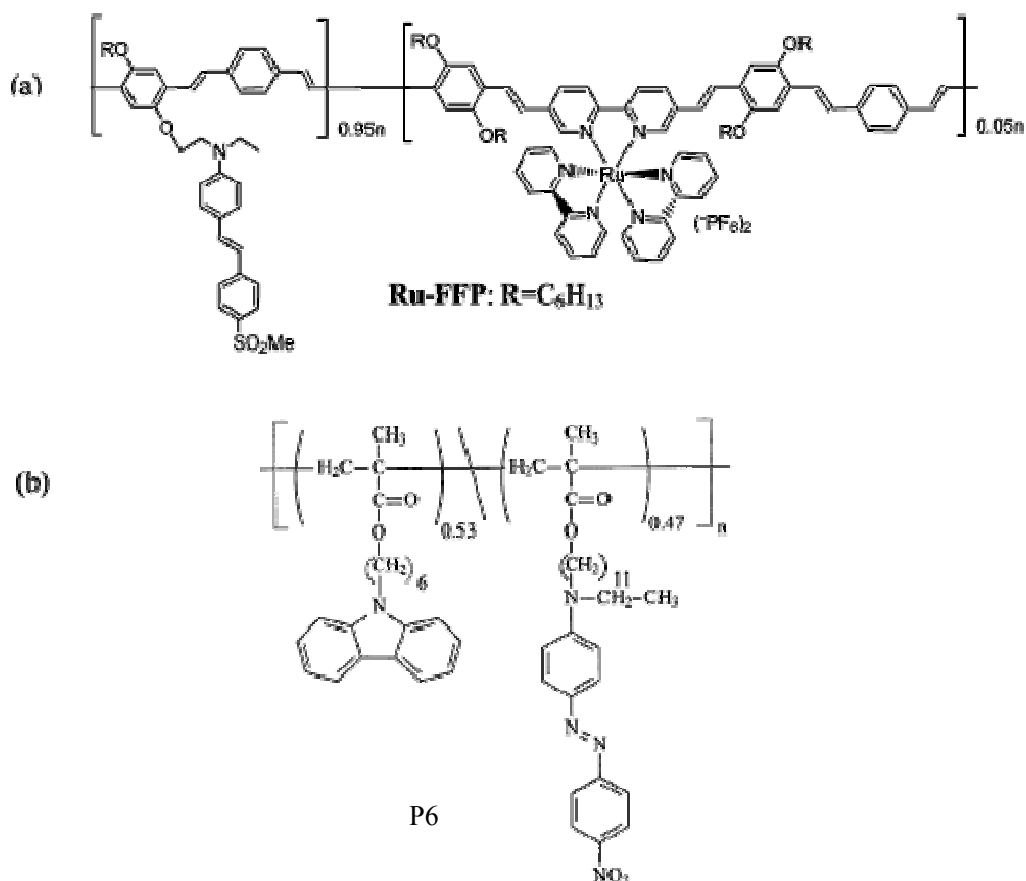


Fig. 2.4. (a) Fully functionalized PR polymer containing ruthenium complex (Ru-FFP). (b) Fully functionalized PR polymethacrylate (P6).

## 2.5 Low $T_g$ and high $T_g$ PR polymers

Based on the glass transition temperature, the PR polymers can also be classified into low  $T_g$  and high  $T_g$  PR polymers.

### 2.5.1 Low $T_g$ PR polymers

Low  $T_g$  PR polymers are the PR polymers which have a glass transition temperature  $T_g$  lower or close to the operating temperature, usually room temperature (RT). Low  $T_g$  PR polymers consists mainly of guest-host type polymers. Because of the

low  $T_g$ , the orientation of the chromophores can be achieved when an electric field is applied without previously heating the polymer. The electric field orientation at RT has important consequences on the properties of such polymers, since the poling field is no longer the external field but the total electric field, namely the superposition<sup>88</sup> of the external field and the internal photogenerated space-charge field, a spatially modulated field. The spatially modulated field will reorient the chromophores and induce a spatially modulated birefringence. This effect is of paramount importance since it can lead to high refractive index modulation. In this case, the refractive index modulation has two contributions: the electro-optic and the birefringence contributions. Moreover, the electro-optic effect is enhanced. Hence, low  $T_g$  polymers usually have very good PR performance. The main problems of low  $T_g$  PR polymers are mechanical and chemical instabilities, which will cause problems such as phase separation and crystallization, as we mentioned for guest-host PR polymers.

### 2.5.2 High $T_g$ PR polymers

High  $T_g$  PR polymers have a glass transition temperature much higher than RT. In this case, in order to obtain macroscopic second-order nonlinear properties, orientational order of the chromophores is induced during the so-called prepoling process, which is needed in order to break the centrosymmetry of the bulk material.<sup>89</sup> In the prepoling process, the polymer sample is first heated above  $T_g$ , then an electric field is applied to induce chromophore reorientation, and finally the polymer is cooled down to RT with the electric field still on. Because of their high  $T_g$ , the polymers are stable at RT. Compared with low  $T_g$  PR polymers, high  $T_g$  PR polymers do not show phase separation or crystallization on long time-scales.<sup>90</sup> However, for the same reason the chromophores cannot move freely at RT, so that no birefringence contribution is present and hence high  $T_g$  polymers usually exhibit lower refractive index modulation and worse PR performance.

## BIBLIOGRAPHY

1. A. Ashkin, G. D. Boyde, J. M. Dziedzic, R. G. Smith, A. A. Ballman, J. J. Levenstein, K. Nassau. *Appl. Phys. Lett.*, **1966**, 9, 72.
2. L. Marín-Gomis, J. Ortiz, F. Fernández-Lázaro, A. Sastre-Santos, B. Elliott, L. Echegoyen. *Tetrahedron*. **2006**, 62, 2102.
3. Sandalphon, B. Kippelen, N. Peyghambarian, S. R. Lyon, A. B. Padias, H. K. Hall, Jr. *Opt. Lett.*, **1994**, 19, 68.
4. S. Ducharme, J. C. Scott, R. J. Twieg, W. E. Moerner. *Phys. Rev. Lett.*, **1991**, 66, 1846.
5. W. E. Moerner, S. M. Silence. *Chem. Rev.*, **1994**, 94, 127.
6. W. E. Moerner, A. Grunnet-Jepsen, C. L. Thomspon. *Ann. Rev. Mater. Sci.*, **1997**, 27, 585.
7. L. M. Wang, Q. Wang, L. P. Yu. *Adv. Mater.*, **2000**, 12, 974.
8. Q. Wang, L. M. Wang, L. P. Yu. *J. Amer. Chem. Soc.*, **1998**, 120, 12860.
9. F. Aslam, D. M. Graham, D. J. Binks, P. Dawson, N. Pickett, P. O'Brien, C. C. Byeon, D. -k. Ko, J. Lee. *J. Appl. Phys.*, **2008**, 103, 093702.
10. F. Aslam, J. Stevenson-Hill, D. J. Binks, S. Daniels, N. L. Pickett, P. O'Brien. *Chem. Phys.*, **2007**, 334, 45.
11. O. Ostroverkhova, W. E. Moerner. *Chem. Rev.*, **2004**, 104, 3267.
12. D. J. Suh, O. O. Park, T. Ahn, Hong-ku Shim. *Opt. Mater.*, **2002**, 21, 365.
13. C. Fuentes-Hernandez, D. J. Suh, S. R. Marder, B. Kippelen. *Proc. SPIE*. **2003**, 5216, 221.
14. D. J. Binks, D. P. West, S. Norager, P. O'Brien. *J. Chem. Phys.*, **2002**, 117, 2425.
15. C. Fuentes-Hernandez, D. J. Suh, B. Kippelen, S. R. Marder. *Appl. Phys. Lett.*, **2004**, 85, 534.
16. F. Aslam, D. J. Binks, M. D. Rahn, D. P. West, P. O'Brien, N. Pickett. *J. Mod. Opt.*, **2005**, 52, 945.
17. J. G. Winiarz, L. Zhang, M. Lal, C. S. Friend, P. N. Prasad. *J. Am. Chem. Soc.*, **1999**, 121, 5287.
18. C. S. Friend, M. Lal, A. Biswas, J. G. Winiarz, L. Zhang, P. N. Prasad. *Proc. SPIE*. **1998**, 3469, 100.
19. E. A. Slivinska, U. Hartwig, K. Buse, K. Meerholz. *Proc. SPIE*. **2004**, 5521, 17.
20. M. Schaerlaekens, C. Engles, A. Hameurlaine, W. Dehaen, A. Persoons. *Proc. SPIE.*, **2003**, 5216, 71.
21. K. R. Chaoudhary, Y. Sahoo, S. Jang, P. N. Prasad. *Adv. Funct. Mater.*, **2005**, 15, 751.
22. K. R. Chaoudhary, Y. Sahoo, P. N. Prasad. *Adv. Mater.*, **2005**, 17, 2877.
23. Y. Yang, J. Huang, Q. Wu, G. Sun, H. Fei, Z. Wei, J. Shen. *Proc. SPIE.*, **1999**, 3740, 384.
24. J. G. Winiarz, L. Zhang, J. Park, P. N. Prasad. *J. Phys. Chem. B*, **2002**, 106, 967.
25. F. Aslam, D. J. Binks, M. D. Rahn, D. P. West, P. O'Brien, N. Pickett, S. Daniels. *J. Chem. Phys.*, **2005**, 122, 184713.
26. F. Aslam, J. Stevenson-Hill, D. J. Binks, S. Daniels, N. L. Pickett, P. O'Brien. *Chem. Phys.*, **2007**, 334, 45.
27. W. You, L. M. Wang, Q. Wang, L. P. Yu. *Macromolecules*. **2002**, 35, 4636.
28. Z. H. Peng, A. R. Gharavi, L. P. Yu. *J. Am. Chem. Soc.*, **1997**, 119, 4622.
29. I. Aiello, D. Dattilo, M. Ghedini, A. Bruno, R. Termine, A. Golemme. *Adv. Mater.*, **2002**, 14, 1233.
30. J. G. Winiarz, L. M. Zhang, M. Lal, C. S. Friend, P. N. Prasad. *J. Am. Chem. Soc.*, **1999**, 121, 5287.



31. J. Winiarz, P. Prasad. *Opt. Lett.*, **2002**, 27, 1330.
32. D. J. Binks, D. P. West, S. Norager, P. O'Brien. *J. Chem. Phys.*, **2002**, 117, 7335.
33. Y. Wang, N. Herron. *Chem. Phys. Lett.*, **1992**, 200, 71.
34. D. J. Suh, O. O. Park, T. Ahn, H. K. Shim. *Opt. Mater.*, **2003**, 21, 365.
35. J. G. Winiarz, L. M. Zhang, M. Lal, C. S. Friend, P. N. Prasad. *Chem. Phys.*, **1999**, 245, 417.
36. D. V. Steenwinckel, E. Hendrickx, A. Persoons. *J. Chem. Phys.*, **2001**, 114, 9557.
37. S. Schlöter, U. Hofmann, P. Strohriegel, H. W. Schmidt, D. Haarer. *J. Opt. Soc. Am. B.* **1998**, 15, 2473.
38. H. Chun, I. K. Moon, D. H. Shin, S. Song, N. Kim. *J. Mater. Chem.*, **2002**, 12, 858.
39. E. Mecher, F. Gallego-Gomez, H. Tillmann, H. H. Horhold, J. C. Hummelen, K. Meerholz. *Nature*, **2002**, 418, 959.
40. D. Wright, M. A. Diaz-Garcia, J. D. Casperson, M. S. DeClue, W. E. Moerner, R. J. Twieg. *Appl. Phys. Lett.*, **1998**, 73, 1490.
41. B. Kippelen, S. R. Marder, E. Hendrickx, J. L. Maldonado, G. Guillemet, B. L. Volodin, D. D. Steele, Y. Enami, Sandalphon, Y. J. Yao, J. F. Wang, H. Rockel, L. Erskine, N. Peyghambarian. *Science*, **1998**, 279, 54.
42. D. Wright, U. Gubler, W. E. Moerner, M. S. DeClue, J. S. Siegel. *J. Phys. Chem. B*, **2003**, 107, 4732.
43. M. S. Bratcher, M. S. DeClue, A. Grunnet-Jepsen, D. Wright, B. R. Smith, W. E. Moerner, J. S. Siegel. *J. Am. Chem. Soc.*, **1998**, 120, 9680.
44. E. Hendrickx, J. Herlocker, J. L. Maldonado, S. R. Marder, B. Kippelen, A. Persoons, N. Peyghambarian. *Appl. Phys. Lett.*, **1998**, 72, 1679.
45. G. Iftime, F. L. Labarthe, A. Natansohn, P. Rochon, K. Murti. *Chem. Mater.*, **2002**, 14, 168.
46. P. M. Borsenberger, D. S. Weiss. *Organic Photoreceptors for Xerography*, Marcel Dekker: New York, **1998**.
47. I. K. Moon, S. Choi, N. Kim. *Polymer*, **2007**, 48, 3461.
48. F. Würthner, R. Wortmann, K. Meerholz. *ChemPhysChem.*, **2002**, 3, 17.
49. M. A. Diaz-Gracia, D. Wright, J. D. Casperson, B. Smith, E. Glazer, W. E. Moerner. *Chem. Mater.*, **1999**, 11, 1784.
50. A. Grunnet-Jepsen, D. Wright, B. Smith, M. S. Bratcher, M. S. DeClue, J. S. Siegel. *Chem. Phys. Lett.*, **1998**, 291, 553.
51. H. J. Bolink, V. V. Krasnikov, P. H. J. Kouwer, G. Hadziioannou. *Chem. Mater.*, **1998**, 10, 3951.
52. S. J. Ziker. *ChemPhysChem.*, **2000**, 1, 72.
53. J. Shi, M. M. Huang, Z. J. Chen, Q. H. Gong, S. K. Cao. *J. Mater. Sci.*, **2004**, 39, 3783.
54. J. V. Grazulevicius, P. Strohriegel, J. Pielichowski, K. Pielichowski. *Prog. Polym. Sci.*, **2003**, 28, 1297.
55. F. Aslam, D. J. Binks, M. D. Rahn, D. P. West, P. O'Brien, N. Pickett. *J. Mod. Opt.*, **2005**, 52, 945.
56. B. Kippelen, F. Meyers, N. Peyghambarian, S. R. Marder. *J. Am. Chem. Soc.*, **1997**, 119, 4559.
57. C. R. Moylan, R. Wortmann, R. J. Twieg, I. H. McComb. *J. Opt. Soc. Am. B*, **1998**, 15, 929.
58. F. Würthner, R. Wortmann, K. Meerholz. *ChemPhysChem.*, **2002**, 3, 17.

59. R. Wortmann, C. Poga, R. J. Twieg, C. Geletneky, C. R. Moylan, P. M. Lundquist, R. G. DeVoe, P. M. Cotts, H. Horn, J. E. Rice, D. M. Burland. *J. Chem. Phys.*, **1996**, 105, 10637.
60. E. Hendrickx, B. L. Volodin, D. D. Steele, J. L. Maldonado, J. F. Wang, B. Kippelen, N. Peyghambarian. *Appl. Phys. Lett.*, **1997**, 71, 1159.
61. K. Meerholz, R. Bittner, Y. DeNardin, C. Brauchle, E. Hendrickx, B. L. Volodin, B. Kippelen, N. Peyghambarian. *Adv. Mater.*, **1997**, 9, 1043.
62. K. Meerholz, Y. De Nardin, R. Bittner, R. Wortmann, F. Wurthner. *Appl. Phys. Lett.*, **1998**, 73, 4.
63. F. Wurthner, C. Yao, T. Debaerdemaeker, R. Wortmann. *J. Am. Chem. Soc.*, **2002**, 124, 9431.
64. M. He, R. Twieg, O. Ostroverkhova, U. Gubler, D. Wright, W. E. Moerner. SPIE Proceedings, SPIE annual meeting, Seattle, WA, **2002**, 4802, 9.
65. A. Goonesekera, S. Ducharme. *J. Appl. Phys.*, **1999**, 85, 6506.
66. D. Van Steenwinckel, E. Hendrickx, A. Persoons, K. Van den Broeck, C. Samyn. *J. Chem. Phys.*, **2000**, 112, 11030.
67. O. Ostroverkhova, K. D. Singer. *J. Appl. Phys.*, **2002**, 92, 1727.
68. E. Hendrickx, B. Kippelen, S. Thayumanavan, S. R. Marder, A. Persoons, N. Peyghambarian. *J. Chem. Phys.*, **2000**, 112, 9557.
69. M. A. Diaz-Garcia, D. Wright, J. D. Casperson, B. Smith, E. Glazer, W. E. Moerner, L. I. Sukhomlinova, R. J. Twieg. *Chem. Mater.*, **1999**, 11, 1784.
70. K. M. Jung, M. J. Cho, Jung-Il Jin, D. H. Choi. *Appl. Phys. Lett.*, **2007**, 90, 181123.
71. M. C. J. M. Donckers, S. M. Silence, C. A. Walsh, F. Hache, D. M. Burland, W. E. Moerner, R. J. Twieg. *Opt. Lett.*, **1993**, 18, 1044.
72. B. Kippelen, Sandalphon, N. Peyghambarian, S. R. Lyon, A. B Padias, H. K. Hall, Jr. *Electronics Lett.*, **1993**, 29, 1873.
73. K. Meerholz, B. Volodin, Sandalphon, B. Kippelen, N. Peyghambarian. *Nature*, **1994**, 371, 497.
74. W. J. Joo, N. J. Kim, H. Chun, I. K. Moon, N. Kim. *Polymer*, **2001**, 42, 9863.
75. O. P. Kwon, S. H. Lee, G. Montemezzani, P. Günter. *Adv. Function. Mater.*, **2003**, 13, 434.
76. L. M. Wang, M. K. Ng, L. P. Yu. *Appl. Phys. Lett.*, **2001**, 78, 700.
77. Q. Wang, L. M. Wang, L. P. Yu. *Macromol. Rapid Commun.*, **2000**, 21, 723.
78. L. P. Yu, W. K. Chan, Z. N. Bao, S. X. F. Cao. *J. Chem. Soc. Chem. Commun.*, **1992**, 1735.
79. L. P. Yu. *J. Polym. Sci. A: Polym. Chem.*, **2001**, 39, 2557.
80. Q. Wang, L. M. Wang, J. J. Yu, L. P. Yu. *Adv. Mater.*, **2000**, 12, 974.
81. D. Van Steenwinckel, C. Engels, E. Gubbelmans, E. Hendrickx, C. Samyn, A. Persoons. *Macromolecules*, **2000**, 33, 4074.
82. C. Engels, D. Van Steenwinckel, E. Hendrickx, M. Schaerlaekens, A. Persoons, C. Samyn. *J. Mater. Chem.*, **2002**, 12, 951.
83. M. K. Ng, L. M. Wang, L. P. Yu. *Chem. Mater.*, **2000**, 12, 2988.
84. S. Schloter, U. Hofmann, K. Hoehstetter, G. Bauml, D. Haarer, K. Ewert, C. D. Eisenbach. *J. Opt. Soc. Am. B*, **1998**, 15, 2560.
85. C. J. Chang, W. T. Whang, K. Y. Hsu. *J. Appl. Polym. Sci.*, **1999**, 74, 1321.
86. Y. W. Chen, Z. J. Chen, Q. H. Gong, M. Schroers. *Mater. Lett.*, **2003**, 57, 2271.
87. W. J. Li, A. Gharavi, Q. Wang, L. P. Yu. *Adv. Mater.*, **1998**, 10, 927.
88. I. K. Moon, C. S. Choi, N. Kim. *J. Photochem. Photobiol. A: Chem.*, **2009**, 202, 57.
89. T. Kolev, B. Stamboliyska, D. Yancheva. *Chem. Phys.*, **2006**, 324, 489.

90. Y. Pan, X. Z. Tang, L. Zhu, Y. W. Huang. *Eur. Polym. J.*, **2007**, 43, 1091.

## Chapter 3

### AZO-POLYMERS:

#### LGHT-INDUCED EFFECTS AND APPLICATIONS

Azo polymers include a -N=N- group within their structure, and can be broadly classified as main-chain or side-chain azo polymers. A wide variety of properties of azo dyes have been studied since their discovery in 1863, and numerous applications have been developed after their initial use as coloring agents<sup>1</sup>, including those based on non-linear optical behaviour, light-induced dichroism and birefringence. The combination of the different properties of azo polymers offers the possibility for multifunctional materials with practical use in electro optics, image recording and more.<sup>1,2</sup> All the properties and applications are based on the photoisomerization of the azo-aromatic moiety.

#### 3.1 Brief history of azobenzene

Since the discovery of the first azo-dye by Martius in 1863,<sup>3</sup> azo and its derivatives were mainly used as dyes, because various colors could be obtained by appropriate substitution on the aromatic rings.<sup>4</sup> In 1957, a polarized light-induced change in a physical property of an azo aromatic compound was first mentioned in the literature.<sup>5</sup> Soon after Neporent et al. found that a viscous solution became dichroic under polarized light, and the photoinduced dichroism could be stable for about one week.<sup>6,7</sup> In their explanation, the photo-absorbing molecules rotated to a preferred direction. Makushenko et al. begun to associate this rotation with the photoinduced isomerization of azobenzene just a few years later.<sup>8,9</sup> Research didn't progress until the first optical application in holography by Todorov, Nikolova, and Tomova in 1983-1984. They used a solid solution of 0.06% methyl orange in poly(vinyl alcohol), in which the photoinduced dichroism and birerfringence was produced by the photoisomerization of azobenzene under polarized laser illumination, orienting the chromophore perpendicularly to the laser polarization.<sup>10</sup> Around 1987, the same phenomenon was observed in liquid crystalline polymers containing azobenzene groups.<sup>11,12</sup> At about the same time, Ichimura proposed the "command surfaces" concept, where a liquid crystalline Langmuir-Blodgett film, acting as "soldiers", aligns with the isomerization of azobenzene, acting as a "commander"

under illumination. From 1991 on, this research field developed rapidly, with hundreds of publications each year and the discovery of many exciting new phenomena, such as the photoinduced orientation in azopolymers,<sup>1,13</sup> the photoalignment in LC polymers,<sup>14,15</sup> photoinduced chirality and switching<sup>2</sup>, surface relief gratings and nonlinear optical effects.<sup>2,13,16,17</sup>

### 3.2 Isomerization of the azo-aromatic group

A chromophore is the part of a molecule which accounts for its absorption of light and its photochemical activity. The absorption of a particular chromophore depends on the type of transition involved in that particular excitation. The promotion of an electron from a  $\pi$ -bonding molecular orbital to a  $\pi$ -antibonding orbital is referred to as a  $\pi,\pi^*$  transition, and the excited state is symbolized as  $(\pi,\pi^*)$ . Promotion of an electron from a nonbonding molecular orbital to a  $\pi$ -antibonding orbital is referred to as an  $n,\pi^*$  transition and symbolized as  $(n,\pi^*)$ . The relative energies of molecular orbitals and the transitions are shown in Fig. 3.1. Because nonbonding molecular orbitals lie at higher energy than bonding ones,  $n,\pi^*$  transitions are of lower energy than the corresponding  $\pi,\pi^*$  transitions. Both  $n,\pi^*$  and  $\pi,\pi^*$  transitions are usually found in the ultraviolet region of the electromagnetic spectrum. It is well-known that the azo aromatic group can exist in two configurations, the trans or “E” form and the cis or “Z” form, as illustrated in Fig. 3.2. Either of the two forms can transfer to the other one by the isomerization process, which is induced by the electronic excitation of an electron from either the highest occupied nonbonding orbital (n) or the highest occupied  $\pi$  orbital to the lowest unoccupied  $\pi$  orbital ( $\pi^*$ ). Generally, the trans form has lower energy and is more stable than the cis form. In the case of azobenzene, the energy difference between the ground state of the trans and cis isomers is about 50 kJ/mol.<sup>18</sup> When exposed to light with wavelength within its absorption band, the stable trans form can be transformed into the cis form, while the reverse can be either a thermal and/or a photochemical process. This phenomenon was first studied with azo dye molecules in solution or dispersed in a variety of polymers.<sup>19</sup>

The mechanism for the trans-cis isomerization has been investigated since the early 1950s.<sup>18</sup> It was first suggested that the isomerization acts via rotation of the -N=N- bond. An alternative mechanism was later proposed, namely that the isomerization acted via the inversion of one or both of the nitrogens through a linear sp-hybridized transition

state with the double bond retained (Fig.3.2). The inversion mechanism was generally accepted to be involved in the thermal isomerization of azo aromatic groups, while both mechanisms are possible in the photochemical isomerization process. The controversy between the rotation and inversion mechanisms is still continuing and further experiments and calculations are being carried out in this area to better understand the mechanism of the isomerization process.<sup>1</sup>

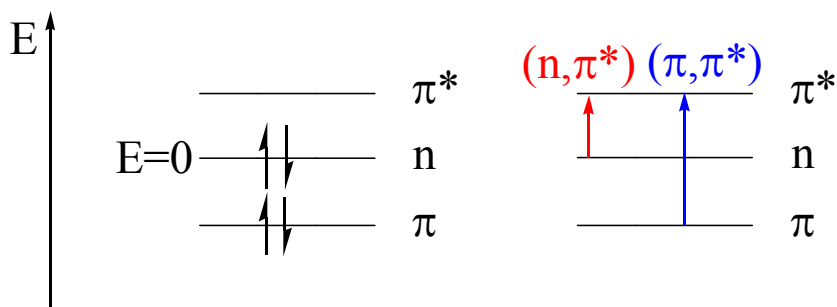


Fig. 3.1. Relative energies of molecular orbitals in azo compounds.

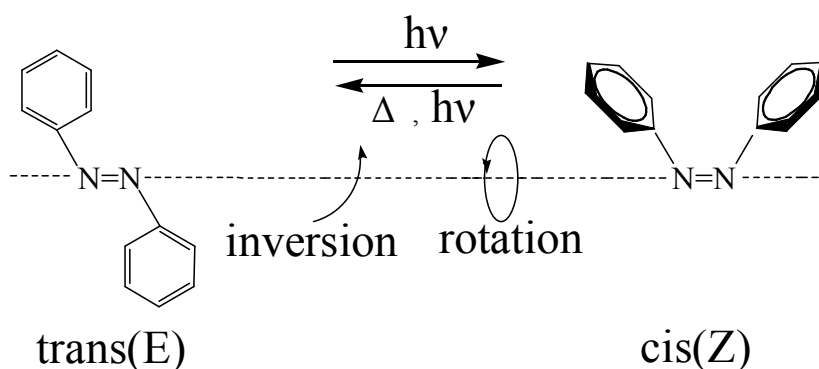


Fig. 3.2. Trans-cis isomerization of azobenzene.

### 3.3 Three classes of azo compounds

Based on the relative energetic order of the  $(n,\pi^*)$  and  $(\pi,\pi^*)$  states, azo compounds can be classified into three classes: the azobenzene type molecules, the aminoazobenzene type molecules, and the pseudo-stilbenes type molecules,<sup>18</sup> as shown in Fig. 3.3. The azobenzene type molecules have a low-intensity  $n-\pi^*$  band in the visible region of the spectrum and a high intensity  $\pi-\pi^*$  band in the UV, hence they can be characterized spectroscopically. For this type of molecule, because of the relatively slow cis-to trans thermal isomerization, it is possible to isolate the cis isomer.

Aminoazobenzene type molecules are characterized spectroscopically according to a close proximity of  $n\text{-}\pi^*$  and  $\pi\text{-}\pi^*$  bands. Pseudo-stilbene type molecules have a long wavelength  $\pi\text{-}\pi^*$  band and the sequence of  $(n,\pi^*)$  and  $(\pi,\pi^*)$  states is reversed on the energy scale, as in stilbene. At room temperature, the aminoazobenzene and pseudo-stilbene type molecules with pull/push substituents can isomerize back very quickly, usually in times of the order of several milliseconds. These differences in the kinetics of cis-to-trans thermal isomerization of different azo groups are very important, and they are critical for the interpretation of the properties and the design of azo polymers.

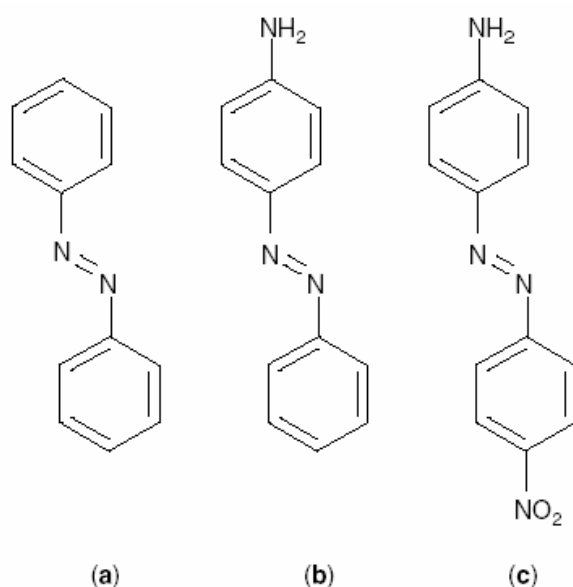


Fig. 3.3. Examples of azomolecules classified as (a) azobenzenes, (b) aminoazobenzenes, and (c) pseudo-stilbenes.

### 3.4 Photo-induced motions in azo-polymers

Because of the photoisomerization, a series of motions of the chromophores will occur in azo-polymers under illumination. Furthermore, nonbound azobenzenes can possibly affect their surrounding environment if they are dissolved in a polymer matrix. Roughly speaking, there are three levels of motions, as illustrated in Fig. 3.4.

The first level is the chromophore motion at the molecular scale. Azobenzenes preferentially absorb light polarized along their transition dipole axis. For trans-azobenzenes, the transition dipole moment is approximately parallel to the molecular long axis; thereby the trans-azobenzenes show angular-dependent absorption of

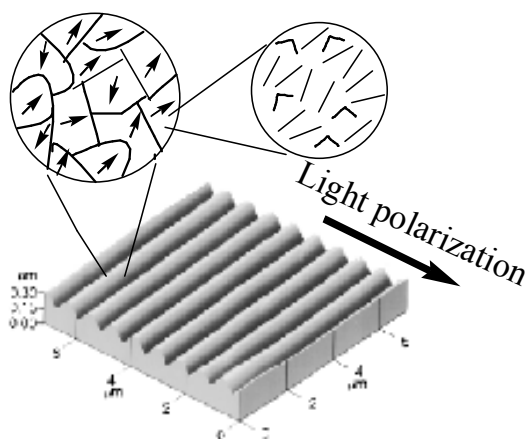


Fig. 3.4 Illustration of the three levels of photo induced motions related to azo isomerization.

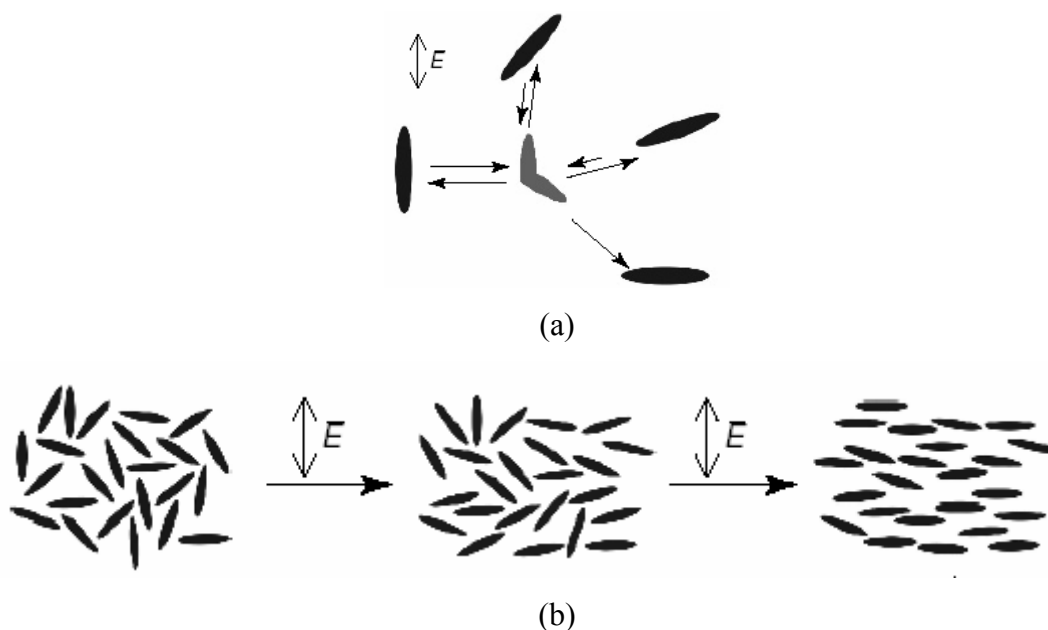


Fig. 3.5. Photoorientation of azobenzene chromophores. (a) The chromophores aligned along the light polarization direction absorb, isomerize, and reorient, while the perpendicularly aligned chromophores cannot absorb and remain fixed. (b) Irradiation of an isotropic samples leads to accumulation of chromophores in the perpendicular direction.

linearly polarized light. The probability of absorption varies as  $\cos^2\phi$ , where  $\phi$  is the angle between the light polarization and the dipole moment. Thus, trans-azobenzene molecules with their transition moments parallel to the polarization direction of linearly polarized



light are activated very effectively to their excited states, followed by trans-cis isomerization, while molecules with their transition moments perpendicular to the polarization direction of light are inactive towards isomerization. For a given initial angular distribution of azobenzene chromophores, many will absorb, convert into the cis form and then revert to the trans form with a new random direction, as shown in Fig. 3.5 (a). Those chromophores that fall perpendicular to the light polarization will no longer isomerize and reorient. After repetition of trans-cis-trans isomerization cycles, there will be a higher population of azobenzene molecules aligned perpendicularly to the light polarization,<sup>20,21</sup> as shown in Fig. 3.5 (b). The reorientation process gives rise to strong birefringence.

The second level of motion occurs roughly at the nanoscale level, and it requires the chromophores to be bound to the polymer matrix or to be involved in a tightly organized structure, such as liquid crystalline, Langmuir-Blodgett or monolayer film. Usually some degree of intrinsic order of the matrix, which can be liquid crystalline, or semicrystalline, is also required. In an ordered structure, the first type of motion will be hindered because of the counteraction of the intrinsic order. However, the driving force to select the direction perpendicular to the light polarization is very strong because of the high quantum yield for photoisomerization, and the whole liquid crystalline or crystalline domains will eventually reorient towards a direction perpendicular to the light polarization. This is a cooperative motion and is very common in ordered materials. Although the order parameter within each domain is not changed, an overall orientation of the whole domain occurs, so that a very strong orientation, much stronger than in amorphous polymers, is created. Compared with the first level motion, the amount of moved material is larger. After illumination, the domain size will probably vary along with the thermal history, but usually it will be still at a nanoscale level.

Finally, the third level of motion, which can be called macroscopic motion, is at an even larger scale. The chromophore is also required to be bound to the polymer, and it drives massive motion of the polymer material by driving forces from pressure gradients created by interfering light and unequal isomerization patterns, or the electric field of the light, depending on which level the mechanism is looked at. This level of motion can produce patterns so big that they have depth and spacing at the micrometer scale on the film surface and are visible with the naked eye. This was an extremely unexpected finding and generated a huge literature after 1995.<sup>2</sup> One important application of this massive

motion is to induce surface relief gratings in azo polymers.

### 3.5 Azo group binding, local free volume and polymer matrix.

Many types of azo-chromophores have been introduced into polymer structures in order to induce some special properties, such as photoinduced birefringence. The azo chromophore can be part of the main chain or in side chains. The spacer length has influence on the photoinduced motion. Usually, the shorter it is, the more restricted is the chromophore motion, making it harder to get photoinduced birefringence. However, this will improve the stability of the photoinduced orientation.<sup>2</sup>

In azo polymers, it is generally recognized that a minimum, critical size of the local free volume in the neighborhood of the chromophore must be satisfied for almost any isomerization. In the case of the inversion mechanism, a free volume of  $0.12 \text{ nm}^3$  is estimated to be necessary for the isomerization of azobenzene in polymers.<sup>22,23</sup> Thus, photochemical and thermal isomerization of the azo dyes with different sizes are valuable in the study of the free volume and of the morphology of polymers.<sup>24,25</sup> The size of the azo dyes, the temperature, and other factors also play important roles for the quantum yield of the trans to cis isomerization. It was also suggested in earlier studies that an additional energy for the rearrangement of the polymer conformations was involved in the isomerization process.<sup>22,26</sup>

The polymer matrix also plays an important role for its power to enable or restrict the motion of the chromophore. For example, binding a tethered azobenzene moiety to a very high Tg polyimide not only allows photoorientation and photoassisted poling at room temperature (which is at least  $190 \text{ }^\circ\text{C}$  below Tg), but also improves much of the photoinduced orientation even at very high temperature, as long as the temperature is below Tg.<sup>27,28</sup> Some other unusual polymer matrices have also been proposed. For example, the synthesis of sol-gel preparation of organic-inorganic hybrid materials is possible by attaching a triethoxysilane group to the chromophore.<sup>29,30</sup> The azo oxides can show photoinduced birefringence and their stability is significantly increased due to the tridimensional structure of the gels.<sup>29</sup> Birefringence can also be induced in nanocomposites of azobenzene and molecular sieves.<sup>31</sup> Another tridimensional structure that can be subjected to photoorientation is purely organic and based on azo-substituted melamine monomers and resins.<sup>32</sup> Cross-linking is also very useful to improve the

stability of the photoinduced orientation.<sup>33</sup>

### 3.6 Experimental methods for the photoorientation investigation

There are many methods to investigate the photoorientation of azo groups. Besides the optical methods which can measure photoinduced birefringence on irradiated spots or diffraction grating efficiency on photoinduced gratings, spectral methods can also provide information on the motion of chromophores. The first and most used method is electronic dichroism (UV-vis spectra and their angular distribution), which can be used to investigate the chromophores distribution and its variations upon irradiation. In addition, there are many other spectroscopic methods which can offer insights into this kind of motion. For example, dielectric relaxation spectroscopy is especially useful for liquid crystalline polymer samples.<sup>34</sup> In chromophores aligned in an electric field, it measures their behavior upon electric field variations. Alternatively, the homeotropic alignment perpendicular to the electrodes used in the dielectric setup can be obtained by light illumination, and the behavior of samples aligned by electric field and light can be compared. These measurements are very valuable, because the frequency and the temperature can be changed. The method has been applied to many materials, such as amorphous azo copolymers<sup>35</sup> and solid solutions of small azo dyes,<sup>36</sup> and to pinpoint cooperative motions in liquid crystalline azo oligomers.<sup>37</sup>

To this date, the most popular and informative spectral method to analyze the photoinduced motion is FTIR.<sup>2</sup> The best procedure is to reduce the intensity of irradiation, thus to slow the photoinduced motion and to follow in situ the changes of the FTIR spectra. It is necessary to perform polarized FTIR analysis, because the absorbance band will change in intensity only for the directions parallel or perpendicular to the polarization of the pump light. A better way to use polarized FTIR is to modulate its polarization. Pézolet et al.<sup>38</sup> have demonstrated the polarization modulation infrared dichroism spectra (PM-IRDC) as a method to monitor in situ the photoinduced motions of the azo chromophores and of a variety of other groups present in the structure of the material. This method can also be used to obtain the order parameter, analyze the kinetic model of changes induced by light, model the overall distribution of the chromophores at the end of each process,<sup>39</sup> and model various matrix-chromophore and chromophore-chromophore interactions.<sup>40</sup>

In addition, Resonance Raman measurements can also provide useful information

on the photoinduced motions,<sup>41</sup> although the most intense area of study was the investigation of macroscopic motion, producing surface relief gratings.

### 3.7 Properties and applications of azopolymers

Polymers containing azo aromatic groups have received tremendous attention because of many special properties. Apart from the good mechanical and thermal properties and low flammability,<sup>41</sup> some other features such as liquid-crystalline properties, nonlinear optical properties, photochromism and optical dichroism are gaining importance and have many potential applications as a consequence of the mentioned three types of photoinduced motions.<sup>2</sup>

#### 3.7.1 Applications based on motions at the molecular level

Considering motions at the molecular level, the most obvious and most mentioned application is in digital optical storage. The phenomenon is reversible and repeatable for tens and even hundreds of thousands of times, especially for amorphous materials. However, the time to write and erase the information is usually of the order of milliseconds, and it is relatively slow. It is better to inscribe as much information as possible at the same time by holographic procedures, thus to decrease the time for a given amount of information. For high T<sub>g</sub> liquid crystalline polymers, where the process occurs only in the amorphous phase, gray levels are possible because of the high photoinduced birefringence.<sup>42</sup> This property has been applied in rewritable optical disk systems.<sup>43</sup> Azo polymers can also be used to make polarization separators<sup>44</sup> by inscribing polarization holograms.<sup>45,46</sup> The device can diffract right circularly polarized light in one direction and left circularly polarized light in the other direction. Not only a single point or a holographic grating, but also a line can be inscribed on an azopolymer film and thus it can act as a waveguide<sup>45</sup> and make it possible to fabricate a whole “photonic printed circuit” on a simple polymer film.<sup>47</sup> In polyurethanes and urethane-urea copolymers, channel waveguides can be obtained by a photobleaching reaction following the photoinduced refractive index change. Apart from the memory application, the holograms obtained by interference of laser beams on azo-doped PMMA have been used for optical processing, such as edge enhancement of various objects, and even moving objects.<sup>48</sup> Azo dyes can also be used to produce high-speed reversible and bistable optical switching in complex

systems based on liquid crystals.<sup>49</sup> Taking advantage of the NLO properties of the azo chromophore, photorefractive properties have been demonstrated by combining the azo chromophore with photoconductive moieties such as carbazole, and this will be discussed later.

### 3.7.2 Applications based on motions at the domain level

#### 1) Photoinduced liquid crystalline phase transitions

As shown in Fig. 3.2, the trans(E) configuration of the azo aromatic group has a rodlike shape and the cis(Z) configuration has a bent shape, which can provide a powerful mesogenic structure (when in the E configuration) and an effective liquid crystalline phase disruptor (when in the Z configuration). Thus, the change in geometry associated with the trans-cis photoisomerization can act as a trigger to either disrupt an ordered phase or to restore or produce an ordered arrangement.<sup>2</sup> In the first reported example a relatively low amount (1%) of azobenzenes was added to liquid crystals to induce the nematic-isotropic transition under illumination, at temperatures just below the normal transition temperature. The liquid crystalline phase can be disrupted by even tiny amounts of azobenzene, due to the shape change from mesogenic (trans) to bent (cis).<sup>50,51</sup> This phenomenon is called light-induced isotropization or isothermal phase transition.

#### 2) Helical structure of macromolecules

In a helical structure, the azobenzene group may affect the supramolecular helical arrangement in many ways, by the photoisomerization effect. The first example was published in 1971,<sup>52</sup> in which the pitch of a cholesteric liquid crystal was changed by photoisomerization of added azobenzene. This process was accompanied by a color change and hence led to a very interesting and useful reversible photochromism. The change in pitch and color can translate into a change in transmittance at a certain wavelength, thus allowing a very elegant and efficient all-optical switch device.<sup>53</sup> Temperature is also very important for the pitch (color) change. For example, in a non-polymer system, it was demonstrated that the color change took place above 87 °C and then was fixed by rapid cooling.<sup>54</sup> The azobenzene moiety can also be used to induce a chirality transfer from the matrix to the aggregated dye by incorporating it into a chiral diblock copolymer.<sup>55</sup> The photoisomerization can also change the helicity of the main chain of helical polypeptides containing azobenzene groups in the side chain.<sup>56</sup> Helical

structures or otherwise organized supramolecular structures are not restricted to polypeptides, and azobenzene has been incorporated into many other polymers to phototrigger the supramolecular organization.

There are also many other application based on motions at the domain level. For example, a) to induce chirality in a structure in which no helical structure was initially present. The proposed mechanism is that the circular momentum transfers from the circularly polarized light to the azobenzene chromophore and was studied deeply by Nikolova et al.<sup>57</sup> The most interesting and intriguing phenomenon is that the left circularly polarized light can induce a left-hand supramolecular helix, and the subsequent irradiation with right circularly polarized light will first destroy the left-hand supramolecular arrangement, and then create a right-hand supramolecular helix.<sup>2</sup> b) to orient liquid crystals by photoisomerization of azo based compounds, considering the intrinsic thermodynamic tendency of liquid crystals to orient along a preferred director. The orientation process is shown in Fig. 3.6.

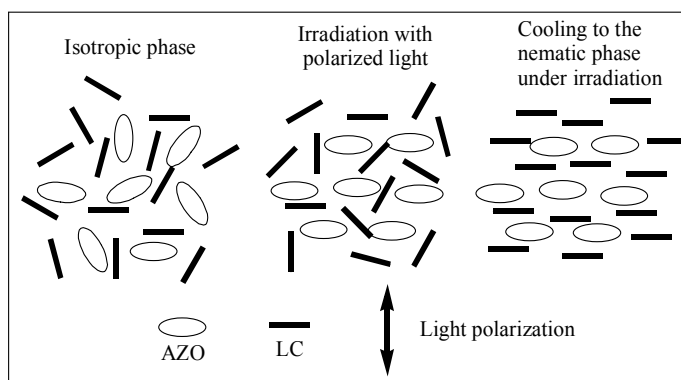


Fig. 3.6. Induction of long-range liquid crystal orientation in the nematic phase due to azo photoisomerization.

### 3.7.3 Applications based on massive macroscopic motions

Surface relief grating (SRG) can be produced on azo polymer films when they are irradiated for a period of time longer than that required for photoinduced orientation. One typical experimental set-up for SRG inscription is shown in Fig. 3.7 and an atomic force microscope surface profile of an optically inscribed SRG is shown in Fig. 3.8. The grating depths depend on the illumination power and light polarization and may approach the scale of hundreds of nanometers.<sup>58</sup> More than one SRG can be induced by consecutive

irradiation with different polarizations, because the inscription of subsequent SRG will not erase the first ones, as shown in Fig. 3.9. It was reported that eight holograms were inscribed on a single spot,<sup>59</sup> but this is obviously not the limit. The SRG inscription on azo polymer is particular because no other photosensitive or photochromic groups would be amenable to such inscription.<sup>2</sup> Besides SRG, different surface deformations can also be created by a variety of single beam irradiation on an azo polymer film surface,<sup>60</sup> as shown in Fig. 3.9. The SRG can be easily erased by heating the azo polymer above  $T_g$ .<sup>28,61</sup>

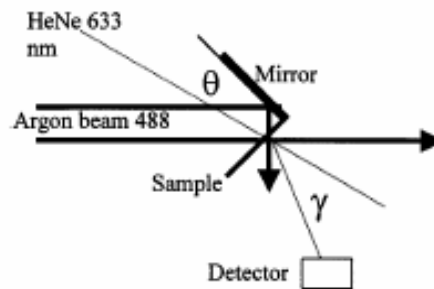


Fig. 3.7. Experimental set-up for SRG inscription.

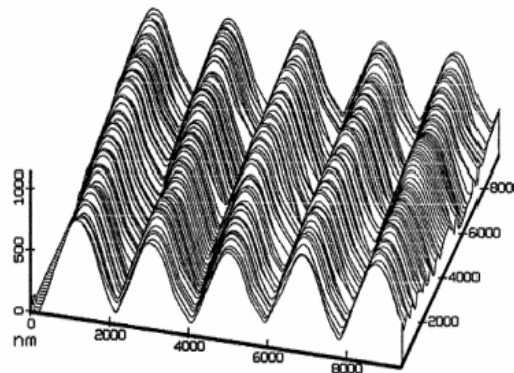


Fig. 3.8. Surface profile of a SRG.

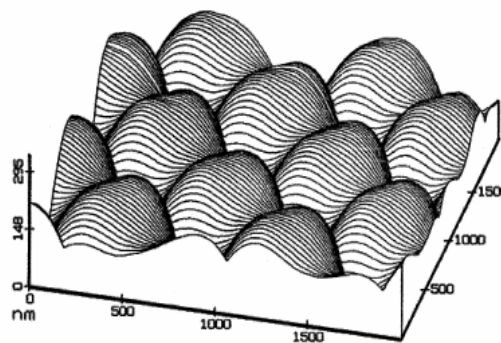


Fig. 3.9. Superposition of SRGs.

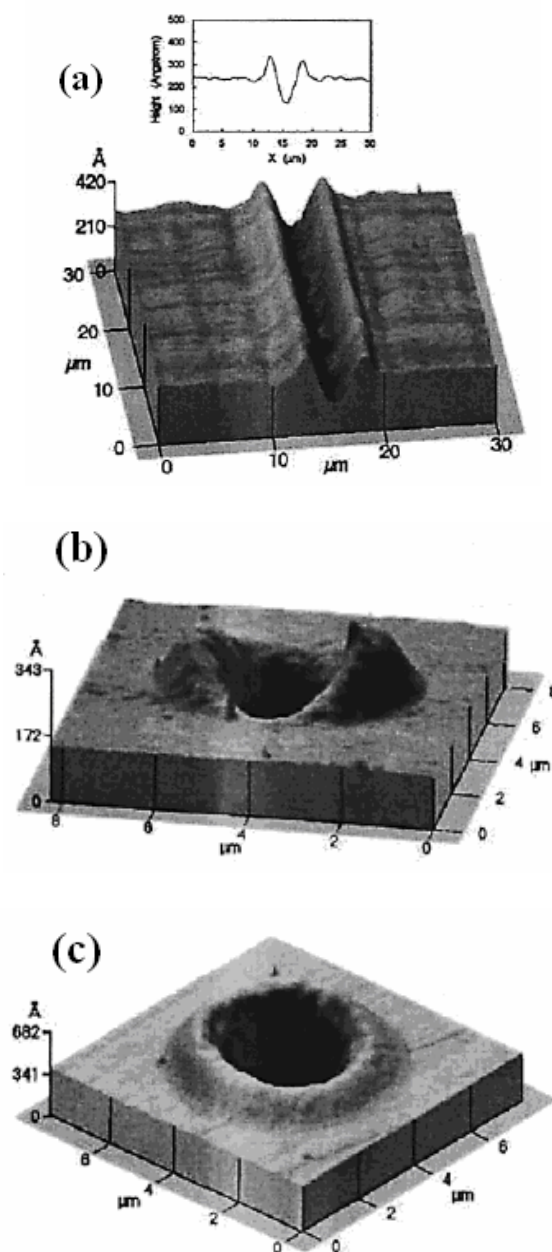


Fig. 3.10. Surface deformations.

There are many applications based on SRG.<sup>2</sup> It has been applied to produce one-step holographic image storage, to couple light into and out of waveguides, to act as orientation layer in a liquid crystal cell and so on.



## BIBLIOGRAPHY

1. S. Xie, A. Natansohn, P. Rochon. *Chem. Mater.*, **1993**, 5, 403.
2. A. Natansohn, P. Rochon. *Chem. Rev.*, **2002**, 102, 4139.
3. J. Griffiths. *Chem. Soc. Rev.*, **1972**, 1, 481.
4. H. Zollinger. *Colour Chemistry. Synthesis, Properties, and Applications of Organic Dyes*, VCH, Weinheim, **1987**.
5. A. Teitel. *Naturwissenschaften*, **1957**, 44, 370.
6. B. S. Neporent, O. V. Stolbova. *Opt. Spectrosc.*, **1961**, 10, 146.
7. B. S. Neporent, O. V. Stolbova. *Opt. Spectrosc.*, **1963**, 14, 331.
8. A. M. Makushenko, B. S. Neporent, O. V. Stolbova. *Opt. Spectrosc.*, **1971**, 31, 295.
9. A. M. Makushenko, B. S. Neporent, O. V. Stolbova. *Opt. Spectrosc.*, **1971**, 31, 397.
10. T. Todorov, L. Nikolova, N. Tomova. *Appl. Opt.*, 1984, 23, 4309.
11. M. Eich, J. Wendorff. *Makromol. Chem.*, **1987**, 8, 467.
12. M. Eich, J. Wendorff, B. Reck, H. Ringsdorf. *Makromol. Chem.*, **1987**, 8, 59.
13. J. A. Delaire, K. Nakatani. *Chem. Rev.*, **2000**, 100, 1817.
14. K. Ichimura. In *Polymers as Electrooptical Components*, V. P. Shibaev (Ed.), Vol. 138, Springer-Verlag, New York, **1996**.
15. K. Ichimura. *Chem. Rev.*, **2000**, 100, 1847.
16. N. K. Viswanathan, D. Y. Kim, S. Bian, J. Williams, W. Liu, L. Li, L. Samuelson, J. Kumar, S. K. Tripathy. *J. Mater. Chem.*, **1999**, 9, 1941.
17. K. G. Yager, C. J. Barrett. *Curr. Opin. Solid State Mater. Sci.*, **2001**, 5, 487.
18. H. Rau. *Photochemistry and Photophysics*, J. F. Rabek, Ed. Vol. II, CRC Press: Boca Raton, FL, **1990**, Vol. 11, Chapter 4.
19. G. Kumar, D. Neckers. *Chem. Rev.*, **1989**, 89, 1915.
20. Y. L. Yu, T. Ikeda. *J. Photochem. Photobiol. C: Photochem. Rev.*, **2004**, 5, 247.
21. Y. Zhao, T. Ikeda. *Smart Light-Responsive Materials: Azobenzene Polymers for Photonic Application*, John Wiley & Sons: New York, USA **2009**.
22. D. Tabak, H. Morawetz. *Macromolecules*, **1970**, 3, 403.
23. T. Naito, K. Horie, I. Mita. *Polym. J.*, **1991**, 23, 809.
24. T. Naito, K. Horie, I. Mita. *Macromolecules*, **1991**, 24, 2907.
25. J. S. Royal, J. G. Victor, J. M. Torkelson. *Macromolecules*, **1992**, 25, 729.
26. C. Paik, H. Morawetz. *Macromolecules*, **1972**, 5, 171.
27. Z. Sekkat, J. Wood, E. F. Aust, W. Knoll, W. Volksen, R. D. Miller. *J. Opt. Soc. Am. B*, **1996**, 13, 1713.
28. D. Y. Kim, L. Li, X. L. Jiang, V. Shivshankar, J. Kumar, S. K. Tripathy. *Macromolecules*, **1995**, 28, 8835.
29. K. Hoffmann, F. Marlow, J. Caro. *Adv. Mater.*, **1997**, 9, 567.
30. A. Stracke, J. H. Wendorff, J. Mahler, G. Rafler. *Macromolecules*, **2000**, 33, 2605.
31. H. Takase, A. Natansohn, P. Rochon. *J. Polym. Sci., Part B: Polym. Phys.*, **2001**, 39, 1686.
32. O. Nuyken. *Encyclopedia of Polymer Science and Engineering*, John Wiley & Sons: New York, **1985**, Vol. 2, p 156.
33. J. Eickmans, T. Bieringer, S. Kostromine, H. Berneth, R. Thoma. *Jpn. J. Appl. Phys.*, **1999**, 38, 1835.
34. S. R. Andrews, G. Williams, L. Lasker, J. Stumpe. *Macromolecules*, **1995**, 28, 8463.
35. A. Fritz, A. Schonhals, B. Sapich, J. Stumpe. *Macromol. Chem. Phys.*, **1999**, 200, 2213.

36. E. Wolarz, D. Kilian, W. Haase, D. Bauman. *J. Polym. Sci.: Part B: Polym. Phys.*, **1999**, 37, 369.
37. N. A. Nikonorova, T. I. Borisova, V. P. Shibaev. *Macromol. Chem. Phys.*, **2000**, 201, 226.
38. T. Buffeteau, M. Pézolet. *Appl. Spectrosc.*, **1996**, 50, 948.
39. T. Buffeteau, M. Pézolet. *Macromolecules*, **1998**, 31, 2631.
40. T. Buffeteau, F. Lagugné Labarthe, M. Pézolet, Sourisseau, C. *Macromolecules*, **1998**, 31, 7312.
41. F. Lagugné Labarthe, C. Sourisseau. *J. Raman Spectrosc.*, **1996**, 27, 491.
42. J. Eickmans, T. Bieringer, S. Kostromine, H. Berneth, R. Thoma. *Jpn. J. Appl. Phys.*, **1999**, 38, 1835.
43. Y. Sabi, M. Yamamoto, H. Watanabe, T. Bieringer, D. Haarer, R. Hagen, S. G. Kostromine, H. Berneth. *Jpn. J. Appl. Phys.*, **2001**, 40, 1613.
44. A. Natansohn, P. Rochon. *Adv. Mater.*, **1999**, 11, 1387.
45. J. J. Couture, R. A. Lessard. *Appl. Opt.*, **1988**, 27, 3368.
46. L. Nikolova, T. Todorov, M. Ivanov, F. Andruzzi, S. Hvilsted, P. Ramanujam. *J. Appl. Opt.*, **1996**, 35, 3835.
47. C. Barrett, A. Natansohn, P. Rochon. *SPIE Proc.*, **1997**, 3006, 441.
48. B. Fleck, D. A. Dowling, L. Wenke. *J. Modern Opt.*, **1996**, 43, 1485.
49. H. Yamane, H. Kikuchi, T. Kajiyama. *Polymer*, **1999**, 40, 4777.
50. T. Ikeda, T. Miyamoto, S. Kurihara, M. Tsukada, S. Tazuke. *Mol. Cryst. Liq. Cryst.*, **1990**, 182 B, 373.
51. S. Kurihara, T. Ikeda, T. Sasaki, H. B. Kim, S. Tazuke. *J. Chem. Soc., Chem. Commun.*, **1990**, 1751.
52. E. Sackmann. *J. Am. Chem. Soc.*, **1971**, 93, 7088.
53. H. K. Lee, K. Doi, H. Harada, O. Tsutsumi, A. Kanazawa, T. Shiono, T. Ikeda. *J. Phys. Chem. B*, **2000**, 104, 7023.
54. N. Tamaoki, S. Song, M. Moriyama, H. Matsuda. *Adv. Mater.*, **2000**, 12, 94.
55. H. Yamane, H. Kikuchi, T. Kajiyama. *Polymer*, **1999**, 40, 4777.
56. T. Ikeda, T. Miyamoto, S. Kurihara, M. Tsukada, S. Tazuke. *Mol. Cryst. Liq. Cryst.*, **1990**, 182 B, 373.
57. L. Nikolova, L. Nedelchev, T. Todorov, Tz. Petrova, N. Tomova, V. Dragostinova, P. S. Ramanujam, S. Hvilsted. *Appl. Phys. Lett.*, **2000**, 77, 657.
58. T. M. Geue, M. G. Saphiannikova, O. Henneberg, U. Pietsch, P. L. Rochon, A. L. Natansohn. *Physical Review E*, **2002**, 65, 052801.
59. A. Natansohn, P. Rochon. In *ACS Symposium Series: Photonic and Optoelectronic Polymers*, K. J. W. Samson A. Jenekhe, Ed., American Chemical Society: Washington, DC, **1997**, Vol. 672, p 236.
60. S. Bian, L. Li, J. Kumar, D. Y. Kim, J. Williams, S. K. Tripathy. *Appl. Phys. Lett.*, **1998**, 73, 1817.
61. D. Y. Kim, S. K. Tripathy, L. Li, J. Kumar. *Appl. Phys. Lett.*, **1995**, 66, 1166.

## Chapter 4

### MEASUREMENT TECHNIQUES

In this chapter we will deal with the experimental techniques necessary to characterize photoconductivity, charge mobility and PR properties in organics. First, the measurement of photoconductivity and charge carrier mobility are introduced. Then a description of standard Two-Beam coupling (2BC) and Four-Wave-Mixing (FWM) methods, which are the basic techniques often used to detect the PR behavior and measure the amplitude of a light-induced refractive index modulation, will be given. As previously mentioned, several phenomena contribute to photorefractivity, such as charge generation, carrier mobility and electro-optic response. Although the presence of all these necessary elements is no guarantee for the observation of the PR effect, it is important to study the contribution of each mechanism to the overall PR performance to determine limiting factors and optimize the behavior.

#### 4.1 Sample preparation

To apply electric field while at the same time allowing light to pass through the samples, polymers are usually sandwiched between two transparent indium-tin oxide (ITO)-coated glasses. First, the proper amount of polymer is put on a piece of ITO glass with the ITO side on top. Some glass spacers are also placed on the corners of the glass. The glass with the polymer is then heated on a hot plate to a temperature above the  $T_g$  of the polymer until it is soft enough. Another piece of ITO glass with the ITO underneath is then squeezed on the polymers to obtain a thin film, and then the sample is cooled down quickly to room temperature. The thicknesses of the polymers is controlled by the spacers and can be measured by interferometry.

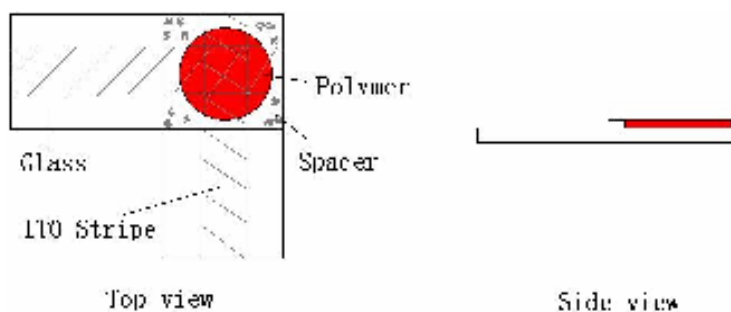


Fig. 4.1. Sample preparation.

The top view and side view of the sample are shown in Fig. 4.1. Sandwiched samples of polymers are not always so easy to prepare because the  $T_g$  and the decomposition temperature ( $T_d$ ) of some polymers can be close to each other and polymers may never become soft enough before they decompose on the hot plate. In these cases, a plasticizer, such as DPP (diphenyl phthalate, Table 2.1), is added to the polymer by dissolving both in a solvent with low boiling point, such as chloroform. The solution is then heated at 50 °C and stirred for 30 minutes. After dropping the solution on a piece of ITO glass on a hot plate at 100 °C to evaporate the chloroform, the resulting blend is processed according to the method described above. The  $T_g$ s of polymers and blends were determined by a Pyris DSC (Perkin-Elmer) at a 10 °C min<sup>-1</sup> heating rate, under a nitrogen flow.

## 4.2 Absorption coefficient measurement

The absorption coefficient  $\alpha$  describes the extent to which the intensity of a light beam is reduced as it passes through a specific material without scattering and reflection. Absorption is important for the photogeneration of the space-charge carriers. The higher it is, the more carriers in a unit time can be produced, which means that a higher PR grating formation speed can be obtained. The absorption coefficient of a material can be measured using the Lambert-Beer law, which states that there is a logarithmic dependence between the transmission of light through a substance and the product of absorption coefficient and the distance the light travels through the material.

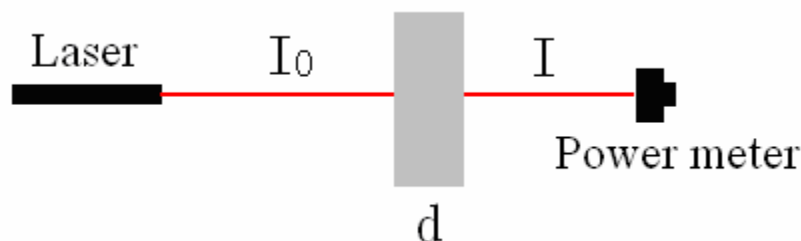


Fig. 4.2. Set-up for  $\alpha$  measurement.

As shown in Fig. 4.2, a light beam with power  $I_0$  passes perpendicularly through a material with thickness  $d$ , and the transmission beam power decreases to  $I$ . Neglecting scattering and reflections, the absorption coefficient of the material can be calculated by

$$\alpha = \frac{1}{d} \ln \frac{I_0}{I} \quad (4.1)$$

### 4.3 Photoconductivity

Photoconductivity  $\sigma_{\text{photo}}$ , a necessary requirement for the observation of the PR effect, refers to the difference of electrical conductivity of a material with and without illumination. Measurements of photoconductivity consist of Current-Voltage measurements conducted under dark and under illumination. A typical set-up for photoconductivity measurements is shown in Fig. 4.3.

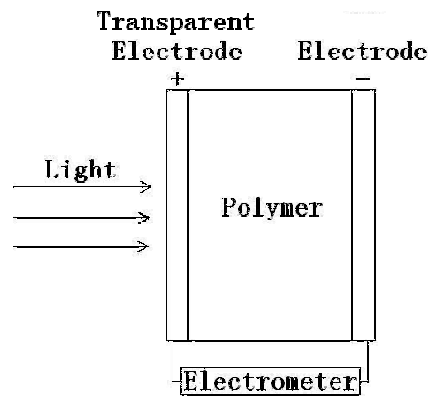


Fig. 4.3. Schematic illustration of photoconductivity measurement set-up.

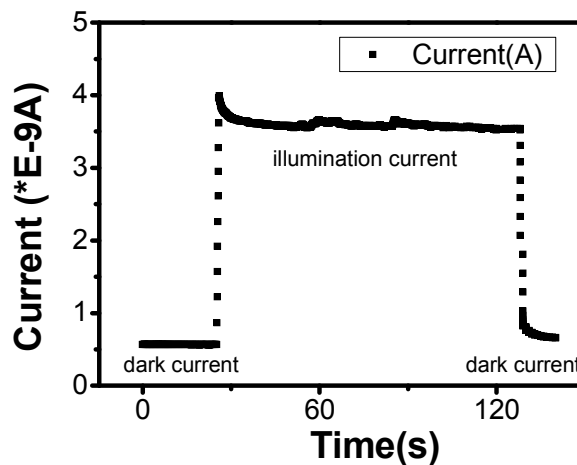


Fig. 4.4. A typical current under dark and illumination during photoconductivity measurement.

At the beginning of the measurement, an electric field supplied by the

electrometer is applied on the polymer sample. The dark current is also measured by the electrometer, which can measure very weak current. When the dark current is constant, the light is turned on and the current under illumination is continuously recorded until it is constant. For a photoconducting material, there will be photogenerated charges and hence the current will increase under illumination. A typical current during the photoconductivity measurement is shown in Fig. 4.4.

When the light is incident perpendicularly on the sample, photoconductivity can be expressed as:

$$\sigma_{photo} = \frac{Id}{VS} \quad (4.2)$$

where  $I$  is the current difference with and without illumination,  $V$  is the voltage,  $d$  is the sample thickness.  $S$  is the area of the sample where the voltage is applied if such area is completely illuminated, otherwise  $S$  is the illumination area. Since photogeneration efficiency depends on light intensity  $I$ , the results are often expressed in terms of the  $\sigma_{photo}/I$  ratio. A typical  $\sigma_{photo}$ - $V$  curve is shown in Fig. 4.5.

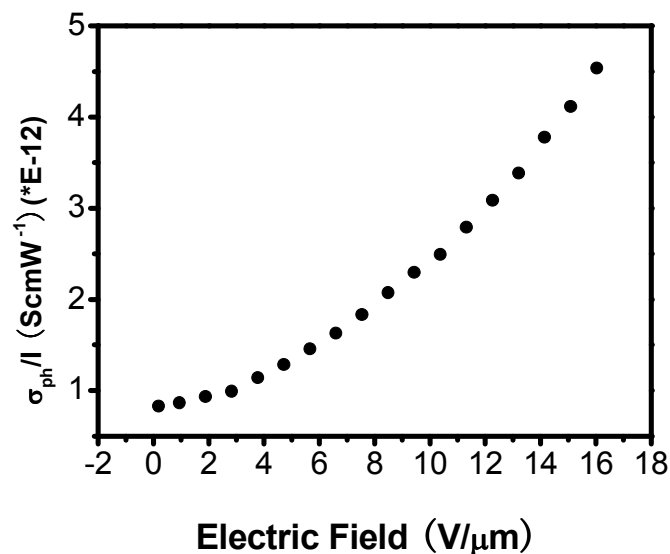


Fig. 4.5. Typical  $\sigma_{photo}$ - $V$  curve.

Illumination wavelength and electric field are important factors determining the continuous wave (cw) photoconductivity of a material. A higher number of charges can be photogenerated at wavelengths where absorption is higher and this will induce a higher current under illumination. The electric field dependence of the cw photocurrent ( $I_{cw}$ ) can

be characterized by a power-law function  $I_{\text{cw}} \propto E^{\alpha_{\text{cw}}}$ , with  $\alpha_{\text{cw}}$  varying between 1.8 and 3.2 in organic films.<sup>1</sup>

#### 4.4 Charge carrier mobility

The response time of an optoelectronic device depends on how fast the charge carriers move in a given electric field.<sup>2</sup> In the best cases, the room temperature mobility of crystalline organic semiconductors can reach the 0.1-20  $\text{cm}^2/\text{Vs}$  range.<sup>3-5</sup> In amorphous materials, the mobility generally drops well below 0.1  $\text{cm}^2/\text{Vs}$ .<sup>6,7</sup> For totally disordered polymer films, charge mobilities are low, in the  $10^{-6}$ - $10^{-3}$   $\text{cm}^2/\text{Vs}$  range. Mobilities significantly increase when the polymer chains present self-assembling properties that can be exploited to generate ordered structures.<sup>8</sup> High mobilities can also be achieved via introduction of a liquid crystal character.<sup>9,10</sup>

The charge carrier mobility  $\mu$  is defined as the ratio between carrier velocity  $\vec{v}$  and applied electric field  $\vec{E}$ , and can be measured by using several different techniques.<sup>11-25</sup> Here we will focus on Time-of-Flight (TOF)<sup>11-14</sup> and Space Charge Limited Current (SCLC)<sup>15,16</sup> experiments.

##### 4.4.1 Time-of-flight

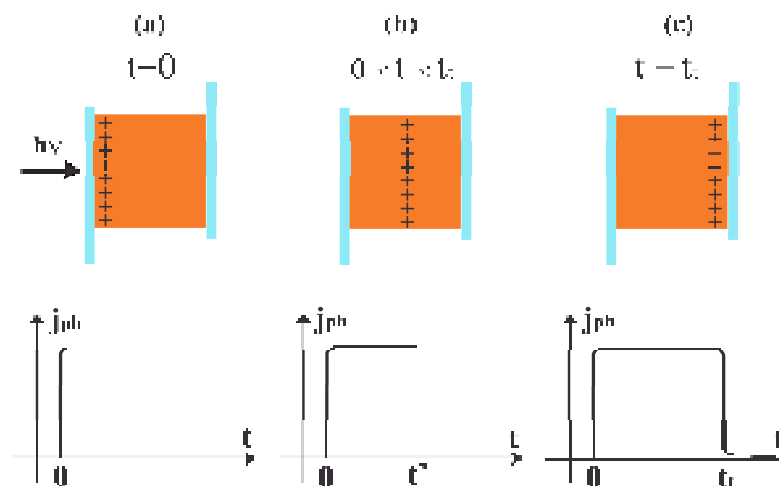


Fig. 4.6. Transient current formation dynamics.

TOF is the most common technique used in order to measure charge mobility in

thick photoconducting samples such as PR polymers. The principle of TOF can be explained with the help of Fig. 4.6. The material is sandwiched between a transparent electrode (typically ITO) and another electrode. A short laser pulse is transmitted through the ITO electrode and is strongly absorbed by the material, and then a sheet of charges is photogenerated (Fig. 4.6 (a)) (or injected in the sample): a rapid increase of the transient current is observed. Then charges move towards the other electrode under the influence of the applied electric field, giving a constant transient current (Fig. 4.6 (b)) until the charges reach the opposite electrode and, at  $t = t_t$ , the current decays ( Fig. 4.6 (c)). The drift mobility  $\mu$  can be expressed as

$$\mu = \frac{d}{t_t E} \quad (4.3)$$

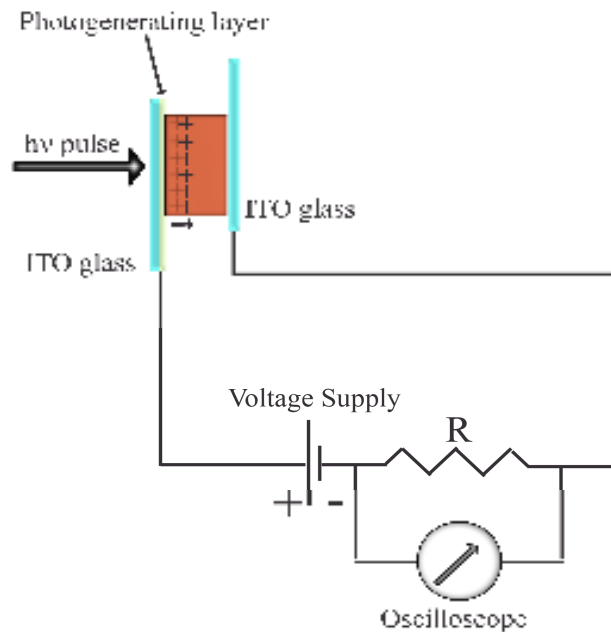


Fig. 4.7. Experimental setup for TOF.

The experimental set-up for TOF experiments is shown in Fig. 4.7 in the case of hole mobility measurements (to determine electrons mobility it is necessary to invert field polarity). The electrodes are connected to a voltage supply and a resistor  $R$ , with a much lower resistance than the internal resistance of the sample, is placed in series with the sample. By photo-excitation of the film on the side of the first electrode by a pulsed laser, a sheet of holes is generated in the material. If the photogeneration process is not efficient enough, a thin layer of a photosensitizer can be deposited between the conducting



material and the electrode. In this case charges photogenerated in the photosensitive layer are injected in the material, where they are transported to the electrode with opposite polarity. The condition  $RC \ll t_t$  ( $C$  = total capacity across the circuit) must be satisfied and to prevent broad edges of the signal, the sheet of charge carriers has to be kept very narrow by using light pulses which are short compared with  $t_t$ , and by keeping the absorption depth of the excitation small compared to the thickness  $d$  of the sample. The behaviour depicted in Fig. 4.6 is typical for a trap free material. However, not many materials show this ideal case of a transient photocurrent and the signal shown in Fig. 4.8 is often observed. This result is due to the presence of deep traps in the material which cause a spread in the charge carriers sheet because they hold several carriers while they travel from one electrode to the other. These transient currents have to be examined in double logarithmic current versus time plots.

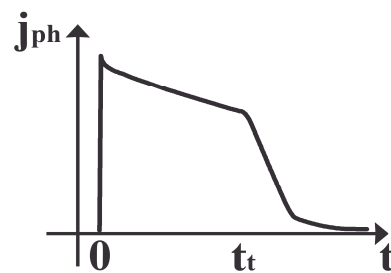


Fig. 4.8. Current transient shape in deep traps experimental conditions

The transient time is then determined by the intersection between two straight lines with different slopes at short and long times of the transient photocurrent (Fig. 4.9).

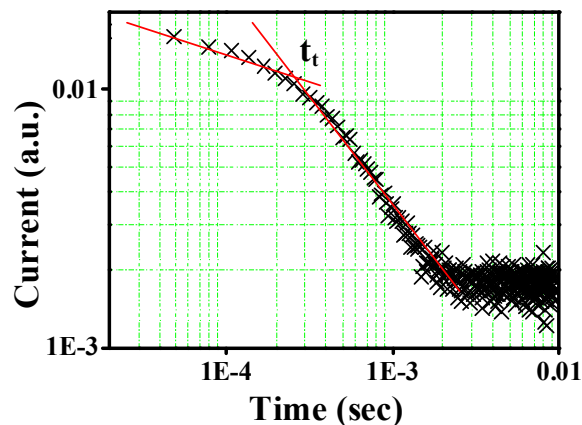


Fig. 4.9. Log-log plot in dispersive transient current.

Typical values for charge mobility in amorphous photoconductors are in the range of  $10^{-3} \text{ cm}^2/\text{Vs}$  for holes and  $10^{-4} \text{ cm}^2/\text{Vs}$  for electrons. The smaller values observed for electron mobility are often correlated with the trapping effects induced by molecular oxygen in these materials.<sup>26</sup>

#### 4.4.2 Space charge limited current

The Space Charge Limited Current (SCLC) model considers a perfectly insulating and completely trap-free material with a negligible concentration of thermally generated charge carriers. It assumes the following:

1. There is only one type of charge carrier present.
2. The material has no intrinsic conductivity, but charges are injected into it from one electrode and captured by the other.
3. The carrier mobility  $\mu$  and the dielectric permittivity  $\epsilon$  are constant throughout the sample.
4. The electric field at the charge-injecting electrode is zero.

In this case the steady-state space-charge limited current  $I$  can be expressed as

$$\frac{I}{S} = \frac{9}{8} \epsilon \epsilon_0 \mu \frac{V^2}{d^3} \quad (4.4)$$

Where  $S$  is the area of the overlap zone between the positive and negative electrodes,  $\epsilon_0 = 8.85 \text{ E-12}$  is the vacuum permittivity,  $\epsilon$  is the relative dielectric constant of the material,  $\mu$  is the drift mobility and  $d$  is the sample thickness. To obtain a trap free regime, where Eq. (4.4) is valid, it is not necessary to have a perfect insulator, since for some values of applied voltage all existing traps can be filled and the current density is described by Eq. (4.4). In order to perform mobility measurement it is enough to implement a I-V measurement, analyze the resulting curve and find a region where the behaviour is quadratic.

A typical I-V curve is illustrated in Fig. 4.10. Part (1) is described by an ohmic regime, and the linear dependence of current on voltage can be described as:

$$\frac{I}{S} = n_{fb} e \mu \frac{V}{d} \quad (4.5)$$

where  $n_{fb}$  is charge density.

Part (2) corresponds to the Mott-Gurney SCLC regime and the quadratic dependence of current on voltage can be described by Eq. (4.4). At the threshold voltage ( $V_T$ ), the slope changes from linear to quadratic, and  $V_T$  is expressed as:

$$V_T = \frac{8}{9} en_b \frac{d^2}{\epsilon \epsilon_0} \quad (4.6)$$

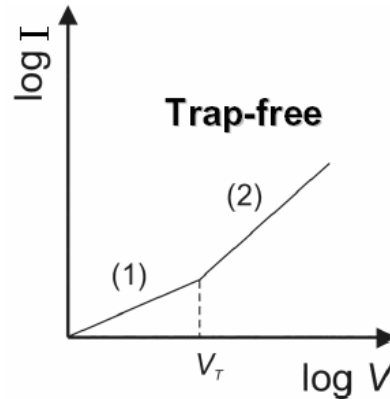


Fig. 4.10. Typical SCLC I-V curve.

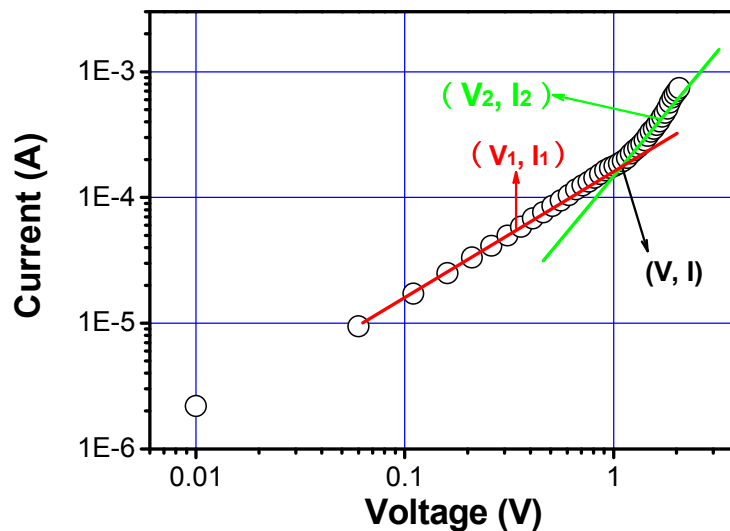


Fig. 4.11. A typical experimental SCLC I-V curve.

A typical experimental log-log I-V curve (open circles) is shown in Fig. 4.11. The linear red straight line and quadratic green straight line are the best fits to the two parts of the I-V curve with different slopes. Point ( $V, I$ ) is the intersection of the two lines.

There are several important steps to check if the I-V curve is believable to obtain mobility value according to Eq. (4.4). First, one point ( $V_2, I_2$ ) on the green line is selected

to calculate the mobility value according to Eq. (4.4), and it can be denoted as  $\mu^*$ . Second, another point ( $V_1, I_1$ ) on the red line is also selected, and then ( $V_1, I_1$ ) and  $\mu^*$  are substituted into Eq. (4.5) to obtain charge density  $n_b$ . Then  $V_T$  can be obtained according to Eq.(4.6).  $\mu^*$  can be trusted as the true mobility value once the difference between  $V_T$  and  $V$  is neglectable.

In experiments, we have to consider the properties of the contact between the material and the injecting electrode: in order to obtain realistic mobility measurements, the material and not the injection must control current flows. In other words, an ohmic contact is necessary, in which the work function of the electrode matches the highest occupied molecular orbital (HOMO) / lowest unoccupied molecular orbital (LUMO) level of the conducting material that is used for hole /electron conduction. An ohmic contact allows carriers to flow in and out of the materials and an ideal ohmic contact must have no effect on device performance, i.e., it must be capable of delivering the required current with no voltage drop between the electrode and materials. In real life, an ohmic contact must have a contact resistance that is as small as possible, to make it negligible in comparison to the bulk resistance of the material. To do this, the difference between the HOMO (LUMO) level and the work function of electrode should be less than 0.3 eV. If this condition is not met, mobility may be underestimated by several orders of magnitude. The work functions of some elements are shown in Table 4.1.

**Table 4.1. Work functions of some elements.**

Element	eV	Element	eV	Element	eV	Element	eV
<u>Ag</u> :	4.52-4.74	<u>Al</u> :	4.06-4.26	<u>Ca</u> :	2.87	<u>Au</u> :	5.1

To measure hole mobility of a polymer, a positive electrode with a work function close the HOMO level of the polymer should be used. Meanwhile, electrons shouldn't be injected from the negative electrode. Hole mobility measurement of a polymer containing carbazole group is shown in Fig. 4.12. The energies of HOMO and LUMO are 5.3 eV and 3.4 eV, respectively. Hence Au can be used as an anode to inject holes into the polymer, while ITO (work function = 4.6 eV) can work as a cathode. Because of the big gap

between the LUMO level of the polymer and the work function of ITO, electrons can't be injected into the polymer. In this way, holes are the only carriers during the measurement.

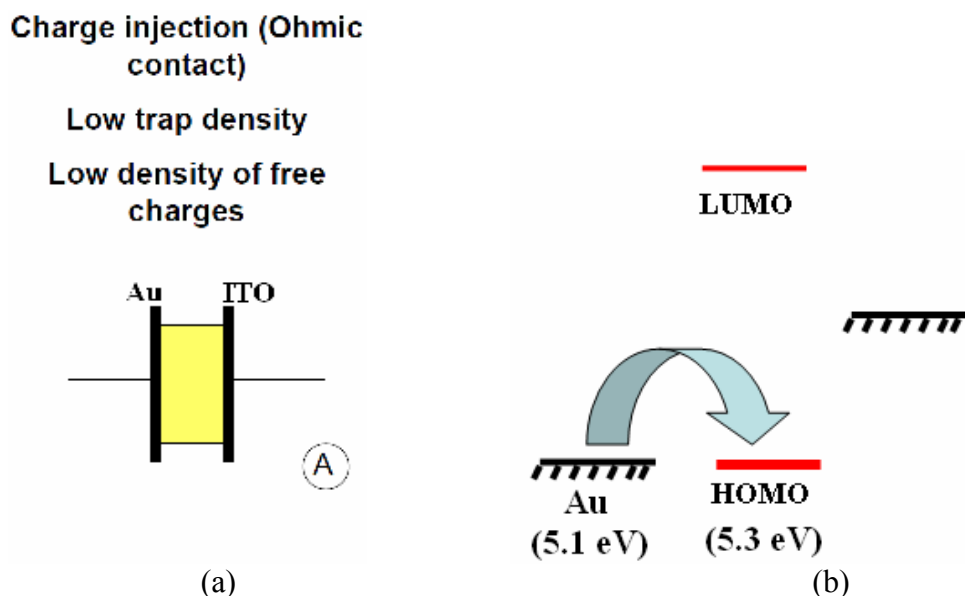


Fig. 4.12. Hole injection in the hole mobility measurement experiment.

The holes transfer can be schematically described as shown in Fig. 2.1. Because of the ohmic contact between Au and the polymer, as shown in step S1, holes will be injected from Au (anode) as shown in step S1. Then the holes will drift within the polymer bulk towards the ITO electrode under the influence of the electric field, as shown in step S2 and S3. Finally, holes will reach the interface between polymer and ITO, and a similar I-V curve as shown in Fig. 4.11 will be obtained. When the electric field is reversed (Au cathode and ITO anode), the contact is not ohmic anymore and neither holes nor electrons can be injected. Hence, a much weaker current will be seen, and the quadratic behaviour will not be observed.

There are several steps to prepare samples for the measurement. (1) Polymers are dissolved in a solvent such as Tetrahydrofuran (THF). (2) The solution is spin-coated on a piece of clean ITO glass to obtain a thin layer of the polymer with a thickness at the range of hundreds of nanometers. Then the sample is put into a vacuum oven, and it is heated for a time long enough to remove residual solvent. (3) A thin layer of metal with a thickness of hundreds of nanometers is deposited on the polymer sample by vacuum evaporation, and the shape of the metal can be controlled using a mask. (4) The thickness of the metal and polymer can be measured using profilometer later. A typical sample with

5 ITO stripes and 4 Au stripes is shown in Fig. 4.13.

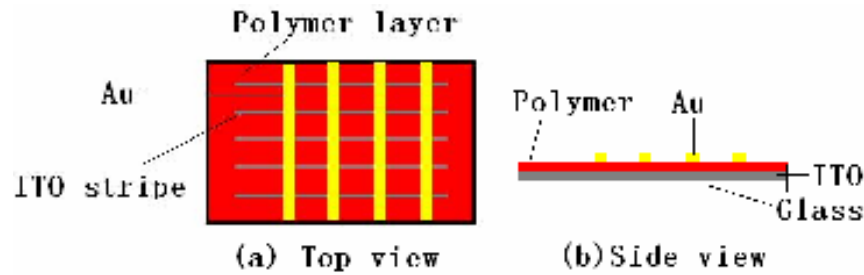


Fig. 4.13. Top and side view of the sample.

#### 4.5 Two-beam coupling

Two-beam coupling (2BC) is one crucial experiment to characterize the PR properties of materials.<sup>27</sup> In this experiment, a uni-directional transfer of energy allows a weak signal to grow exponentially with distance at the expense of the pump beam.<sup>28,29</sup> For inorganic crystals, the exponential gain coefficient is generally in the range of 10 to 100  $\text{cm}^{-1}$ , with the highest observed in  $\text{LiNbO}_3:\text{Fe},\text{Tb}$ .<sup>30</sup> In organic materials, the largest gain coefficient reported for photorefractive materials is 3700  $\text{cm}^{-1}$  as measured in a photorefractive polymer.<sup>31,32</sup>

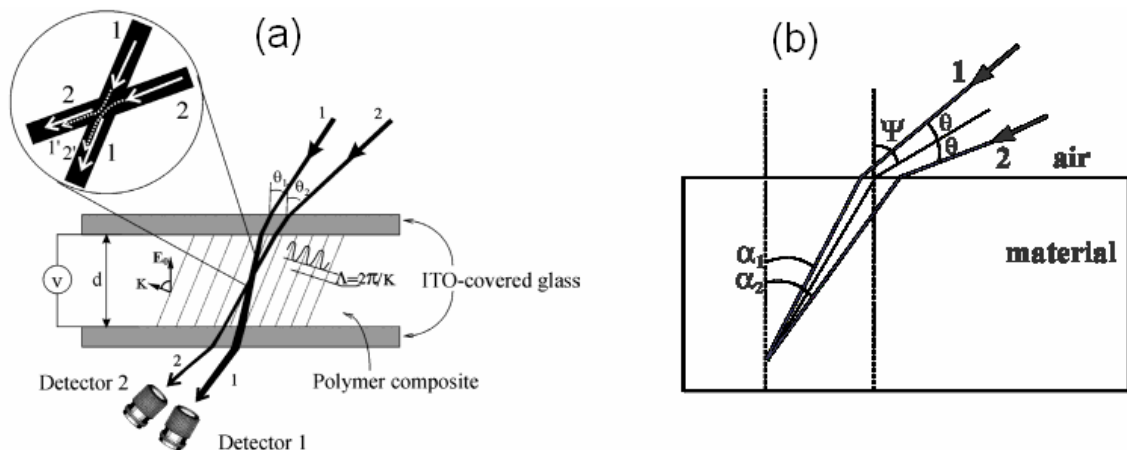


Fig. 4.14. 2BC experiment set-up.

In the PR effect, as mentioned above, an applied electric field plays an important role in both the photogeneration and the charge transport processes. Moreover, the electric field is also essential for the poling and consequently for the electro-optic properties of the polymer film. A convenient way to apply an electric field is to sandwich the

photorefractive polymers between two transparent electrodes such as ITO (indium tin oxide)-coated glass slides, with the thickness of the sample controlled by glass spacers. The electric field is then applied in the direction perpendicular to the polymer film as shown in Fig. 4.14 (a). Optical beams 1 and 2 with the same wavelength and polarization are incident at angles  $\theta_1$  and  $\theta_2$ , respectively, on the same side of the sample normal, and interfere in the PR material. In this way a sinusoidal light intensity modulation is obtained. The period ( $\Lambda$ ) of the light pattern depends on the geometry as shown in Fig. 4.14 (b) and can be calculated according to the equation (4.7):

$$\Lambda = \frac{\lambda}{2n \sin[(\alpha_2 - \alpha_1)/2]} \quad (4.7)$$

where  $n$  is the refractive index of the material and  $\lambda$  is the wavelength of the light, while  $\alpha_1$  and  $\alpha_2$  are the angles between the interfering beams and the sample normal inside the material. The connection among angles inside and outside the photorefractive sample is provided by the following equations:

$$\begin{aligned} \alpha_1 &= \arcsin\left[ \frac{\sin(\Psi - \theta)}{n} \right] \\ \alpha_2 &= \arcsin\left[ \frac{\sin(\Psi + \theta)}{n} \right] \end{aligned} \quad (4.8)$$

where  $\Psi$  is the tilt angle between the sample normal and the beams bisector outside the sample and  $\theta$  is half of the angle between the two light beams outside of the sample.

An important factor to take into account in 2BC is the diffraction regime of the resulting grating. Depending on experimental conditions, it is possible to be in two different regimes of diffraction: the thin grating regime, also called Raman-Nath regime, or the volume grating regime, also called Bragg regime. In order to identify the diffraction regime, it is useful to evaluate the parameter  $Q$ <sup>33</sup>:

$$Q = \frac{2\pi d \lambda}{\Lambda^2 n} \quad (4.9)$$

where  $\lambda$  is the light wavelength,  $d$  is the thickness of the sample,  $\Lambda$  is the grating spacing and  $n$  is the refractive index of the material. If  $Q \ll 1$  the grating is considered thin, while for  $Q \gg 1$  it is a volume grating. Experimentally, the difference between the two diffraction regimes is evident: in volume gratings only one order of diffraction is observed, while in thin gratings several diffraction orders may be obtained.

In the Bragg regime, if the material is photorefractive, the refractive index will be

sinusoidally modulated and there will be a phase shift between the refractive index modulation and the light pattern, creating a nonlocal ( $\Theta \neq 0$ ) diffraction grating (The electric field in Fig. 4.14 (a) supplies a component along the grating vector  $\vec{K}$  and assists the charge transport). Then, the same beams 1 and 2 are partially diffracted by the grating they have just created (beams 1' and 2' in the inset of Fig. 4.14 (a)). Because of the nonlocality of the grating,<sup>34</sup> one diffracted beam (for example, 1') interferes destructively with its companion beam 2, while the other diffracted beam 2' interferes constructively with beam 1. As a result, beam 1 is amplified (energy gain) while beam 2 is attenuated (energy loss). Usually the transmitted beam intensities are measured as a function of time and one typical energy exchange in 2BC experiment is shown in Fig. 4.15. In the Raman-Nath regime, there are many diffraction orders and the energy exchange may be attributed to couplings involving diffracted beams rather than to a phase shift. For this reason, in order to attribute the asymmetric energy exchange to a PR behaviour, 2BC experiments should be carried out in the Bragg regime.

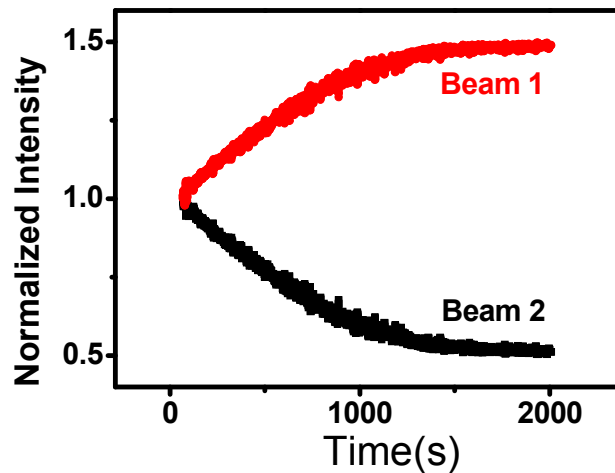


Fig. 4.15. Energy exchange in 2BC.

The energy exchange can be explained by the Kogelnik coupled wave theory<sup>33</sup>, that will be discussed in the following in a very simplified form.<sup>28</sup> First, let's assume that there is a static grating as shown in Fig. 4.16. It consists of a slab of material in which the periodic relative dielectric constant,  $\epsilon_r$ , varies as a function of  $z$  in the form:

$$\epsilon_r = \epsilon_{r0} + \epsilon_{r1} \cos Kz \quad (4.10)$$

where  $\epsilon_{r0}$  is the dielectric constant of the material in the absence of grating,  $\epsilon_{r1}$  is the



amplitude of the dielectric grating, and  $\vec{\kappa}$  is the the grating vector defined in Eq.(4.11), with the direction illustrated in Fig. 4.16.  $\Lambda$  is the grating spacing.

$$\kappa = \frac{2\pi}{\Lambda} \quad (4.11)$$

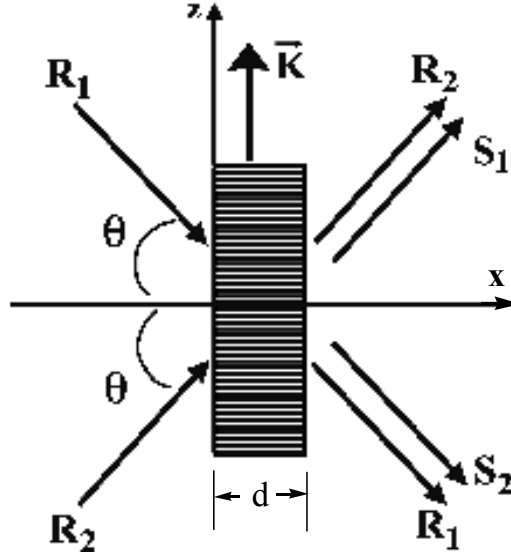


Fig. 4.16. Diffraction of light from a grating.

Now we assume there are two interfering waves,  $R_1$  and  $R_2$ , incident upon the grating, and they have phase angles  $\phi_1$  and  $\phi_2$  respectively. If we assume that the  $R_1$  and  $R_2$  can be expressed as plane waves, then

$$\begin{aligned} R_1 &= A_1 e^{i\phi_1} \cos \kappa x \\ R_2 &= A_2 e^{i\phi_2} \cos \kappa x \end{aligned} \quad (4.12)$$

where  $A_1$  and  $A_2$  are their amplitudes and the coupling constant  $\kappa$  is defined as

$$\kappa = \frac{\epsilon_{r1} \kappa}{4\pi\epsilon_{r0} \cos \theta} \quad (4.13)$$

If the Bragg diffraction condition

$$\Lambda = \frac{\lambda}{2 \sin \theta} \quad (4.14)$$

is satisfied, the two waves will be partially transmitted, with the other part diffracted into the beams  $S_1$  and  $S_2$ , respectively, as shown in Fig. 4.16. The amplitudes of the output waves are given by the expressions

$$R_1 = A_1 e^{i\phi_1} \cos v \quad (4.15)$$

$$R_2 = A_2 e^{i\phi_2} \cos \nu \quad (4.16)$$

$$S_1 = -iA_1 e^{i\phi_1} \sin \nu \quad (4.17)$$

$$S_2 = -iA_2 e^{i\phi_2} \sin \nu \quad (4.18)$$

where, if  $d$  is the thickness of the grating,

$$\nu = \kappa d \quad (4.19)$$

When only beam 1 is incident, since light intensity is proportional to the squared modulus of the amplitude, the output intensities in the direction of beams 1 and 2 are

$$\begin{aligned} I_{11} &= A_1^2 \cos^2 \nu \\ I_{12} &= A_1^2 \sin^2 \nu \end{aligned} \quad (4.20)$$

Analogously, when only beam 2 is incident, the output intensities in the direction of beams 1 and 2 are

$$\begin{aligned} I_{21} &= A_2^2 \cos^2 \nu \\ I_{22} &= A_2^2 \sin^2 \nu \end{aligned} \quad (4.21)$$

When both beams are incident, the output intensity in the direction of beam 1 is then:

$$\begin{aligned} I_1 &= \left| A_1 e^{i\phi_1} \cos \nu - iA_2 e^{i\phi_2} \sin \nu \right|^2 \\ &= A_1^2 \cos^2 \nu + A_2^2 \sin^2 \nu + A_1 A_2 \sin 2\nu \sin(\phi_2 - \phi_1) \end{aligned} \quad (4.22)$$

and the output intensity in the direction of beam 2 is

$$\begin{aligned} I_2 &= \left| A_2 e^{i\phi_2} \cos \nu - iA_1 e^{i\phi_1} \sin \nu \right|^2 \\ &= A_1^2 \sin^2 \nu + A_2^2 \cos^2 \nu - A_1 A_2 \sin 2\nu \sin(\phi_2 - \phi_1) \end{aligned} \quad (4.23)$$

when  $\phi_2 - \phi_1 = 0$ , the output intensities may be obtained by simply adding the intensities when only one or the other beam is present, i.e.

$$I_1 = I_{11} + I_{21} \quad \text{and} \quad I_2 = I_{12} + I_{22} \quad (4.24)$$

It is important to emphasize that when  $\phi_2 - \phi_1 \neq 0$ , we have the interaction term  $A_1 A_2 \sin 2\nu \sin(\phi_2 - \phi_1)$  which adds to the intensity of one output beam and subtracts from the intensity of the other beam, namely energy exchange between the two beams. In PR materials the grating is induced by the two interfering beams and the phase difference  $\phi_2 - \phi_1$  can then be thought of as the phase difference between interference pattern and refractive index grating. In conclusion, the detection of an asymmetrical exchange of energy between the two beams is a proof of the non-local, i.e. photorefractive nature of

the grating.

A typical experimental set-up to perform 2BC is illustrated in Fig. 4.17. The laser beam passes through a polarizer P and reaches a beam splitter where half of the light is transmitted and half is reflected towards the two mirrors M which direct the resulting beams towards the sample. In order to control the polarization and the power density of the beams, half-wave plates and lenses are placed before the sample. The outgoing intensities are passing through a chopper and then they are acquired by two photodiodes placed directly along the path of the two beams. A third photodiode is necessary to measure the intensity of the first order diffraction beam. The acquisition is managed by a software that, working as a lock-in amplifier, acquires only the signals at the chopper frequency. The same software controls the voltage applied on the sample and acquisitions of light intensity versus time or field can be performed. The voltage applied on the sample is generated by a power supply.

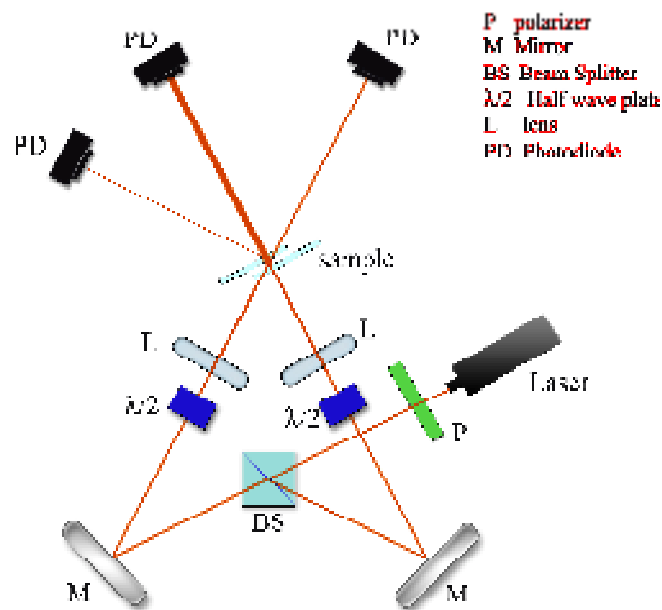


Fig. 4.17. Experimental set-up for 2BC.

The energy exchange can be quantitatively characterized by gain coefficient  $\Gamma$ . According to the coupled waves model<sup>35</sup> it is possible to define  $\Gamma$  as:

$$\Gamma = \frac{2\pi}{\lambda} \Delta n \sin \Theta \quad (4.25)$$

where  $\Theta$  is the phase shift between light pattern and refractive index grating and  $\Delta n$  is the

index modulation amplitude. Higher  $\Gamma$  value means a better PR performance in which more energy is exchanged between the two beams in 2BC. Since it is possible to obtain  $\Theta$  experimentally, from measurement of  $\Gamma$  it is possible to evaluate  $\Delta n$ . The gain coefficient can be extracted from 2BC experiments by using<sup>36</sup>:

$$\Gamma d = \cos \alpha_1 \ln \frac{I_1(I_2 \neq 0)}{I_1(I_1 = 0)} - \cos \alpha_2 \ln \frac{I_2(I_1 \neq 0)}{I_2(I_1 = 0)} \quad (4.26)$$

where  $d$  is the thickness of the sample and  $\alpha_1$  and  $\alpha_2$  are the angles defined in Fig. 4.14 (b).  $I_1(I_2 \neq 0)$  and  $I_1(I_2 = 0)$  are the intensities of beam 1 beyond the sample with beam 2 on and off, respectively. Similar definitions apply to  $I_2(I_1 \neq 0)$  and  $I_2(I_1 = 0)$ . The direction of energy transfer depends on the sign of the applied electric field and on the sign of  $\Delta n$ : by reversing the electric field polarity, it is possible to change the sign of the energy transfer.

#### 4.6 Four-wave mixing experiment

In a Four-wave mixing (FWM) experiment, a reading beam is diffracted by the grating induced by two interfering writing beams. The photorefractive properties of the material are investigated by measuring the diffraction efficiency  $\eta$  defined as the ratio between the intensity of the diffracted beam measured after the sample and the intensity of the incident reading beam measured before the sample.<sup>37</sup> In FWM, information on not only the diffraction efficiency, but also on the grating dynamics can be gathered. The experimental geometry for the FWM experiment is quite similar to that of 2BC. The difference is that in the FWM experiment, in addition to the writing beams 1 and 2, there is also a probe (reading) beam (beam 3 in Fig. 4.18) that is being partially diffracted from the grating created by the writing beams to create a fourth beam (beam 4). In order to minimize the effects of the reading beam on the grating, its intensity should be much weaker than the intensity of the writing beams. The wavelength of the reading beam can be the same as or different from the wavelength of the writing beams. In the degenerate FWM geometry, which is common in PR measurements, beam 3 has the same wavelength as the writing beams and it is usually chosen to be counter-propagating to one of the writing beams in order to satisfy the Bragg diffraction conditions. To probe the grating, it is important that beam 3 does not affect the grating or interact with the writing beams. This can be assured by making the probe beam much weaker than the pump beams and/or by having the probe beam polarized orthogonally to the writing beams. Because

p-polarized beams experience larger diffraction efficiency due to the polarization dependence of the OE response of the material,<sup>38</sup> in most FWM experiments beam 3 is typically p-polarized, while beams 1 and 2 are s-polarized.

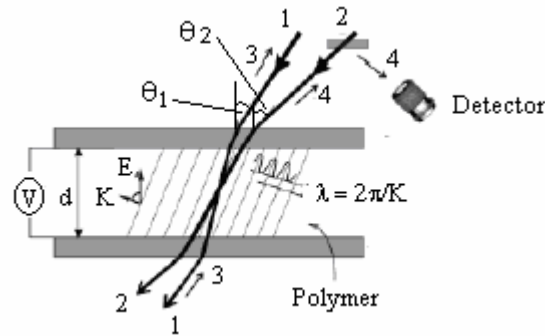


Fig. 4.18. Four-wave Mixing geometry.

A typical FWM experimental set-up is shown in Fig. 4.19. Light passes through the polarizer P and reaches the pellicle beam splitter BS1 where about 10% is transmitted while 90% is reflected. The reflected beam is split in two beams by beam splitter BS2: each beam is reflected by a mirror (M1 and M2) towards a polarizing beam splitter (PBS1 and PBS2), where both beams are reflected (since they are s-polarized) and reach mirrors M3 and M4, respectively. The position of these last mirrors is very important since it defines the grating spacing: after this last reflection the beams reach the sample where they interfere. Turning back to the light transmitted by the beam splitter BS1, it passes through a 1% filter and then through a half-wave plate to rotate the polarization from the s to the p state. Then the beam is reflected by mirrors M5 and M6 in order to have the same direction as writing beam 1. The reading beam now matches the Bragg conditions and for this reason, in the presence of a grating, part of the light will be transmitted and part will be diffracted. The transmitted and diffracted beams follow the reverse path with respect to the writing beams: they are reflected by mirrors M3 and M4 and reach the polarizing beam splitters PBS1 and PBS2, where they are transmitted because they are p-polarized. The intensities of transmitted and diffracted beams are collected by photodiodes PD1 and PD2, respectively. The acquisition system is the same as the one described for 2BC experiment.

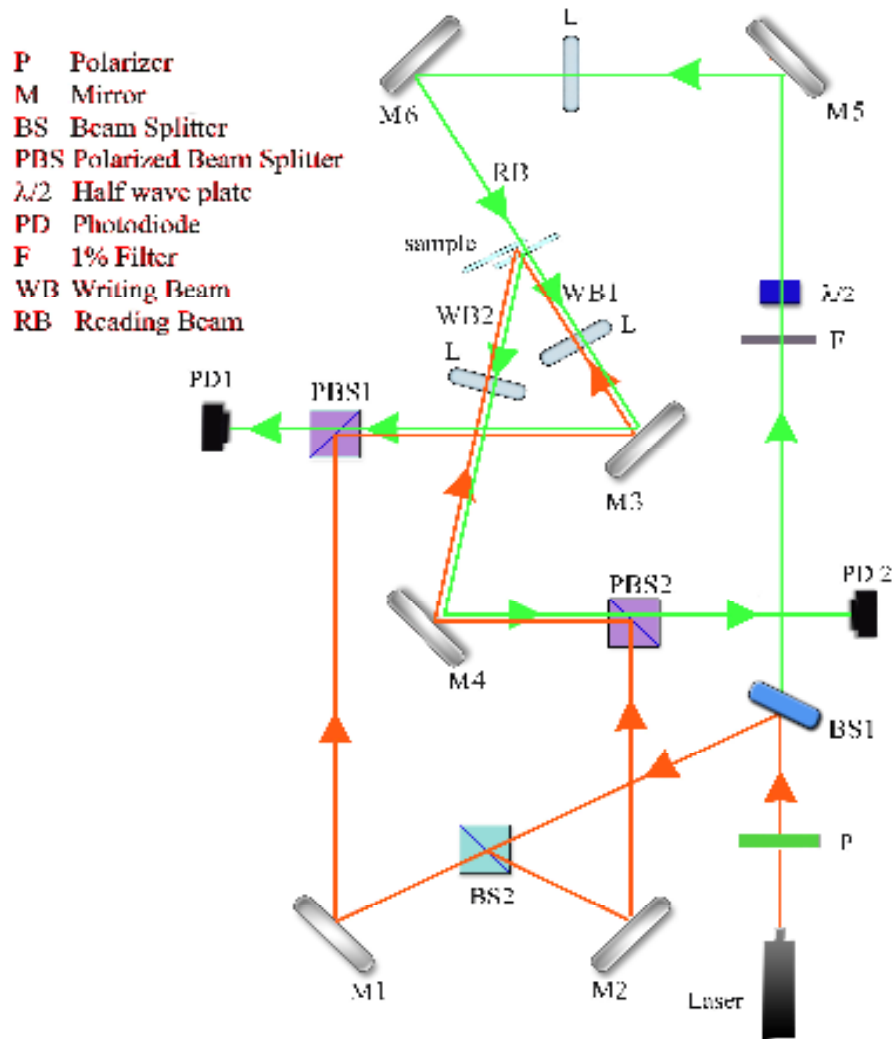


Fig. 4.19. FWM experimental setup.

Results of FWM experiments can be expressed in terms of internal or external diffraction efficiency. The internal diffraction efficiency  $\eta_{\text{int}}$  is given by the following relation:

$$\eta_{\text{int}} = \frac{I_{\text{diffr}}}{I_{\text{diffr}} + I_{\text{trans}}} \quad (4.27)$$

where  $I_{\text{diffr}}$  and  $I_{\text{trans}}$  are the diffracted and the transmitted beam intensities, respectively.

The external diffraction efficiency  $\eta_{\text{ext}}$  is defined as:

$$\eta_{\text{ext}} = \frac{I_{\text{diffr}}}{I_{\text{inc}}} \quad (4.28)$$

where  $I_{\text{inc}}$  is the reading beam intensity before the sample. It is clear that the external

efficiency considers all losses due to reflections, scattering and absorption and measures the net efficiency of the whole process, while the internal efficiency measures directly how well the recorded grating diffracts light. As in 2BC experiments, the measurement of  $\eta_{\text{int}}$  and  $\eta_{\text{ext}}$  are usually performed versus the applied electric field or versus time.

In addition to measurements of steady-state diffraction efficiency, which is an important parameter for application, the FWM experiment is widely used for temporal studies (e.g. formation and erasure) of the PR grating. Furthermore, the FWM experiment is ideally suited to measure the dark decay of gratings, i.e., the decay after both writing beams are turned off.<sup>39-41</sup>

### 4.7 Steady state ellipsometry

Ellipsometry is based on the principle that a sample, due to the birefringence induced by an external electric field or other sources, can act as a retarding wave plate changing the polarization of a light beam. The simple experimental set-up is shown in Fig. 4.20, with the sample placed between two crossed polarizers. A Soleil-Babinet compensator (a variable phase retarder) is placed beyond the sample. The probe light beam passing through the set-up is forming an angle of  $45^\circ$  with respect to the sample normal and its polarization forms a  $45^\circ$  angle with the p-plane. To avoid unwanted effect induced by absorption of probe light beam, the light intensity should be as low as possible. If the sample is completely amorphous (isotropic) and if no phase retardation is introduced by the compensator, the beam polarization is not changed and no light intensity can be detected beyond the analyzer.

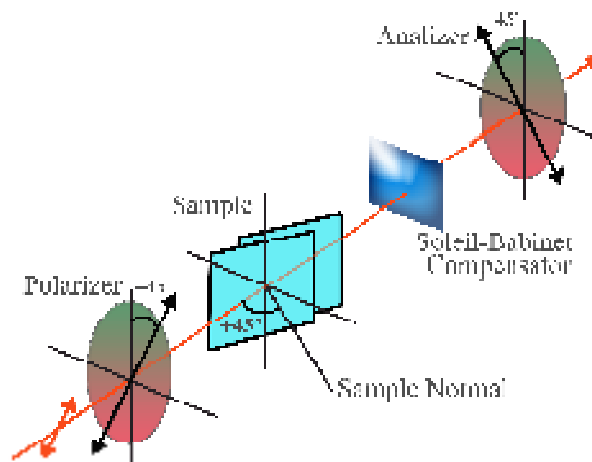


Fig. 4.20. Ellipsometry set-up.

The light intensity passing through the analyzer can be changed by a phase retardation introduced by the compensator as shown in Fig. 4.21: by increasing the phase retardation  $\theta$  the light intensity will increase and decrease sinusoidally, with minima corresponding to multiples of  $2\pi$  in phase delay. The same trend can be observed if phase retardation is caused by birefringence ( $\Delta n$ ) in the sample, due to an applied electric field or to other sources.  $\Delta n$  is defined as:

$$\Delta n = n_p - n_s \quad (4.29)$$

where  $n_p$  and  $n_s$  are the refractive indices for light polarized in the p and in the s planes, respectively. Depending on the compensator setting, it is possible to perform different measurements. By setting  $\theta$  so that the intensity of light is in a minimum, it is possible to calculate  $\Delta n$  by the following equation<sup>42</sup>:

$$\Delta n = \frac{\lambda \cos \xi_{\text{int}}}{2\pi d} \arcsin \sqrt{\frac{I}{I_{\text{max}}}} \quad (4.30)$$

where  $d$  is the thickness of the sample,  $\lambda$  is the wavelength of the light,  $\xi_{\text{int}}$  is the angle inside the material between the sample normal and the light direction,  $I$  is the light passing through the setup and  $I_{\text{max}}$  is the maximum light intensity passing through the system, measured by changing the phase retardation of the compensator.

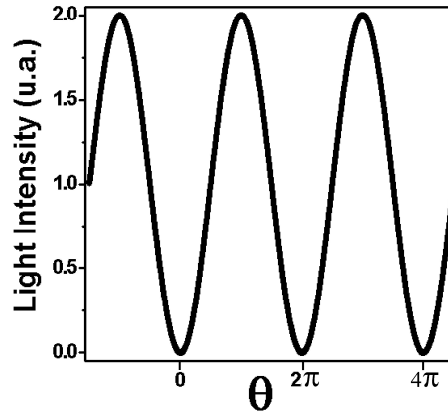


Fig. 4.21. Variation of light intensity as a function of the phase retardation of the Soleil-Babinet compensator.

Several steps should be done for measurement of light-induced birefringence. First, probe beam and writing beam should have different polarizations to avoid interference, and probe beam should be much weaker than writing beam. Usually the writing beam is



set to s-polarized or p-polarized. The diameter of probe beam should also be smaller than that of writing beam, to make sure that the probe beam passes through the bulk of the sample covered by the writing beam, as shown in Fig. 4.22. Second, the Soleil-Babinet compensator is modulated to find the maximum and minimum of the transmission intensity of the probe beam when the writing beam is off. Then the intensity is set back to minimum. Finally the writing beam is turned on and the time dependence of the transmission intensity of the probe beam is recorded. During the experiment, the transmission intensity of the probe beam will increase until saturation and light-induced birefringence can be calculated according to Eq. (4.30).

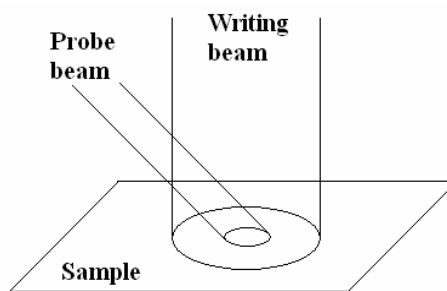


Fig. 4.22. Probe beam and writing beam for the light-induced birefringence measurement. The writing beam propagates along the sample normal and the probe beam forms an angle of  $45^\circ$  with respect to the sample normal.

## 4.8 Transient ellipsometry

For the experiments described above, interesting information can be obtained if an AC field is used. By applying an AC electric field with a DC bias, like the one described in the inset of Fig. 4.23, it is possible to distinguish whether the refractive index modulations is due to a reorientational mechanism or to electrooptic properties or to both<sup>43</sup> mechanisms.

One of the main differences between the two effects consists in the time necessary to obtain the refractive index modulation. The orientational effect is relatively slow because the refractive index modulation is achieved by reorienting molecules or larger objects, while the electrooptic effect is based on electron displacement and it is much faster. Such difference in speed can be exploited in order to distinguish between the two mechanisms by using the same experimental set-up used for steady state ellipsometry (Fig. 4.20), adjusting the compensator in order to have a minimum of light passing through the

system and then applying an electric field such as the one illustrated in the inset of Fig. 4.23. Chromophores are reoriented by the field bias and the resulting loss of centrosymmetry allows the Pockels effect. The AC component of the field modulates the refractive index and the light intensity passing through the system, as a function of the frequency of the electric field, is measured. If the refractive index modulation is observed even for high frequency, then the mechanism is electrooptic, while if light intensity drops down with frequency, the mechanism is orientational. Signal acquisition is usually carried out with a lock-in amplifier at the field frequency.

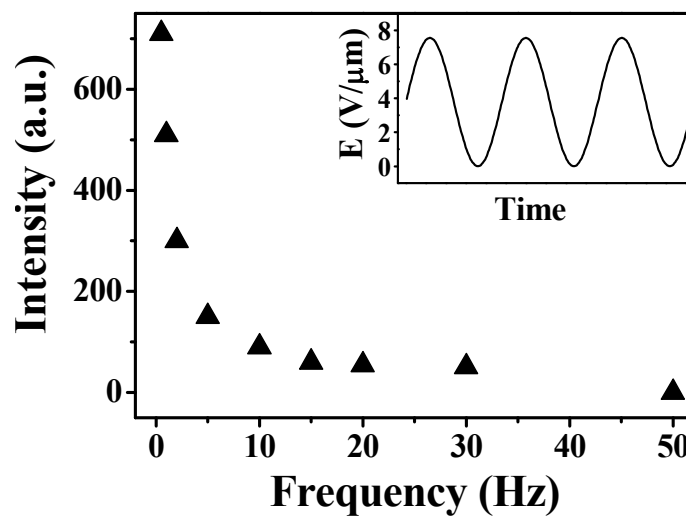


Fig. 4.23. Light intensity versus frequency in transient ellipsometry experiment.

In Fig. 4.23 a typical light intensity/frequency graph for a sample showing only orientational refractive index modulation is shown. At low frequency, chromophores are able to follow the modulating electric field while above a few Hz the efficiency of the induced reorientation process drops.

#### 4.9 Moving grating technique for phase shift measurement

As already mentioned, in a PR material there is a phase shift between the light pattern and the refractive index hologram. This is illustrated in Fig. 4.24 in the case of an illumination that is produced by two interfering beams. In addition to the refractive index grating, there may be an absorption grating. The moving grating technique can determine not only the amplitudes of both the absorption and refractive index gratings, but also their phase shift with respect to the interference pattern.<sup>44</sup>

The experiment can be performed by using the same experimental set-up as for 2BC, depicted in Fig. 4.17. A phase shift  $\Theta$  will be induced when the photorefractive grating is written and reaches a steady state, as shown in Fig. 4.24. Then the sample is translated along the direction of the grating vector  $\vec{k}$  and the intensities of the two transmitted beams are measured as a function of the fringe pattern position or time. If the translation time is much shorter than the time needed to build up a new refractive index grating, the refractive index grating in Fig. 4.24 will be translated along the direction of grating vector  $\vec{k}$ , while the light pattern is maintained fixed. In this way, the phase shift value will be changed between 0 and  $2\pi$ , inducing a sinusoidal variation of the intensities according to Eq. (4.25).

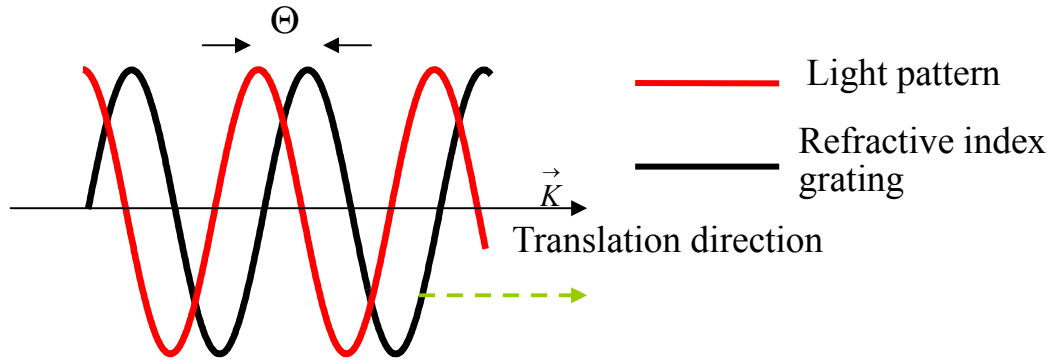


Fig. 4.24. Phase shift measurement.

Typical variations of the beams intensities are shown in Fig. 4.25 (a). When both an absorption and a phase grating are present, the intensity of each beam at the exit of the sample is given by:

$$I_1 = I_0(1 - 2A \cos \Theta_A + 2P \sin \Theta_P) \quad (4.31)$$

$$I_2 = I_0(1 - 2A \cos \Theta_A - 2P \sin \Theta_P) \quad (4.32)$$

where  $I_0$  is the intensity of the beams beyond the sample when no grating is present,  $A$  and  $P$  are the diffraction amplitudes of the absorption and phase gratings, respectively, and  $\Theta_A$  and  $\Theta_P$  are the phase shifts of the two gratings with respect to the fringe pattern. By summing and subtracting Eqs. (4.31) and (4.32) we obtain:

$$I^+ = I_0(2 - 4A \cos \Theta_A) \quad (4.33)$$

$$I^- = 4I_0P \sin \Theta_P \quad (4.34)$$

where  $I^+$  means the sum of the two transmission beams and  $I^-$  means their difference. It is

clear that the modulation of  $I^+$  depends on the amplitude and phase of the absorption grating while amplitude and phase of the refractive index grating can be obtained from  $I^-$  as shown in Fig. 4.25 (b).

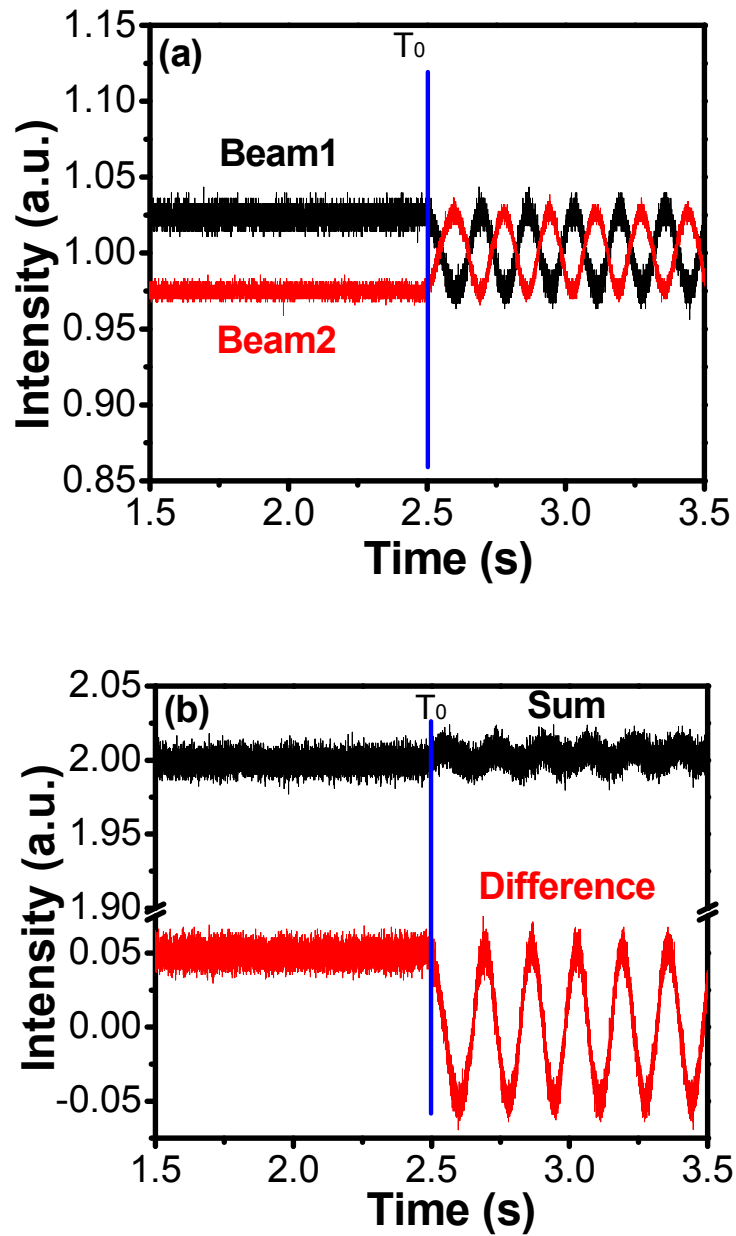


Fig. 4.25. Light intensities of the two transmission beams as a function of time during the translation of the grating, starting at  $T_0 = 2.5$  s.

## BIBLIOGRAPHY

1. J. Day, S. Subramanian, J. E. Anthony, Z. Lu, R. J. Twieg, O. Ostroverkhova. *J. Appl. Phys.*, **2008**, 103, 123715.
2. F. Laquai, G. Wegner, H. Bässler. *Phil. Trans. R. Soc. A*, **2007**, 365, 1473.
3. N. Karl. *Synth. Met.*, **2003**, 133, 649.
4. W. Warta, N. Karl. *Phys. Rev. B*, **1985**, 32, 1172.
5. V. Podzorov, V. M. Pudalov, M. E. Gershenson. *Appl. Phys. Lett.*, **2003**, 82, 1739.
6. Y. J. Shirota. *Mater. Chem.*, **2005**, 15, 75.
7. T. Kreouzis, D. Poplavskyy, S. M. Tuladhar, M. Campoy-Quiles, J. Nelson, A. J. Campbell, D. D. C. Bradley. *Phys. Rev. B*, **2006**, 73, 235201.
8. H. Sirringhaus, P. J. Brown, R. H. Friend, M. M. Nielsen, K. Bechgaard, B. M. W. Langeveld-Voss, A. J. H. Spiering, R. A. J. Janssen, E. W. Meijer, P. Herwig, D. M. de Leeuw. *Nature*, **1999**, 401, 685.
9. I. McCulloch, M. Heeney, C. Bailey, K. Genevicius, I. Macdonald, M. Shkunov, D. Sparrowe, S. Tierney, R. Wagner, W. M. Zhang, M. L. Chabinye, R. J. Kline, M. D. McGehee, M. F. Toney. *Nat. Mater.*, **2006**, 5, 328.
10. H. Sirringhaus, R. J. Wilson, R. H. Friend, M. Inbasekaran, W. Wu, E. P. Woo, M. Grell, D. D. C. Bradley. *Appl. Phys. Lett.*, **2000**, 77, 406.
11. O. Ostroverkhova, K. D. Singer. *J. Appl. Phys.*, **2002**, 92, 1727.
12. T. Jakob, S. Schloter, U. Hofmann, M. Grasruck, A. Schreiber, D. Haarer. *J. Chem. Phys.*, **1999**, 111, 10633.
13. A. Goonesekera, S. Ducharme, J. M. Takacs, L. Zhang. *J. Chem. Phys.*, **1997**, 107, 8709.
14. A. Goonesekera, S. Ducharme. *J. Appl. Phys.*, **1999**, 85, 6506.
15. M. A. Lampert, P. Mark. 'Current Injection in Solids', Academic Press, New York, **1970**.
16. V. D. Mihailetschi, J. K. J. Van Duren, P. W. M. Blom, J. C. Hummelen, R. A. Janssen, J. M. Kroon, M. T. Rispens, W. J. H. Verhees, M. M. Wienk. *Adv. Funct. Mater.*, **2003**, 13, 43.
17. G. G. Malliaras, V. V. Krasnikov, H. J. Bolink, G. Hadziioannou. *Phys. Rev. B*, **1995**, 52, 14324.
18. S. J. Zilker, M. Grasruck, J. Wolff, S. Schloter, A. Leopold, M. A. Kol'chenko, U. Hofmann, A. Schreiber, P. Strohmriegel, C. Hohle, D. Haarer. *Chem. Phys. Lett.*, **1999**, 306, 285.
19. S. Bartkiewicz, A. Miniewicz, B. Sahraoui, F. Kajzar. *Appl. Phys. Lett.*, **2002**, 81, 3705.
20. G. Juska, K. Arlauskas, M. Viliunas, J. Kocka. *Phys. Rev. Lett.*, **2000**, 84, 4946.
21. G. Juska, K. Arlauskas, M. Viliunas, K. Genevicius, R. Osterbacka, H. Stubb. *Phys. Rev. B*, **2000**, 62, R16235.
22. G. Juska, K. Genevicius, K. Arlauskas, R. Osterbacka, H. Stubb. *Phys. Rev. B*, **2002**, 65, 233208.
23. L. Kulikovskiy, D. Neher, E. Mecher, K. Meerholz, H. H. Horhold, O. Ostroverkhova. *Phys. Rev. B*, **2004**, 69, 125216.
24. N. Marc, J. Y. Moisan, N. Wolffer, B. Andre, R. Lever. *Philos. Mag. B*, **1996**, 74, 81.
25. D. Basu, L. Wang, L. Dunn, B. Yoo, S. Nadkarni, A. Dodabalapur. *Appl. Phys. Lett.*, **2006**, 89, 242104.
26. P. Günter, J.-P. Huignard. 'Photorefractive Materials and Their Applications 2'.

- Springer, 2007.
27. C. A. Walsh, W. E. Moerner. *J. Opt. Soc. Am. B*, **1992**, 9, 1642.
  28. L. Solymar, D. J. Webb, A. Grunnet-Jepsen. *The Physics And Applications Of Photorefractive Materials*, Oxford University Press, Oxford, **1996**.
  29. D. R. Evans, G. Cook. *J. Nonlinear Opt. Phys. Mater.*, **2007**, 16, 271.
  30. G. Cook, C. J. Finnan, D. C. Jones. *Appl. Phys. B*, **1999**, 68, 911.
  31. F. Kajzar, S. Bartkiewicz, A. Miniewicz. *Appl. Phys. Lett.*, **1999**, 74, 2924.
  32. S. Bartkiewicz, K. Matczyszyn, A. Miniewicz, F. Kajzar. *Opt. Commun.*, **2001**, 187, 257.
  33. H. Kogelnik. *Bell Sys. Tech. J.*, **1969**, 48, 2909.
  34. O. Ostroverkhova, W. E. Moerner, *Chem. Rev.*, **2004**, 104, 3267.
  35. P. Yeh. *Introduction to Photorefractive Nonlinear Optics*, Wiley, New York, **1993**.
  36. G. P. Wiederecht, B. A. Yoon, M. R. Wasielewski. *Adv. Mater.*, **1996**, 8, 535.
  37. B. Kippelen, K. Meehrholz, N. Peyghambarian. *An Introduction to Photorefractive Polymers* in *Nonlinear Optics of Organic Molecules and Polymers*, H. S. Nalwa and S. Miyata Eds., CRC Press Inc., London, **1997**.
  38. W. E. Moerner, A. GrunnetJepsen, C. L. Thompson. *Annu. Rev. Mater. Sci.*, **1997**, 27, 585.
  39. O. Ostroverkhova, W. E. Moerner, M. He, R. J. Twieg. *ChemPhysChem.*, **2003**, 4, 732.
  40. O. Ostroverkhova, U. Gubler, D. Wright, W. E. Moerne, M. He, R. Twieg. *Adv. Function. Mater.*, **2002**, 12, 621.
  41. R. Bittner, K. Meerholz, G. Steckman, D. Psaltis. *Appl. Phys. Lett.*, **2002**, 81, 211.
  42. Sandalphon, B. Kippelen, N. Peyghambarian, K. Meehrholz. *Appl. Opt.*, **1996**, 35, 2346.
  43. W. E. Spear. *J. Non-Cryst. Solids*, **1969**, 1, 197.
  44. K. Sutter, P. Günter. *J. Opt. Soc. Am. B*, **1990**, 7, 2274.

## Chapter 5

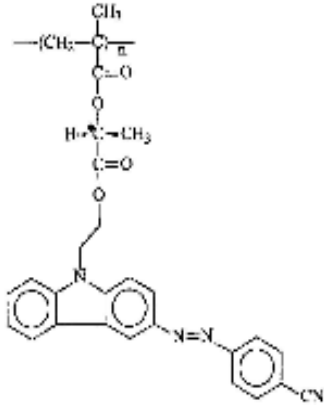
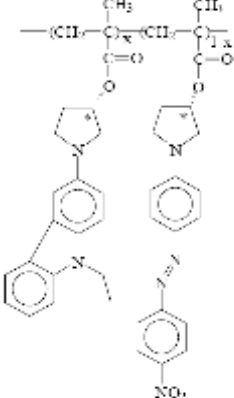
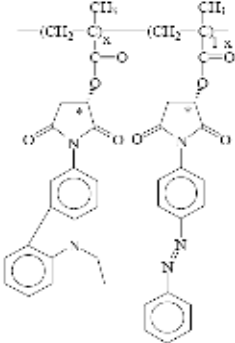
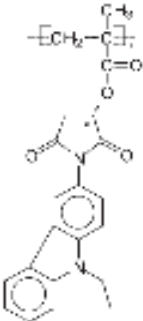
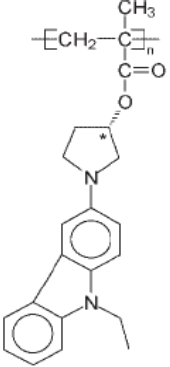
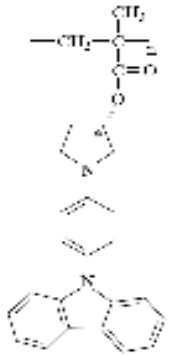
### RESULTS: PHOTOCONDUCTIVITY AND MOBILITY

#### 5.1 Azo-polymers: structures and UV-Vis spectra

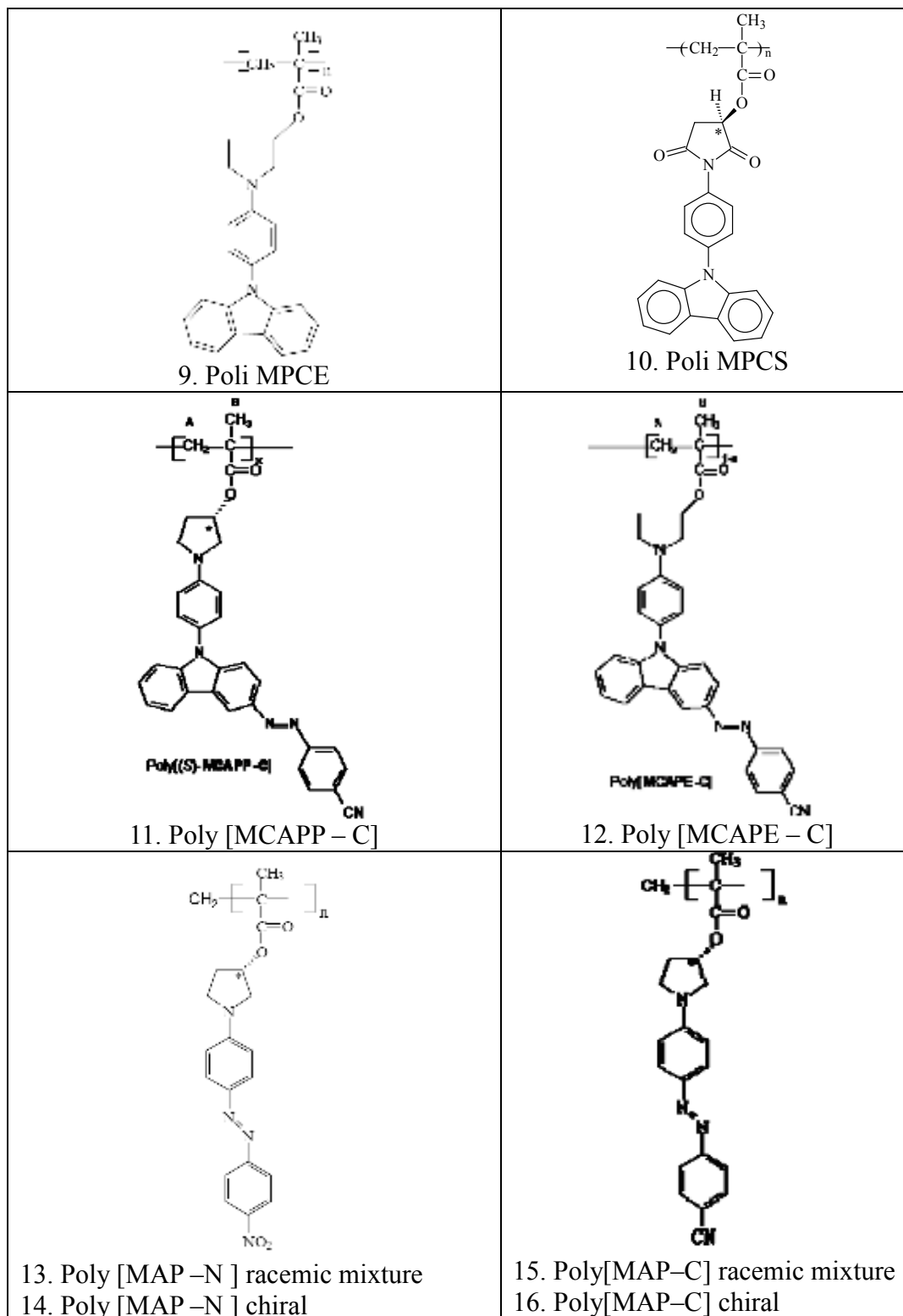
In the previous chapters we have discussed about the PR effect, PR polymers and azo-polymers. As described in section 2.1, polymers are superior choices for PR materials and several azo-polymers have demonstrated PR properties in addition to a number of interesting light-induced effects. The chemical structures of the studied polymers are shown in Table 5.1, and there are stereogenic centers, carbazole and azo moieties, which can induce chiral, semiconducting, photochromic and nonlinear optical properties. All the polymers can be classified as fully functionalized polymers. In this chapter we will focus on the photoconducting properties of these azo-polymers because, as explained in detail in chapter 1, photoconductivity is a prerequisite for the PR effect. Since photoconductivity is related to HOMO-LUMO levels and to charge carriers mobility, we also show results of experiments performed to obtain information on these two parameters.

Appropriate optical absorption is very important to obtain photogenerated charges. Absorption should not be too low, otherwise no charge can be generated, but it should also not be too high, because if a light beam cannot pass through the sample, charges will not be generated throughout the sample thickness. An analysis of the UV-Vis spectra is then necessary in order to find the proper light sources to be used. The normalized absorption spectra of some of the polymers in solution (supplied by the Department of Industrial Chemistry and Materials, University of Bologna) are shown in Fig. 5.1 - 5.3. Spectra show moderate absorption at  $\lambda = 532$  nm and  $\lambda = 632.8$  nm, where inexpensive CW laser sources exist, so that these two wavelengths seem to be suitable in order to conduct experiments regarding photoconducting and photorefractive properties.

Table 5.1. Chemical structures of the azo-polymers used in this work.

 <p>1. Poly (S) MLECA</p>	 <p>2. Poli [(S) - MECP - co -(S) MAP-N], <math>x = 0.5</math></p>
 <p>3. Poli [(S) - MECSI - co -(S) MOSI] <math>x = 0.24</math></p> <p>4. Poli [(S) - MECSI - co -(S) MOSI] <math>x = 0.76</math></p> <p>5. Poli [(S) - MECSI - co -(S) MOSI] <math>x = 0.5</math></p>	 <p>6. Poli [(S) - MECSI]</p>
 <p>7. Poli [(S) - MECPP]</p>	 <p>8. Poli MCPP</p>





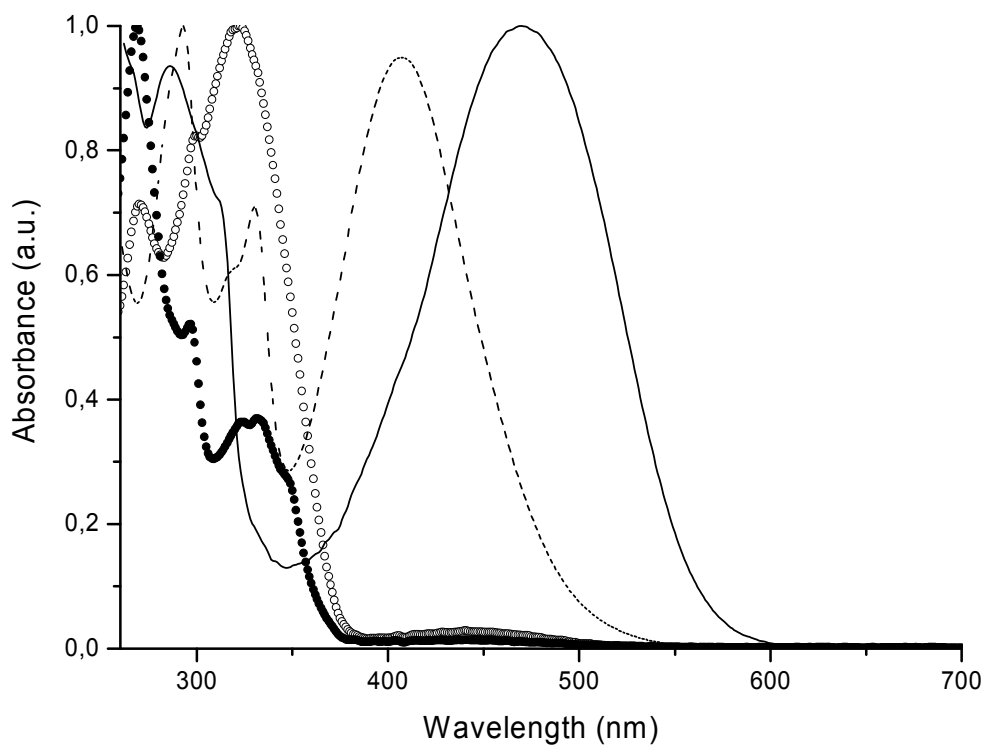


Fig. 5.1. Normalized UV-vis absorption spectra in  $\text{CHCl}_3$  of **1** (----), **2** (—), **3** (○○○) and **4** (●●●).

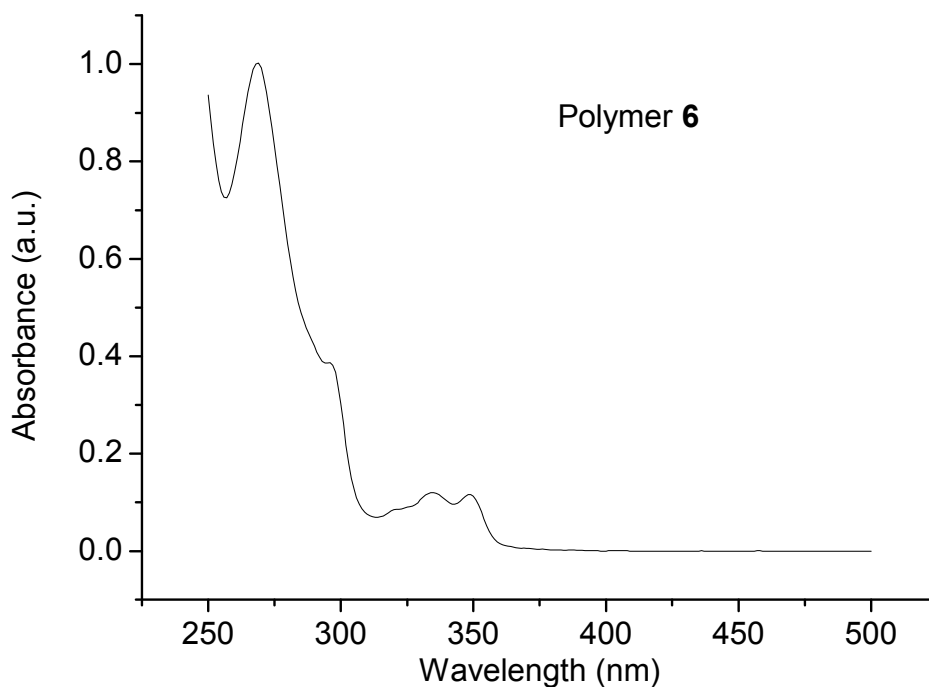


Fig. 5.2. Normalized UV-vis absorption spectra in  $\text{CHCl}_3$  of polymer **6**.

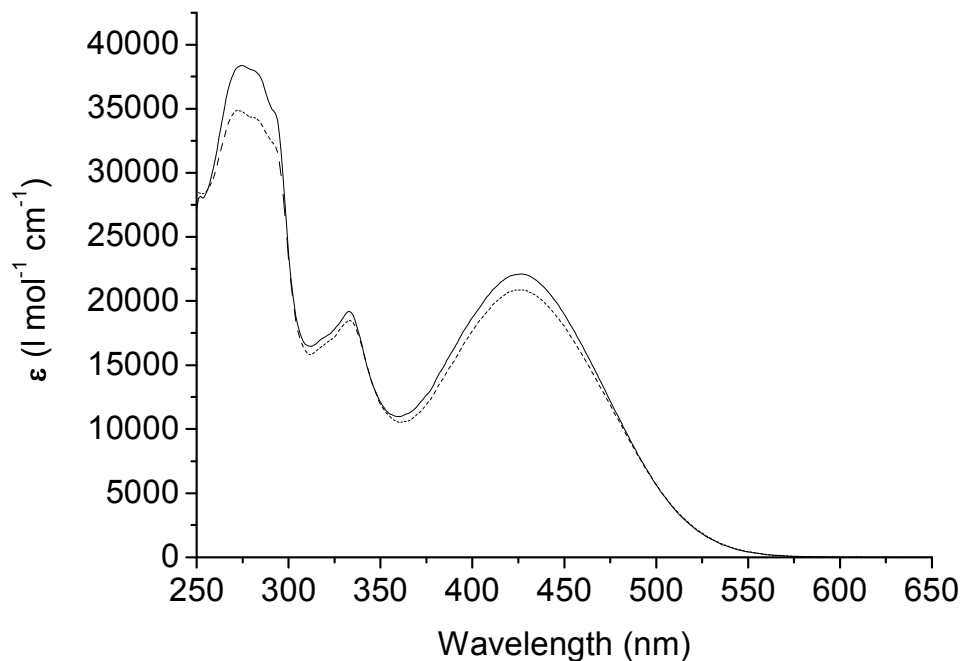


Fig. 5.3. UV-vis spectra in Dimethylformamide ( DMF) solution of polymer **11** (—) and polymer **12**[(*S*)-MCAPP-C] (---).

The absorption coefficients of the polymers were also measured, using the technique described in section 4.2, and their values are shown in Table 5.2.

Table 5.2. Absorption coefficients of polymers **1-15**.

Polymers (% DPP)	$\alpha$ 532nm ( $\text{cm}^{-1}$ )	$\alpha$ 633nm ( $\text{cm}^{-1}$ )
<b>1</b>	1811	168
<b>2</b> (20%)	/	692
<b>3</b>	358	68
<b>4</b>	527	75
<b>6</b> (20%)	987	/
<b>7</b> (20%)	1267	/
<b>8</b>	147	/
<b>9</b> (15%)	78	/
<b>10</b> (15%)	118	/
<b>11</b> (10%)	1857	94
<b>12</b>	2271	129
<b>15</b>	/	120

## 5.2 HOMO and LUMO levels of the polymers

The HOMO and LUMO levels of the polymers were measured by cyclic voltammetry and the values are shown in Table 5.3. The energy of the LUMO level of some of the polymers is not present in Table 5.3, because their values are higher than the detection limit (3.0 eV) of the experimental set-up.

Table 5.3. HOMO and LUMO levels of the polymers.

Polymer	LUMO (eV)	HOMO (eV)	Polymer	LUMO (eV)	HOMO (eV)
<b>1</b>	3.1	5.7	<b>8</b>		5.1
<b>2</b>	3.4	4.8	<b>9</b>		5.1
<b>3</b>		5.3	<b>10</b>		5.4
<b>4</b>		5.3	<b>11</b>	3.1	5.3
<b>6</b>		5.3	<b>12</b>	3.1	5.2
<b>7</b>		4.8	<b>15,16</b>	3.0	5.5

Some considerations can be done if we compare the energy of HOMO levels with the chemical structures of polymers. Four different polymers are shown in Fig. 5.4, with the HOMO levels increasing from left to right. The increase of the HOMO levels correlates well with the electron-withdrawing or electron-donating properties of the linking groups shown in Fig. 5.5, where, from left to right, their ability to donate electron is stronger and stronger. In polymer **1**, the linking group (Fig. 5.5a) is an electron-acceptor, and the electron density on carbazole, which is the moiety involved in electron transfer, is decreased. In polymer **7**, the linking group (Fig. 5.5d) is instead an electron-donor, having the opposite effect. In this way, the electron density on carbazole, from left to right as shown in Fig. 5.4, is higher and higher, resulting in an increasing HOMO orbital energy.

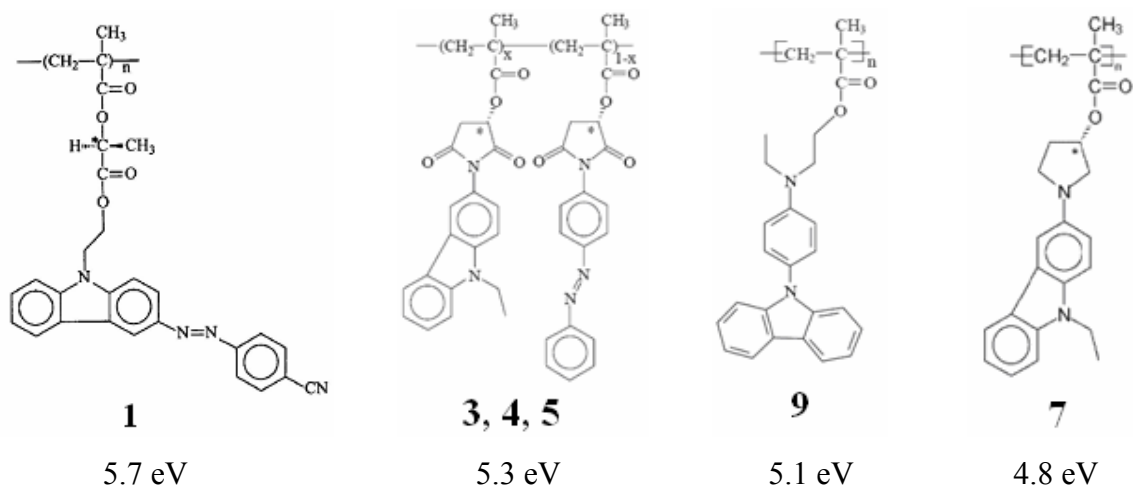


Fig. 5.4. HOMO levels of polymers **1**, **3**, **4**, **5**, **7** and **9**.

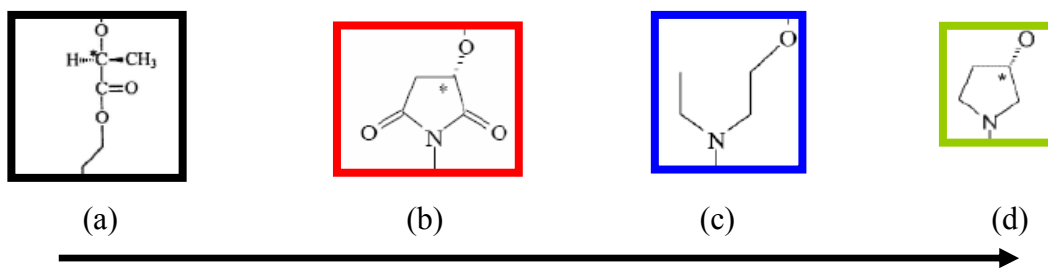


Fig.5.5. Linking groups (a), (b), (c) and (d) in the polymers.

The effect of delocalization in determining HOMO levels can be evinced by considering polymers **7**, **8** and **11**. As shown in Fig. 5.6 and 5.7, wider carbazole-containing structures correspond to more stable HOMO orbitals, as expected.

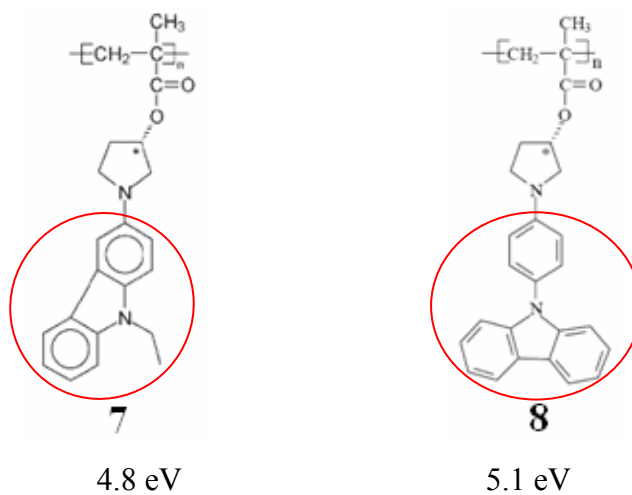


Fig. 5.6. HOMO levels of polymers **7** and **8**.

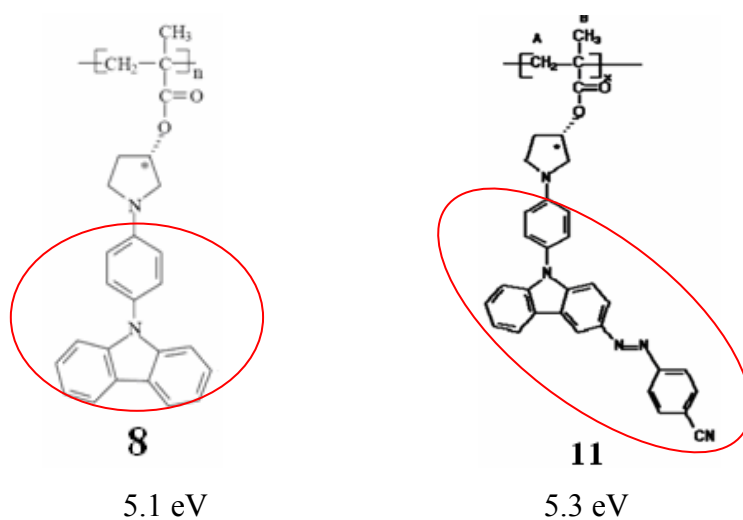


Fig. 5.7. HOMO levels of polymers **8** and **11**.

Polymer **3**, **4**, **5** and **6** have the same HOMO levels, as shown in Fig. 5.8. The only difference between their chemical structures is the absence of the azo chromophore group in **6**. Considering their identical HOMO level, it is reasonable to conclude that the azo chromophore in these polymers is irrelevant in determining the HOMO level. The same can be said for **2** and **7**, as shown in Fig. 5.9.

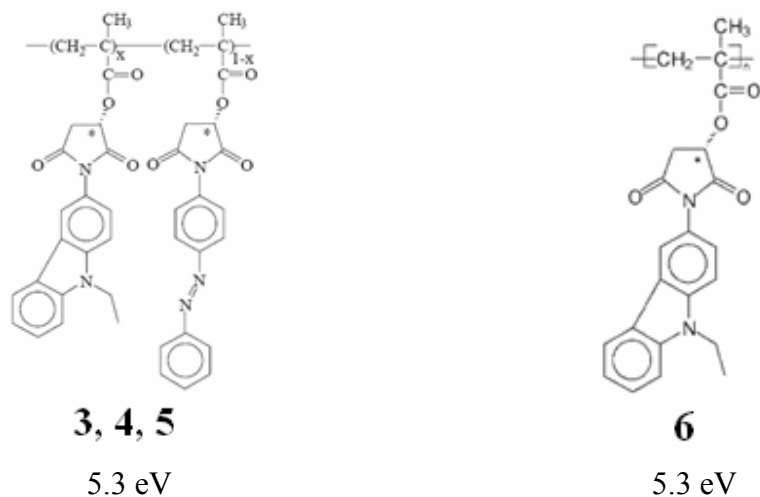


Fig. 5.8. HOMO levels of polymers **3**, **4**, **5** and **6**.

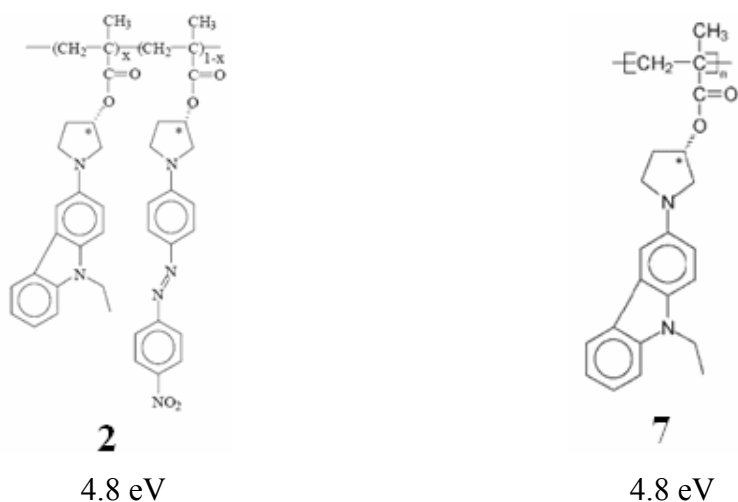
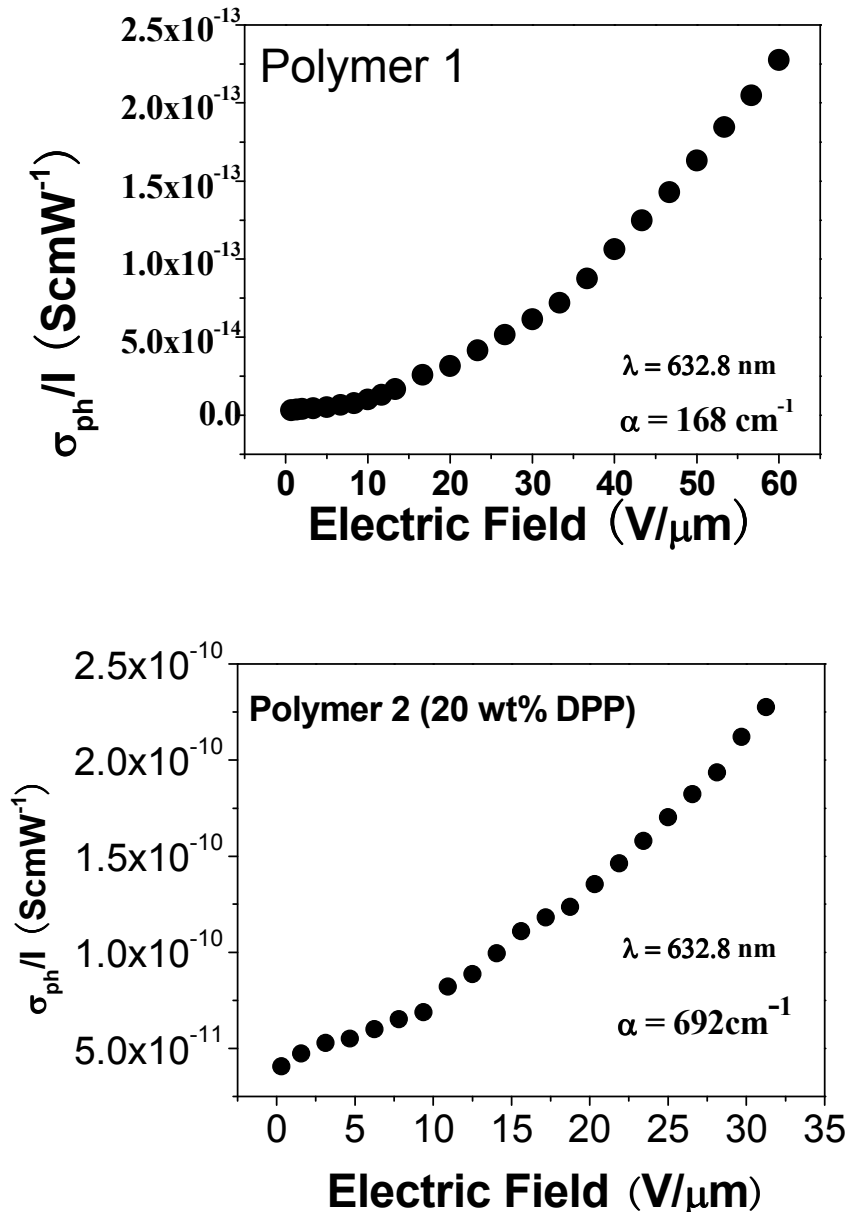


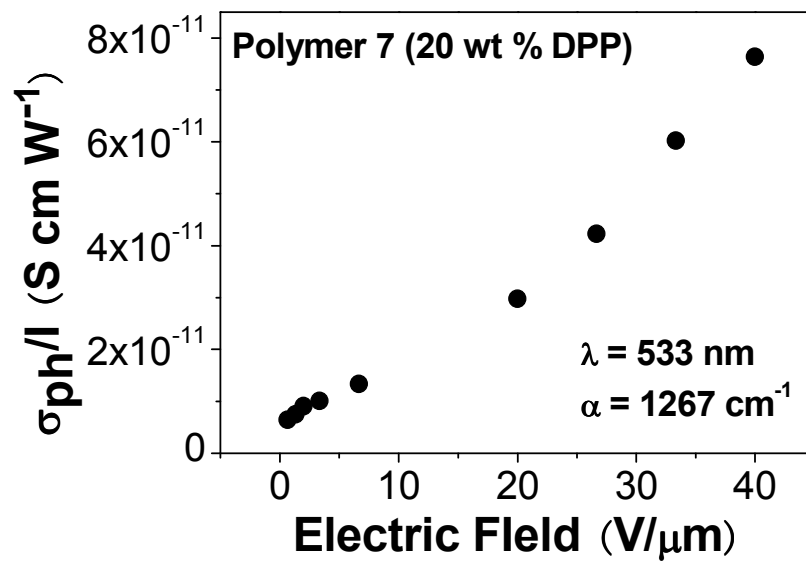
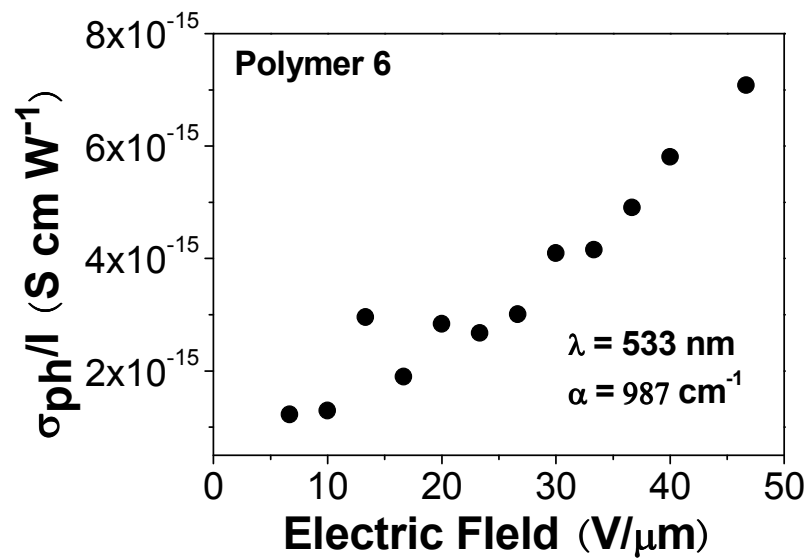
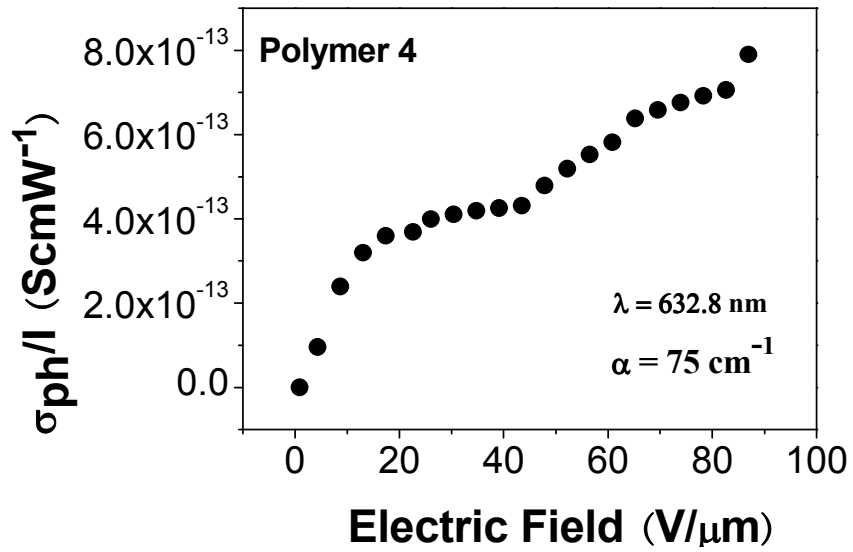
Fig. 5.9. HOMO levels of polymers **2** and **7**.

### 5.3 Photoconductivity measurements

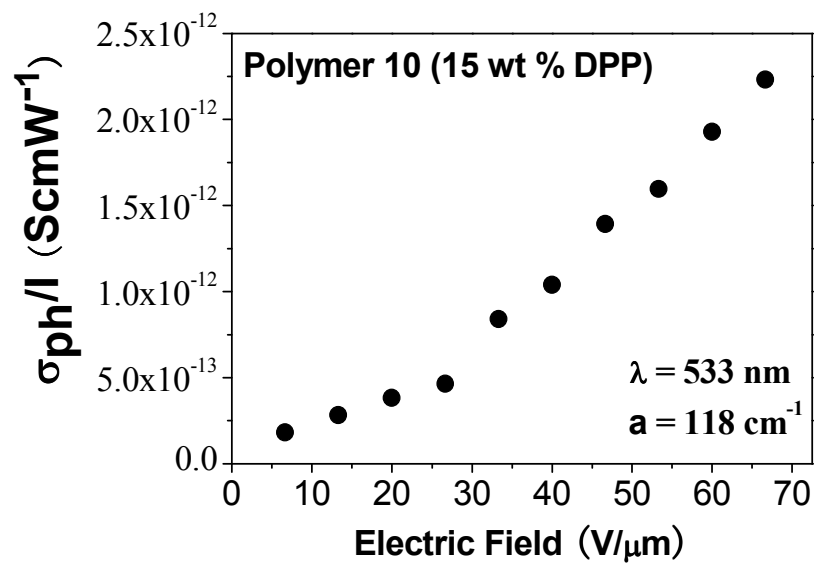
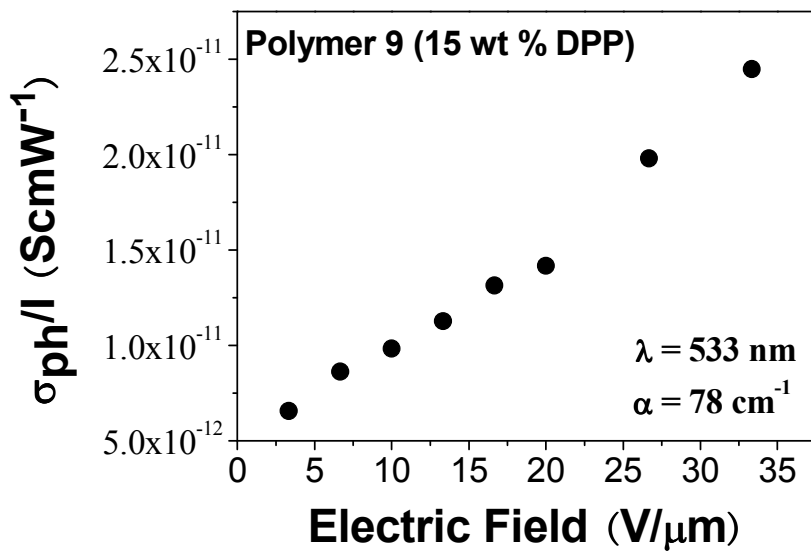
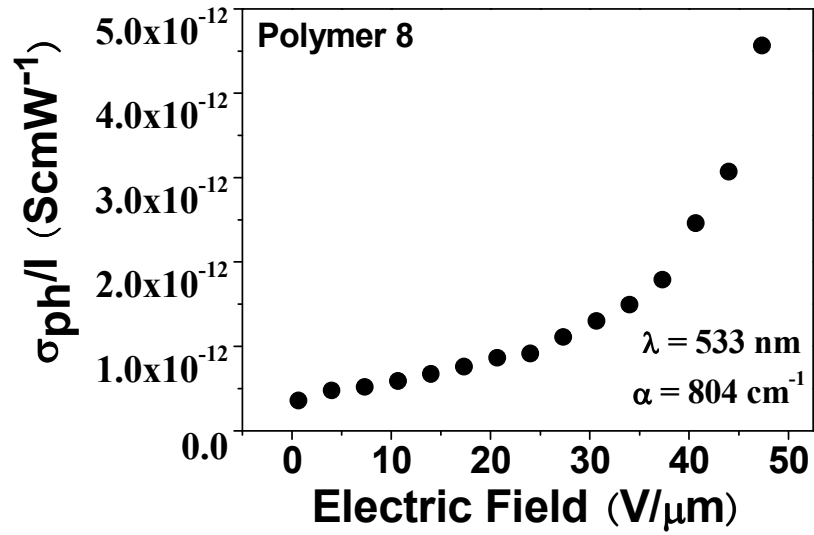
As already discussed in section 1.3, photoconductivity is a necessary prerequisite to observe the PR effect. The photoconductivities of the polymers were measured by the method described in section 4.3. The illumination was provided by either a He-Ne laser ( $\lambda = 632.8$  nm) or a Diode-Pumped Solid-State (DPSS) laser ( $\lambda = 532$  nm). The current

was measured using a Keithley 6517A electrometer at a light intensity  $I \approx 0.8 \text{ W cm}^{-2}$ . All the results are shown in Fig. 5.10 and listed in Table 5.4.









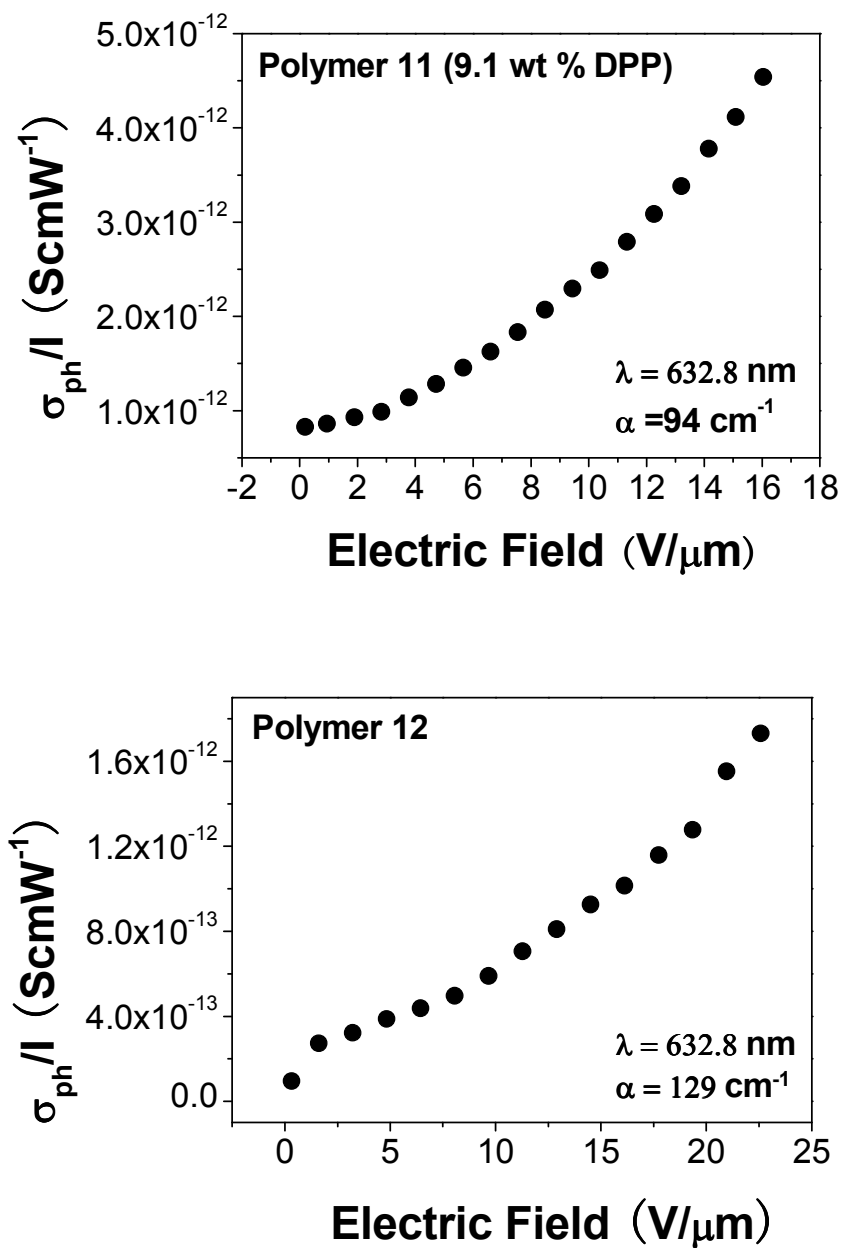


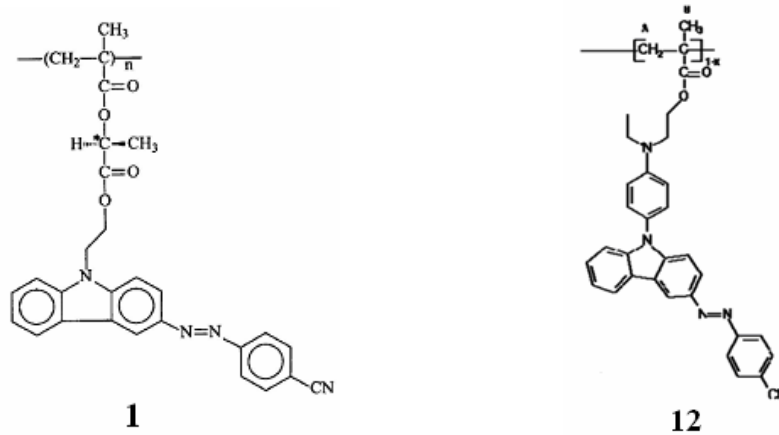
Fig. 5.10. photoconductivity of the polymers containing carbazole groups.

Table 5.4. Photoconductivity of the polymers.

Polymer (% DPP)	$\sigma/I$ 532 nm 18 V/ $\mu\text{m}$	$\sigma/I$ 632.8 nm 18 V/ $\mu\text{m}$	$\sigma/\alpha I$ 532 nm 18 V/ $\mu\text{m}$	$\sigma/\alpha I$ 632.8 nm 18 V/ $\mu\text{m}$	$\sigma/I$ 35V/ $\mu\text{m}$	$\sigma/\alpha I$ 35V/ $\mu\text{m}$
<b>1</b>		$2.9 \cdot 10^{-14}$		$1.7 \cdot 10^{-16}$	$8.0 \cdot 10^{-14}$ @ 632.8	$4.8 \cdot 10^{-16}$ @ 632.8
<b>2</b> (20%)		$1.2 \cdot 10^{-10}$		$1.7 \cdot 10^{-13}$	$2.3 \cdot 10^{-10}$ @ 632.8	$3.3 \cdot 10^{-13}$ @ 632.8
<b>3</b>	$<10^{-15}$	/	$<10^{-15}$	/	$<10^{-15}$	/
<b>4</b>		$3.7 \cdot 10^{-13}$		$4.9 \cdot 10^{-15}$	$4.3 \cdot 10^{-13}$ @ 632.8	$5.7 \cdot 10^{-15}$ @ 632.8
<b>6</b> (20%)	$2.3 \cdot 10^{-15}$		$2.3 \cdot 10^{-18}$		$4.3 \cdot 10^{-15}$ @ 532	$4.3 \cdot 10^{-18}$ @ 532
<b>7</b> (20%)	$2.6 \cdot 10^{-11}$		$2.0 \cdot 10^{-14}$		$6.4 \cdot 10^{-11}$ @ 532	$5.5 \cdot 10^{-14}$ @ 532
<b>8</b>	$7.8 \cdot 10^{-13}$		$5.3 \cdot 10^{-15}$		$1.6 \cdot 10^{-12}$ @ 532	$1.1 \cdot 10^{-14}$ @ 532
<b>9</b> (15%)	$1.3 \cdot 10^{-11}$		$1.6 \cdot 10^{-15}$		$2.4 \cdot 10^{-11}$ @ 532	$3.1 \cdot 10^{-15}$ @ 532
<b>10</b> (15%)	$3.5 \cdot 10^{-13}$		$3.0 \cdot 10^{-15}$		$8.3 \cdot 10^{-13}$ @ 532	$7.0 \cdot 10^{-15}$ @ 532
<b>11</b> (10%)		$4.5 \cdot 10^{-12}$		$4.8 \cdot 10^{-14}$	/	/
<b>12</b>		$1.2 \cdot 10^{-12}$		$9.3 \cdot 10^{-15}$	/	/
<b>13</b>						
<b>14</b>	/	/	/	/	/	/
<b>15</b>		$1.0 \cdot 10^{-13}$		$8.3 \cdot 10^{-16}$	$1.6 \cdot 10^{-13}$ @ 632.8	$1.3 \cdot 10^{-15}$ @ 632.8
<b>16</b>	/	/	/	/	/	/

In Fig. 5.11 we show the structure of **1** and **12**. Their large difference in photoconductivity can be explained by their different linking groups. The donor group in polymer **12** can induce two effects: the first one is connected to the formation of a push-pull system, in conjunction with the presence of the cyano group. Push-pull systems are known to increase photogeneration efficiency, as they favour charge separation at the initial stages of the photogeneration process. In addition, as discussed in section 5.2, the donor group raises the HOMO level of **12**. The higher HOMO level makes it easier for holes to hop between carbazole moieties. In a word, the donor group in **12** can improve both photogeneration efficiency and charge mobility, with both effects contributing to the higher photoconductivity of **12** when compared to **1**.

Similarly, as shown in Fig. 5.12, the presence of the donor group in **7** can explain the higher photoconductivity of **7** when compared to **6**. The higher photoconductivity of **11** with respect to **12**, as shown in Fig. 5.13, can also be explained by the stronger donor group present in **11**, but since the difference between the electron-donating properties of the two groups is not large, the difference in photoconductivity is also not large.



$$\sigma/\alpha I = 1.7 \cdot 10^{-16} \text{ Scm}^2\text{W}^{-1}$$

$$\sigma/\alpha I = 9.3 \cdot 10^{-15} \text{ Scm}^2\text{W}^{-1}$$

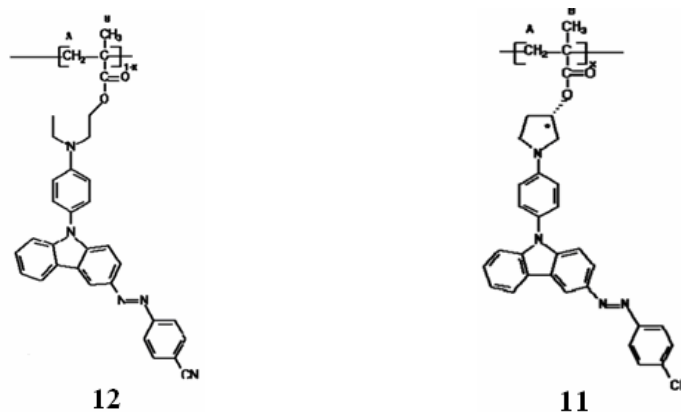
Fig. 5.11. Photoconductivity of polymers **1** and **12**, at  $\lambda = 632.8\text{nm}$  and electric field  $E = 18 \text{ V}/\mu\text{m}$ .



$$\sigma/\alpha I = 4.3 \cdot 10^{-18} \text{ Scm}^2\text{W}^{-1}$$

$$\sigma/\alpha I = 5.5 \cdot 10^{-14} \text{ Scm}^2\text{W}^{-1}$$

Fig. 5.12. Photoconductivity of polymers **6** and **7**, with  $\lambda = 532\text{nm}$  and electric field  $E = 35 \text{ V}/\mu\text{m}$ .



$$\sigma/\alpha I = 9.3 \cdot 10^{-15} \text{ Scm}^2\text{W}^{-1}$$

$$\sigma/\alpha I = 4.8 \cdot 10^{-14} \text{ Scm}^2\text{W}^{-1}$$

Fig. 5.13. Photoconductivity of polymer **11** and **12**, with  $\lambda = 632.8 \text{ nm}$  and electric field  $E = 18 \text{ V}/\mu\text{m}$ .

However, a higher HOMO energy does not always correspond to a higher photoconductivity. Let us focus on the photoconductivity of **8** and **9**, as shown in Fig. 5.14, as an example. Although the linking group in **8** is a better electron-donating group, the photoconductivity in **8** is lower than in **9**. This might be explained with the lower mobility of the carbazole pendant in **8**, due the presence of a closed ring in the linking group. Such reduced mobility might in fact hinder the possibility of obtaining favourable (for charge transfer) relative orientations among the carbazole pendants.

Considering the results shown in Fig. 5.11-14, we can say that in general the presence of a chemical entity with electron-donating properties coupled with the carbazole group can improve photoconductivity, although this is certainly not the only relevant factor.

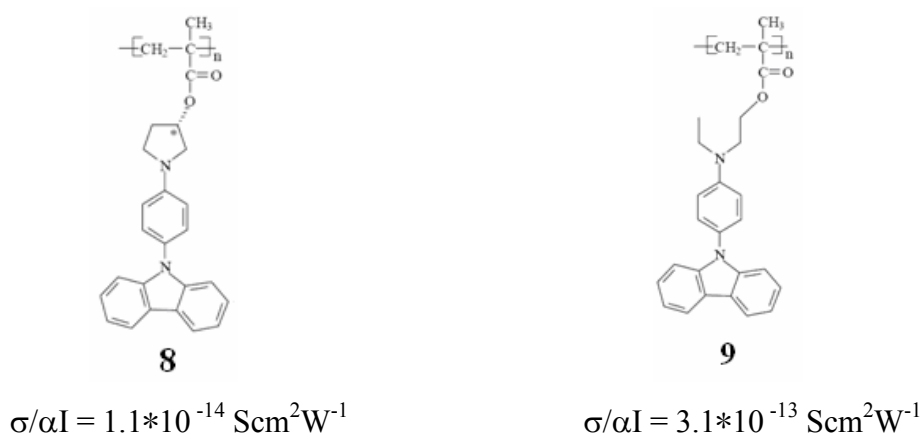


Fig. 5.14. Photoconductivity of polymers **8** and **9**, with  $\lambda = 532\text{nm}$  and electric field =  $35 \text{ V}/\mu\text{m}$ .

#### 5.4 Photoconductivity of azo-polymers without carbazole

In addition to polymers **1** - **12**, we also studied polymers **13** – **16**, which do not contain a carbazole group, as shown in Table. 5.1. Polymers **13** and **14** share the same chemical structure, but polymer **13** is a racemic mixture while polymer **14** is not. The preparation of samples with **13** and **14** using the method described in section 4.1 proved to be problematic because the polymers never became soft enough before their decomposition on the hot plate. After several failed attempts, we decided to study instead polymers **15** and **16**, which were easier to handle. Again, polymers **15** and **16** share the same chemical structure but polymer **15** is racemic mixture while polymer **16** is not. Because of the lack of a carbazole group, we initially assumed that both polymers were

not photoconductors. However, tests were carried out in order to experimentally verify such assumption. The photoconductivity performance of polymer **15** is shown in Fig. 5.15: not only we measured a photoconductivity, but its value is even comparable to the photoconductivity of some polymers with carbazole groups, such as polymers **1** and **4**, and even higher than the photoconductivity of polymer **6**. The photoconductivity of polymer **16** is similar to that of polymer **15**. To our knowledge, this is the first time that photoconductivity is recorded in azo-polymers.

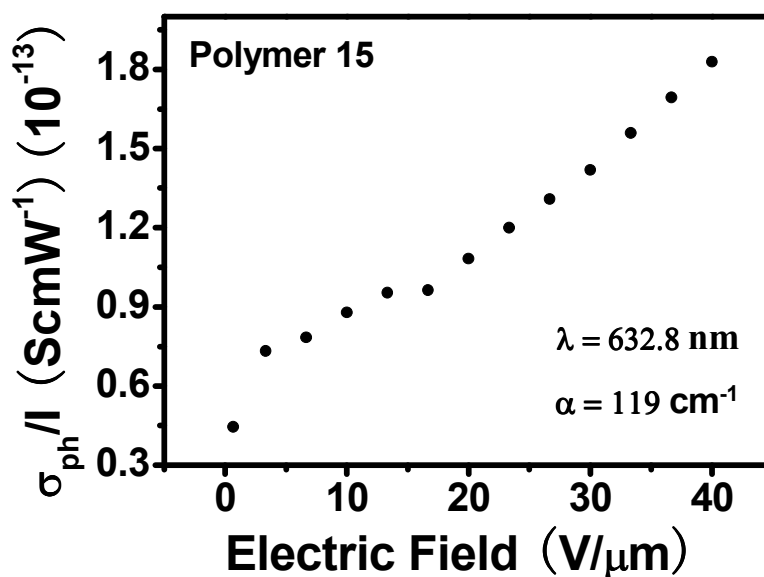


Fig. 5.15. Photoconductivity of polymer **15**.

### 5.5 Hole mobility measurement

The photoconductivity of polymers **1** – **12** is based on the presence of a carbazole group, which is well known for its hole transporting properties. The mobility can be measured using several techniques, including TOF and SCLC, that were described in section 4.4. We first tried to perform TOF experiments, but we were not able to obtain current curves good enough to extract a mobility value. We then tried to obtain mobility using the SCLC technique. An ohmic contact is necessary for SCLC. Considering the HOMO levels of the polymers, we chose Au (5.1 eV) as anode and ITO (4.6 eV) as cathode: the general set-up is shown in Fig. 4.12. Polymer **1** and **10** were excluded from measurements because their HOMO level is too far from the work function of Au. We tried to prepare samples of the other polymers using the method described in section 4.4.2.

However, we were only able to obtain good samples for **3**, **6**, **7** and **9**. For the other polymers, we could not get good samples by spin-coating because the resulting surfaces were rough or because of the presence of pinholes that shorted the electrodes.

The measurement results for **3** are shown in Fig. 5.16. The red line in Fig. 5.16 represents a linear dependence of current on electric field, while the green line represents quadratic dependence. The intersection point of the two straight lines is ( $V$ ,  $I$ ) and the  $V_T$  value can be obtained as described in section 4.4.2.

### Polymer 3:

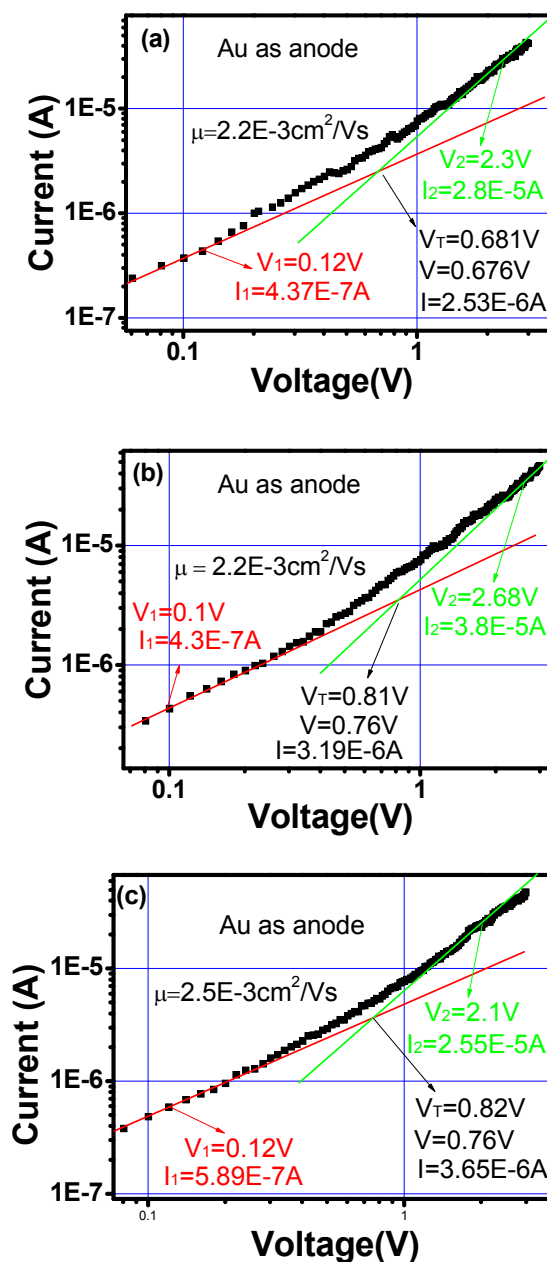


Fig.5.16. I-V curve of polymer **3** with Au as anode and ITO as cathode.

The results in Fig. 5.16 were obtained on three different pixels on the same sample. The thickness of **3**, measured by a profilometer, was  $d = 1.35 \mu\text{m}$  and the relative dielectric constant  $\epsilon = 10.7$ . The width of the ITO stripe was 0.5 mm and the width of Au was 2.15 mm in Fig. 5.16 (a), (b) and 1.15 mm in Fig. 5.16 (c). The difference between the  $V_T$  and  $V$  as shown in Fig. 5.17 is small; hence the I-V curve is believable for the calculation of mobility. The hole mobility  $\mu$  was calculated according to Eq. (4.4) and it ranges between  $2.2 \text{ E-3 cm}^2/\text{Vs}$  to  $2.5 \text{ E-3 cm}^2/\text{Vs}$ .

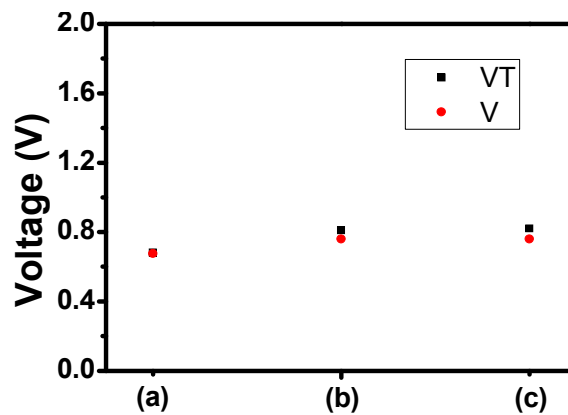


Fig. 5.17.  $V_T$  and  $V$  obtained from I-V curves of polymer **3**.

After the measurements, the electric field was inverted. As we have discussed in section 4.4.2, the current should be lower and the quadratic behavior should not be seen. Results, as shown in Fig. 5.18, confirmed these expectations.

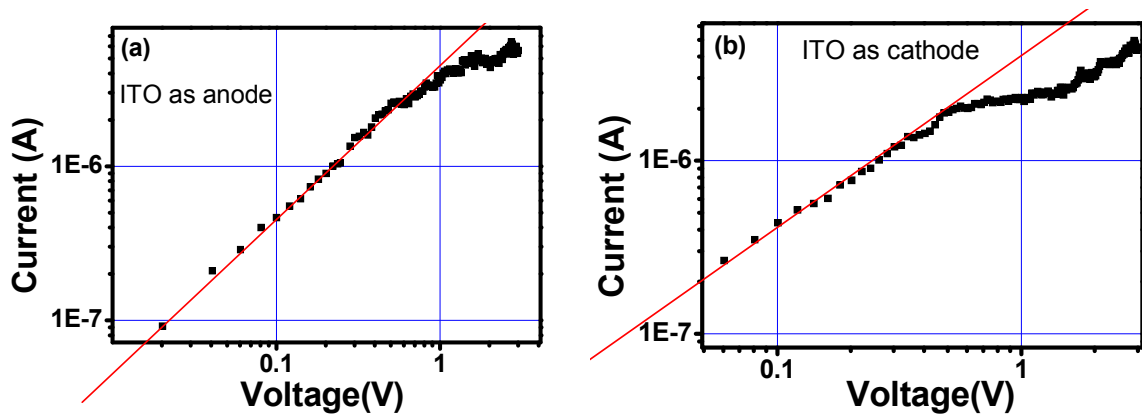


Fig. 5.18. I-V curve of polymer **3** with Au as cathode and ITO as anode.



## Polymer 6:

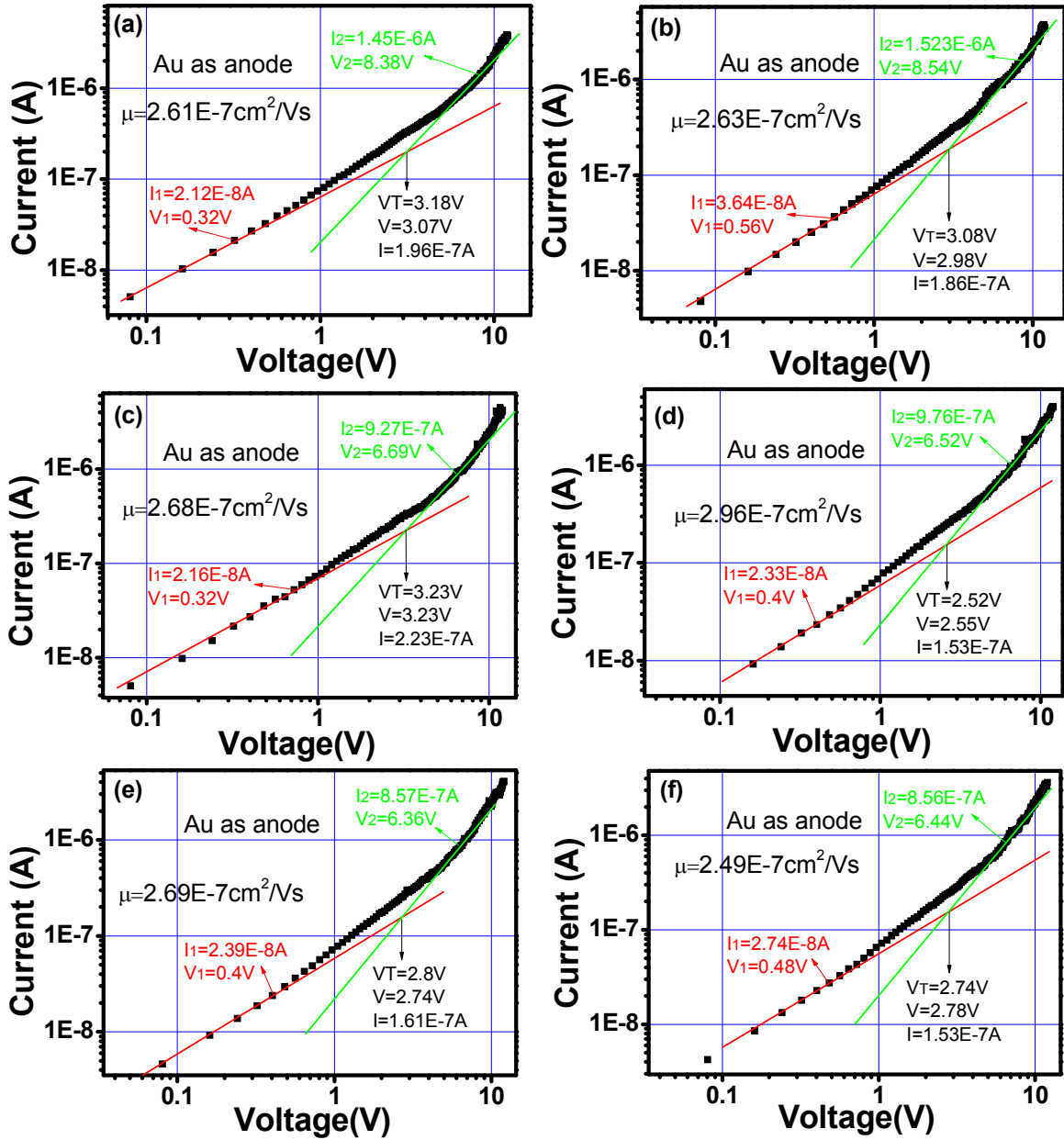


Fig. 5.19. I-V curve of polymer 6 with Au as anode and ITO as cathode.

All the results in Fig. 5.19 were obtained on the same pixel of a sample and are shown to illustrate reproducibility. The thickness of the polymer was  $d = 500 \text{ nm}$  and the relative dielectric constant  $\epsilon = 10$ . The width of the ITO stripe was  $0.5 \text{ mm}$  and the width of Au was  $1.5 \text{ mm}$ . The difference between  $V_T$  and  $V$  as shown in Fig. 5.20 is small enough, and hole mobility ranges between  $2.49 \text{ E-}8 \text{ cm}^2/\text{Vs}$  to  $2.96 \text{ E-}8 \text{ cm}^2/\text{Vs}$ .

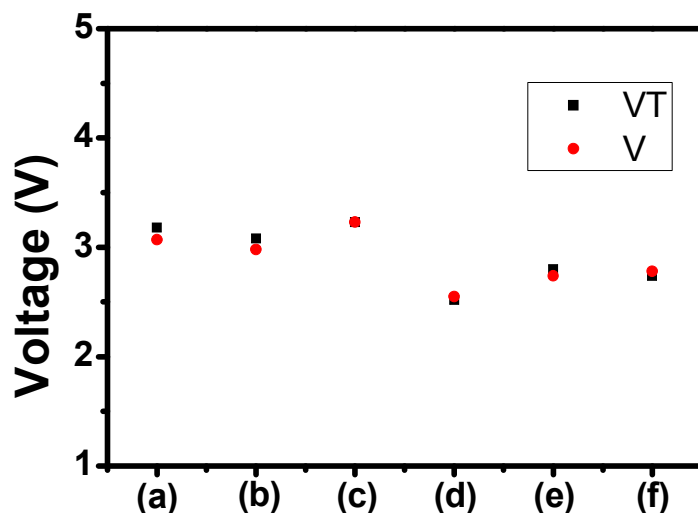


Fig. 5.20.  $V_T$  and  $V$  obtained from I-V curves of polymer 6.

After the measurements, the electric field was inverted and the resulting I-V curves are shown in Fig. 5.21. Because the HOMO level of polymer 6 (5.3 eV) is far from the work function of ITO, holes were not injected from ITO (anode), the currents were much lower than in the other case (Au as anode) and quadratic behavior in the current was not observed.

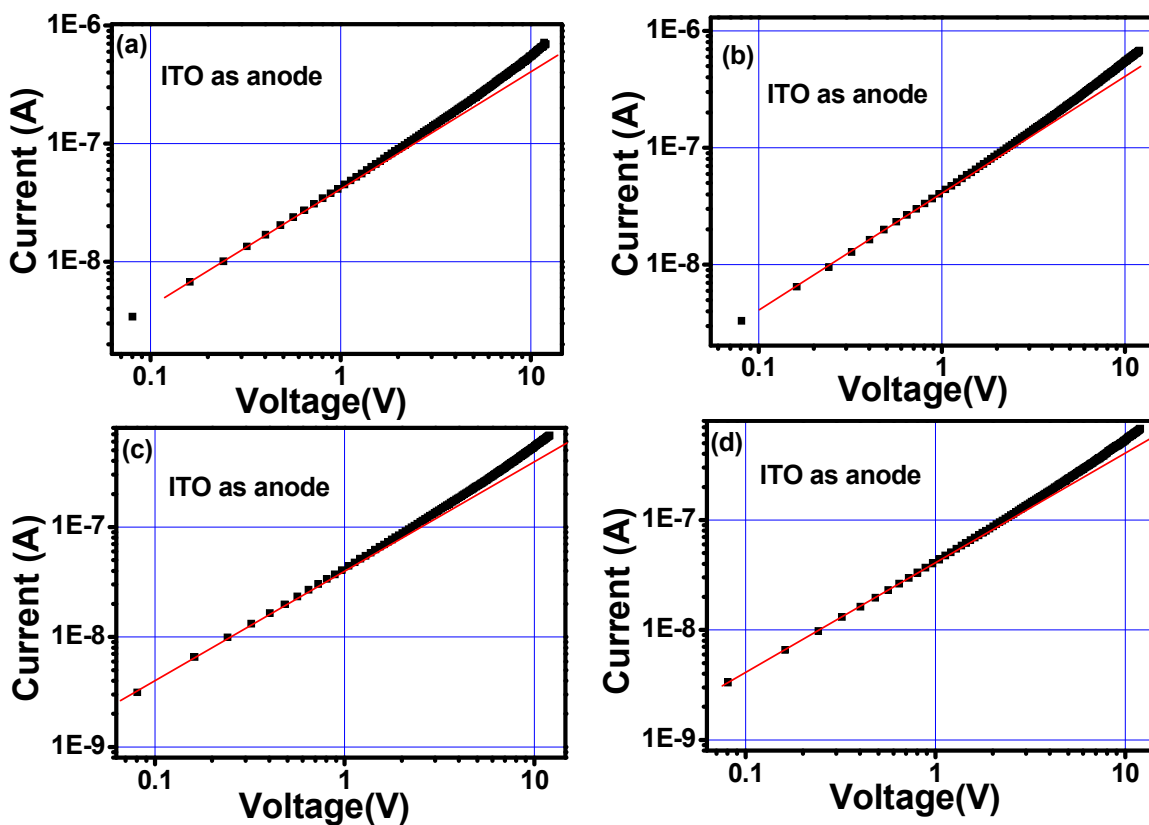


Fig. 5.21. I-V curve of polymer 6 with Au as cathode and ITO as anode.

## Polymer 7:

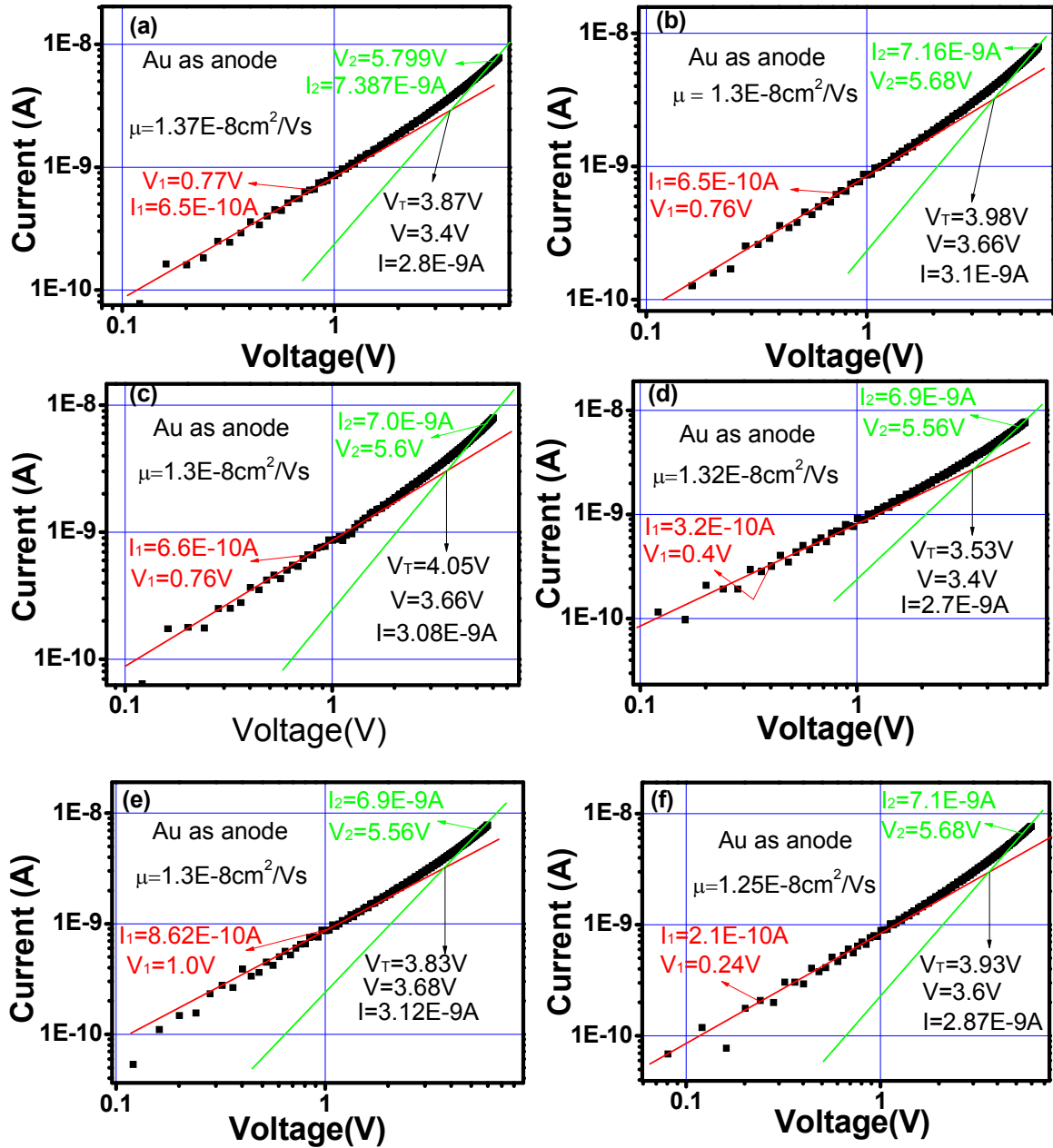


Fig. 5.22. I-V curve of polymer 7 with Au as anode and ITO as cathode.

The results shown in Fig. 5.20 were obtained on the same sample. The results in Fig. 5.22 (a), (b), (c) were obtained on the same pixel, and the results in Fig. 5.22 (d), (e), (f) were obtained on another pixel of the same sample. The thickness of 7 was  $d = 700$  nm and the relative dielectric constant  $\epsilon = 10.7$ . The width of the ITO stripe was 0.5 mm and the width of Au was 1.85 mm in Fig. 5.22 (a), (b), (c) and 1.65 mm in Fig. 5.22 (d), (e), (f). The difference between the  $V_T$  and  $V$  as shown in Fig. 5.23 is small enough, and

hole mobility ranges between  $1.25 \text{ E-}8 \text{ cm}^2/\text{Vs}$  to  $1.37 \text{ E-}8 \text{ cm}^2/\text{Vs}$ .

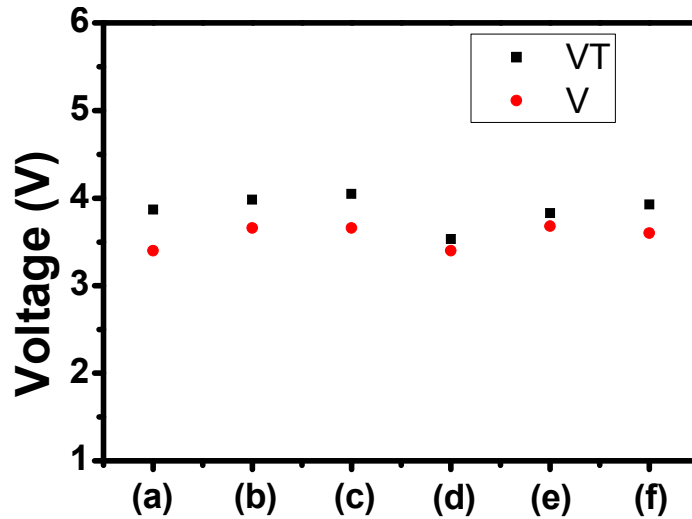


Fig. 5.23.  $V_T$  and  $V$  obtained from I-V curves of polymer 7.

After the measurements, the sign of the electric field was inverted (ITO anode) and the I-V curves on the same pixels are shown in Fig. 5.24 (a) and (b), respectively. In contrast to the results obtained for **3** and **6**, the current was of the same order as in the case of the Au anode and both linear and quadratic behaviors were observed. This can be understood if we consider that the HOMO level of **7** is 4.8 eV. Since this value is close to both the work function of Au (5.1 eV) and ITO (4.6 eV), holes can be injected equally well from both electrodes, i. e. the contact is Ohmic in both cases.

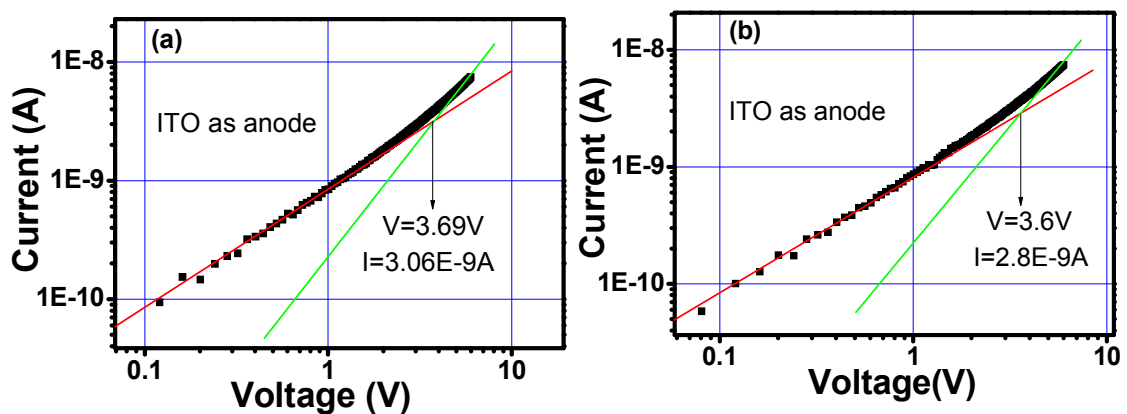


Fig. 5.24. I-V curve of polymer 7 with Au as cathode and ITO as anode.

## Polymer 9:

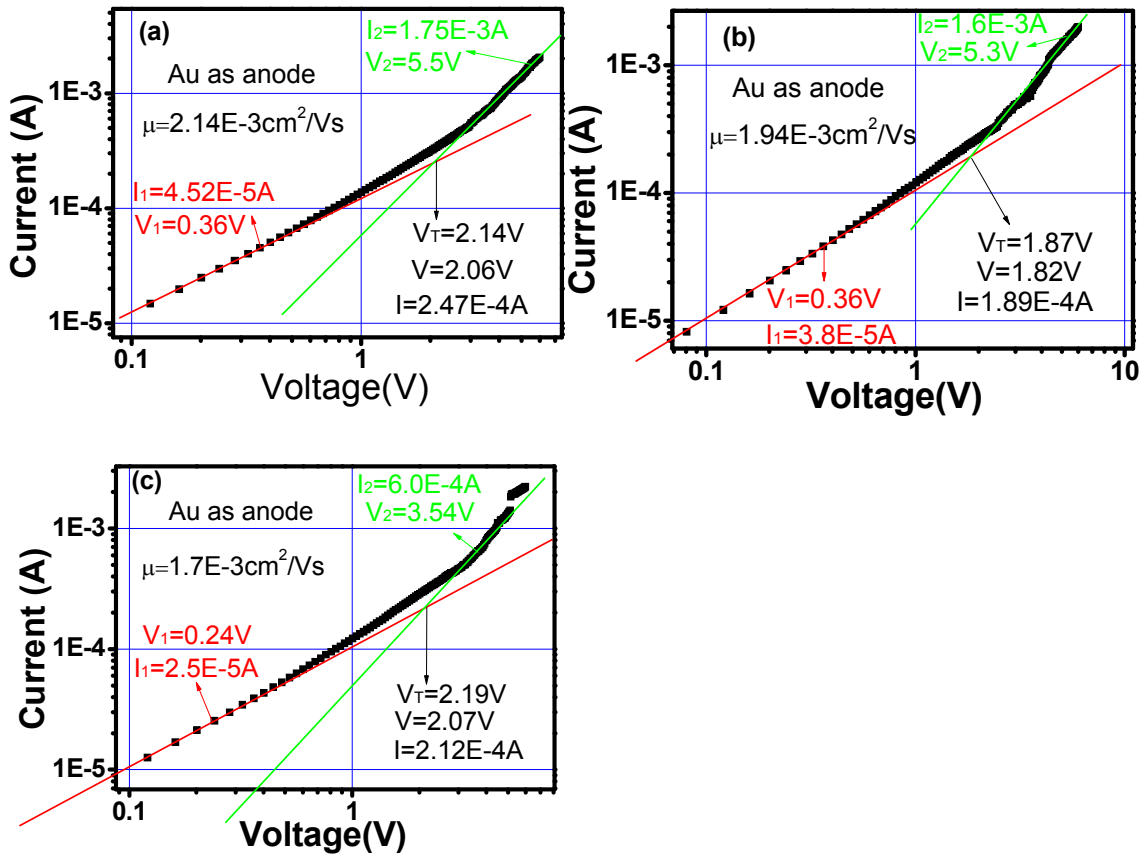
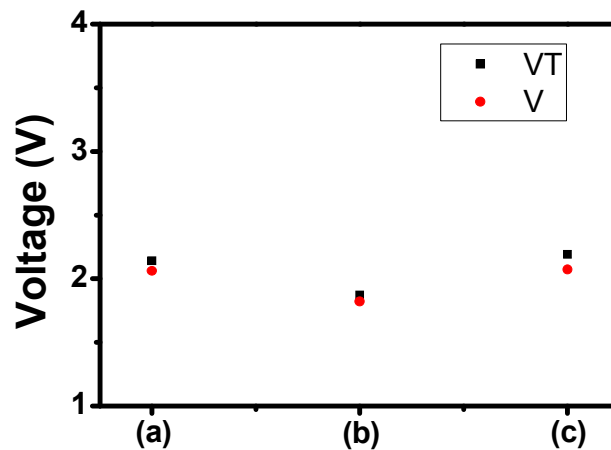


Fig. 5.25. I-V curve of polymer 9 with Au as anode and ITO as cathode.

Fig. 5.26.  $V_T$  and  $V$  obtained from I-V curves of polymer 9.

The results shown in Fig. 5.25 were obtained on the same pixel. The thickness of polymer 9 was  $d = 400 \text{ nm}$  and the relative dielectric constant  $\epsilon = 2.9$ . The width of the

ITO stripe was 0.5 mm and the width of Au was 1.3 mm. The difference between the  $V_T$  and  $V$  as shown in Fig. 5.26 is small enough, and the hole mobility ranges between  $1.7 \text{ E-3 cm}^2/\text{Vs}$  to  $2.14 \text{ E-3 cm}^2/\text{Vs}$  as shown in Fig.5.25.

After the measurements, the electric field was inverted and the I-V curve is shown in Fig. 5.27. We found that the current measured using ITO as anode is of the same order as the current obtained for the Au anode, but without quadratic behavior. This fact is probably linked to the fact that, given the value of the HOMO (5.1 eV), the contact is just at the limit between an Ohmic and a non-Ohmic behaviour when the ITO electrode is the anode.

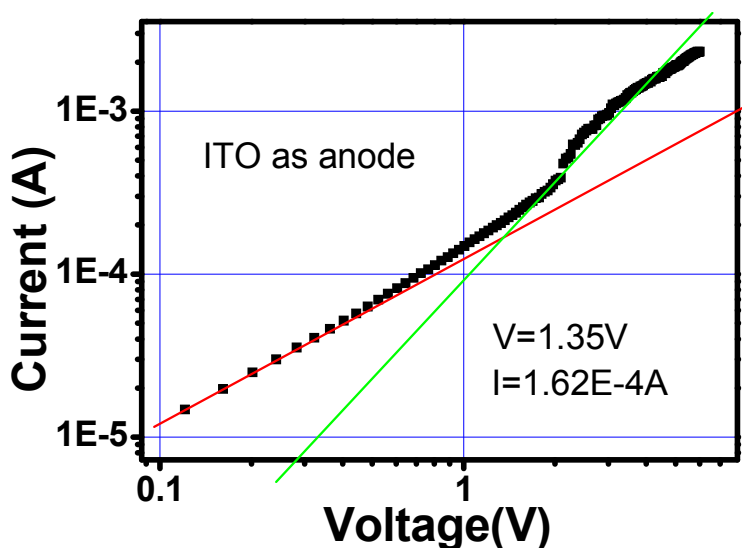


Fig. 5.27. I-V curve of polymer **9** with Au as cathode and ITO as anode.

Summarizing, we found that the hole mobilities of **3** and **9** are of the order of  $1.5\text{-}2.5 \text{ E-3 cm}^2/\text{Vs}$ , which is several orders of magnitude higher than the mobility of **6** and **7**. Polymers **3** and **6** have the same HOMO level (5.3 eV), but there is a huge difference between their hole mobility. Similarly, the higher HOMO level of **7** (4.8 eV) does not reflect a higher mobility. This indicates that the HOMO level does not play an important role in determining mobility. Comparing **3** and **6** the much higher mobility of **3** might be connected with the higher conformational freedom expected in co-polymers or with some other effect due to the azo chromophore group.

One important result comes from the comparison of the photoconducting properties of **6** and **7**. Polymer **6** shows a slightly higher hole mobility but a photoconductivity that is 4 orders of magnitude lower than in **7**. As photoconductivity is

the combined effect of mobility and charge photogeneration, this can only be explained by assuming for **7** a photogeneration efficiency which is several orders of magnitude higher than in **6**. Although more detailed analyses are required, this result seems to correlate a higher photogeneration efficiency with the electron-donating properties of the linking group.

**BIBLIOGRAPHY**

1. J. Day, S. Subramanian, J. E. Anthony, Z. Lu, R. J. Twieg, O. Ostroverkhova. *J. Appl. Phys.*, **008**, 103, 123715.
2. J. V. Grazulevicius, P. Strohhriegl, J. Pielichowski, K. Pielichowski. *Prog. Polym. Sci.*, **2003**, 28, 1297.
3. W. E. Moerner, A. Grunnet-Jepsen, C. L. Thompson. *Annu. Rev. Mater. Sci.*, **1997**, 27, 583.
4. P. N. Prasad, M. E. Orczyk, J. Zieba. *J. Phys. Chem.*, **1994**, 98, 8699.
5. K. Meerholz, B. Volodin, B. Sandalphon, N. Kippelen, N. Peyghambarian. *Nature* **1994**, 371, 497.
6. I. K. Moon, S. Choi, N. Kim. *Polymer*, **2007**, 48, 3461.
7. S. Ducharme, J. C. Scott, R. J. Twieg, W. E. Moerner. *Phys. Rev. Lett.*, **1991**, 66, 1846.
8. D. Wright, M. A. Diaz-Garcia, J. D. Casperson, M. DeClue, W. E. Moerner, R. J. Twieg. *Appl. Phys. Lett.*, **1998**, 73, 1490.
9. F. Würther, R. Wortmann, K. Meerholz. *ChemPhysChem.*, **2002**, 2, 17.
10. O. Ostroverkhova, W. E. Moerner. *Chem. Rev.*, **2004**, 104, 3267.
11. M. A. Diaz-Gracia, D. Wright, J. D. Casperson, B. Smith, E. Glazer, W. E. Moerner. *Chem. Mater.*, **1999**, 11, 1784.
12. A. Grunnet-Jepsen, D. Wright, B. Smith, M. S. Bratcher, M. S. DeClue, J. S. Siegel. *Chem. Phys. Lett.*, **1998**, 291, 553.
13. H. J. Bolink, V. V. Krasnikov, P. H. J. Kouwer, G. Hadziioannou. *Chem. Mater.*, **1998**, 10, 3951.
14. S. J. Ziker. *ChemPhysChem.*, **2000**, 1, 72.
15. J. Shi, M. M. Huang, Z. J. Chen, Q. H. Gong, S. K. Cao. *J. Mater. Sci.*, **2004**, 39, 3783.
16. S. Grigalevicius. *Synth. Met.*, **2006**, 156, 1.
17. F. Laquai, G. Wegner, H. Bässler. *Phil. Trans. R. Soc. A*, **2007**, 365, 1473.
18. N. Karl. *Synth. Met.*, **2003**, 133, 649.
19. W. Warta, N. Karl. *Phys. Rev. B*, **1985**, 32, 1172.
20. V. Podzorov, V. M. Pudalov, M. E. Gershenson. *Appl. Phys. Lett.*, **2003**, 82, 1739.
21. Y. J. Shirota. *Mater. Chem.*, **2005**, 15, 75.
22. T. Kreouzis, D. Poplavskyy, S. M. Tuladhar, M. Campoy-Quiles, J. Nelson, A. J. Campbell, D. D. C. Bradley. *Phys. Rev. B*, **2006**, 73, 235201.
23. H. Siringhaus, P. J. Brown, R. H. Friend, M. M. Nielsen, K. Bechgaard, B. M. W. Langeveld-Voss, A. J. H. Spiering, R. A. J. Janssen, E. W. Meijer, P. Herwig, D. M. de Leeuw. *Nature*, **1999**, 401, 685.
24. I. McCulloch, M. Heeney, C. Bailey, K. Genevicius, I. Macdonald, M. Shkunov, D. Sparrowe, S. Tierney, R. Wagner, W. M. Zhang, M. L. Chabinyc, R. J. Kline, M. D. McGehee, M. F. Toney. *Nat. Mater.*, **2006**, 5, 328.
25. H. Siringhaus, R. J. Wilson, R. H. Friend, M. Inbasekaran, W. Wu, E. P. Woo, M. Grell, D. D. C. Bradley. *Appl. Phys. Lett.*, **2000**, 77, 406.
26. O. Ostroverkhova, K. D. Singer. *J. Appl. Phys.*, **2002**, 92, 1727.
27. T. Jakob, S. Schloter, U. Hofmann, M. Grasruck, A. Schreiber, D. Haarer. *J. Chem. Phys.*, **1999**, 111, 10633.
28. A. Goonesekera, S. Ducharme, J. M. Takacs, L. Zhang. *J. Chem. Phys.*, **1997**, 107, 8709.
29. A. Goonesekera, S. Ducharme. *J. Appl. Phys.*, **1999**, 85, 6506.



30. M. A. Lampert, P. Mark. '*Current Injection in Solids*', Academic Press, New York, **1970**.
31. V. D. Mihailetschi, J. K. J. Van Duren, P. W. M. Blom, J. C. Hummelen, R. A. Janssen, J. M. Kroon, M. T. Rispens, W. J. H. Verhees, M. M. Wienk. *Adv. Funct. Mater.*, **2003**, 13, 43.
32. G. G. Malliaras, V. V. Krasnikov, H. J. Bolink, G. Hadziioannou. *Phys. Rev. B.*, **1995**, 52, 14324.
33. S. J. Zilker, M. Grasruck, J. Wolff, S. Schloter, A. Leopold, M. A. Kol'chenko, U. Hofmann, A. Schreiber, P. Strohhriegl, C. Hohle, D. Haarer. *Chem. Phys. Lett.*, **1999**, 306, 285.
34. S. Bartkiewicz, A. Miniewicz, B. Sahraoui, F. Kajzar. *Appl. Phys. Lett.*, **2002**, 81, 3705.
35. G. Juska, K. Arlauskas, M. Viliunas, J. Kocka. *Phys. Rev. Lett.*, **2000**, 84, 4946.
36. G. Juska, K. Arlauskas, M. Viliunas, K. Genevicius, R. Osterbacka, H. Stubb. *Phys. Rev. B*, **2000**, 62, R16235.
37. G. Juska, K. Genevicius, K. Arlauskas, R. Osterbacka, H. Stubb. *Phys. Rev. B*, **2002**, 65, 233208.
38. L. Kulikovskiy, D. Neher, E. Mecher, K. Meerholz, H. H. Horhold, O. Ostroverkhova. *Phys. Rev. B*, **2004**, 69, 125216.
39. N. Marc, J. Y. Moisan, N. Wolffer, B. Andre, R. Lever. *Philos. Mag. B*, **1996**, 74, 81.
40. D. Basu, L. Wang, L. Dunn, B. Yoo, S. Nadkarni, A. Dodabalapur. *App. Phys. Lett.*, **2006**, 89, 242104.
41. P. Günter, J.-P. Huignard. '*Photorefractive Materials and Their Applications 2*', Springer, **2007**.

## Chapter 6

### RESULTS: PHOTOREFRACTIVITY

As already discussed, photorefractive polymers may be divided in two general classes: low  $T_g$  PR polymers and high  $T_g$  PR polymers, depending on their  $T_g$ s being above or below the operational temperature, usually room temperature (RT). Low  $T_g$  PR polymers usually show better PR performance because of the two contributions to the modulation of the refractive index: the electro-optic and the birefringence contributions. However, low  $T_g$  polymers are often mechanically and chemically instable. High  $T_g$  PR polymers are more stable, but their PR performance is worse, since no birefringence contribution is present. All the azo-polymers listed in Table 5.1 have high  $T_g$ , above 100 °C, and this makes them stable at room temperature. As discussed in chapter 3, photoorientation and photoassisted poling are allowed for high  $T_g$  azo-polymers at room temperature. In this chapter, we will describe our attempts at exploiting such light-induced mobility in order to add a birefringence contribution to the refractive index modulation and to improve the PR performance at room temperature in these high  $T_g$  azo-polymers.

#### 6.1 Polymers and their functional groups

Polymers **1 - 4** shown in Table 5.1 were first chosen to study the PR properties in high  $T_g$  multifunctional media. All the four polymers can be classified as fully functionalized polymers. Homopolymeric polymer **1** bears three distinct functional groups (i.e., the azoaromatic, carbazole and chiral groups of one single configuration) directly linked to a single side chain. Copolymeric compounds **2 - 4** have two different side-chains: one co-monomer with either a (*S*)-3-hydroxy pyrrolidinyll (**2**) or a (*S*)-2-hydroxy succinimide (**3,4**) ring as a chiral moiety, covalently linked to a photochromic azoaromatic group, substituted (**2**) or not (**3,4**) in the 4'-position with a nitro (electron withdrawing) residue. In the side-chain of the second kind of co-monomer, the same chiral rings are linked to photoconductive carbazolic chromophores. In **2 - 4**, the conformationally rigid pyrrolidine or succinimide rings increase the stiffness of the macromolecules and induce high  $T_g$  values (see Table 6.1).

Table 6.1. Relevant characterization data of the investigated polymeric derivatives.

Compound	$\bar{M}_n$ [a]	$\bar{M}_w/\bar{M}_n$ [a]	$\alpha$ [b]	$T_g$ [c]	$T_d$ [d]	$\sigma_{ph}/I$ [e]
	(g mol <sup>-1</sup> )		(cm <sup>-1</sup> )	(°C)	(°C)	( $\Omega^{-1}$ cm W <sup>-1</sup> )
<b>1</b>			1811			
Poly[( <i>S</i> )-MLECA]	13400	1.8	168	147	363	$6.15 \cdot 10^{-14}$
<b>2</b>						
Poly[( <i>S</i> )-(-)-MECP-co-( <i>S</i> )-MAP-N] x = 0.25	6700	1.5	(692)	(107)	328	$(2.12 \cdot 10^{-10})$
<b>3</b>						
Poly[( <i>S</i> )-(+)-MECSI-co-( <i>S</i> )-(+)-MOSI] x = 0.24	9400	1.9	68	227	297	$< 10^{-15}$
<b>4</b>						
Poly[( <i>S</i> )-(+)-MECSI-co-( <i>S</i> )-(+)-MOSI] x = 0.76	10200	2.0	75	228	298	$4.10 \cdot 10^{-13}$

[a] Determined by SEC in THF solution at 25°C, [b] Measured on solid films at  $\lambda = 632.8$  nm (between brackets the values for the mixtures containing 20% of the DDP plasticizer), [c] Glass transition temperature of pure compounds determined by DSC at 10°C/min heating rate under nitrogen flow (between brackets the values for the mixtures containing 20% of the DDP plasticizer), [d] Initial decomposition temperature as determined by TGA at 20°C/min heating rate under air flow, [e] Photoconductivity normalized with respect to the light intensity  $I = 0.8$  W/cm<sup>2</sup>, measured at an applied field  $E = 30$  V/ $\mu$ m, using light with a wavelength  $\lambda = 632.8$  nm (between brackets the values for the mixtures containing 20% of the DDP plasticizer).

## 6.2 Light induced birefringence

Light induced birefringence of polymer **1** was measured at room temperature by

using the steady state ellipsometry set-up already shown in Fig. 4.20, using sample thicknesses in the 20-30  $\mu\text{m}$  range. The wavelengths of the writing beam and probe beam were both  $\lambda = 632.8 \text{ nm}$ . The intensity of the writing beam was  $I_W = 0.8 \text{ W/cm}^2$ , while the intensity of the probe beam was only  $I_P = 4 \times 10^{-4} \text{ W/cm}^2$ . The diameter of the writing beam was 2 mm while the diameter of the probe beam was only 0.8 mm.

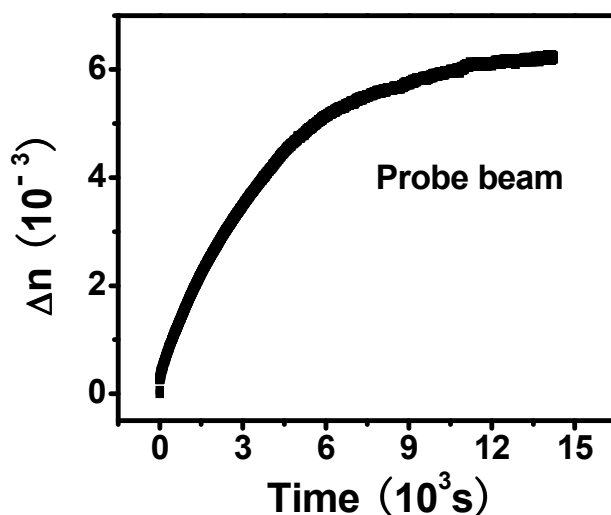


Fig. 6.1. Light-induced birefringence in the sample of polymer 1.

Light-induced birefringence is clear in Fig. 6.1 and the increase of the transmission can be explained by the photoorientation of azobenzene chromophores as shown in Fig. 3.5.

The same experiments were also carried out on samples of polymers 2 - 4, with the same conditions. Similar values of birefringence were also obtained for polymer 2. For polymers 3 and 4, light-induced birefringence was hardly detectable at  $\lambda = 632.8 \text{ nm}$  because of the lower absorption, but it became again of the order of  $1 \times 10^{-3}$  when the wavelength of the writing beam and probe beam were  $\lambda = 532 \text{ nm}$ , where absorption is higher (see Table 5.2). The light-induced birefringence proves that chromophores reorientation in our azo-polymers can be induced by light at temperature well below  $T_g$  (see Table 6.1).

Similar experiments were also carried out without the writing beam, but applying an electric field  $E = 20 \text{ V}/\mu\text{m}$  along the sample normal, in order to test if the field can also reorient azobenzene chromophores. However, no field-induced birefringence was

detected, as it was expected given their high  $T_g$  values.

### 6.3 Light-induced surface relief grating

As we have discussed in section 3.4 and 3.7.3, there is another light-induced phenomenon associated with trans-cis isomerization in azo-polymers, namely the formation of surface relief gratings which are associated with the movement of massive amounts of material over large distances, even micrometers.<sup>4</sup> This phenomenon is also known to be active at temperatures well below  $T_g$ .<sup>5,6</sup>

In order to provide further evidence of the existence of light-induced molecular mobility in the polymers under investigation, the inscription of SRG at room temperature on polymer **1** was investigated (in the Department of Industrial Chemistry and Materials, University of Bologna). The resulting 2D and 3D images of the obtained SRG are shown in Fig. 6.2.

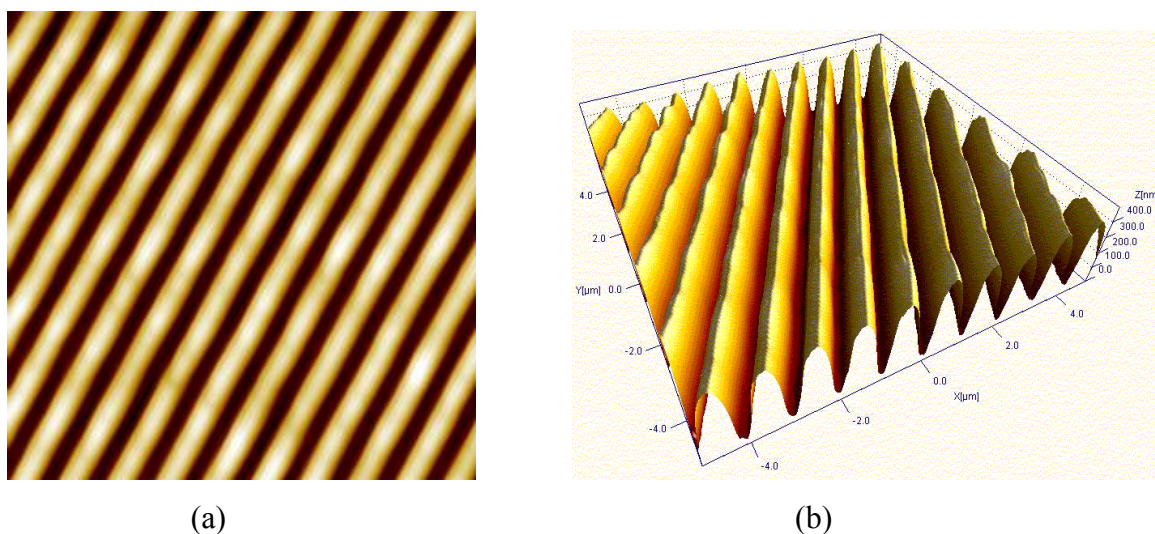


Fig. 6.2: (a) 2D AFM image 10x10  $\mu\text{m}$ , (b) relative 3D AFM image of a 400 nm thick film of polymer **1** after inscription at room temperature of surface relief grating (SRG) on the sample surface.

Based on the light-induced birefringence and surface relief grating at room temperature, we can conclude that chromophores reorientation in these azo-polymers can be induced by light at temperatures well below  $T_g$ .

## 6.4 Effect of illumination with a single light beam

One beam experiments were carried out in order to study light-induced effects in the simplest possible experimental conditions. The set-up shown in Fig. 4.2 was used, but the power meter was substituted by a photodiode detector and the intensity of the transmission beam as a function of time was recorded. The wavelength of the linearly polarized laser was  $\lambda = 632.8$  nm and its intensity was  $I = 0.8$  W/cm<sup>2</sup>. The result on polymer **1** is shown in Fig. 6.3.

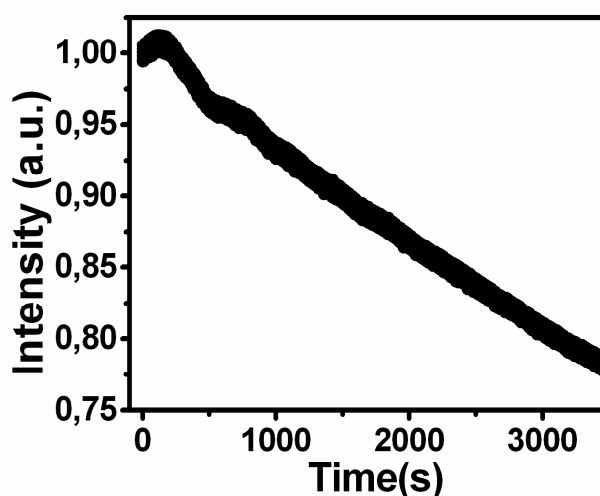


Fig. 6.3. Time dependence of light transmission through a 20  $\mu\text{m}$  thick oxidized sample of polymer **1**. The light was linearly polarized, with intensity  $I = 0.8$  W cm<sup>-2</sup> and  $\lambda = 632.8$  nm, and its propagation direction was along the sample normal.

Considering the trans-cis photoisomerization, the transmission intensity was expected to increase during irradiation, as the population of molecular transition dipoles along the direction of polarization of the laser beam is depleted. However, we observed a decrease of transmission, except for an initial increase, more evident in older samples, as shown in Fig. 6.3. The same experiments were also carried out on polymers **2** - **4**. The decrease was also found for polymer **2**, but there was no change of the transmission for polymers **3** and **4**.

The increase at the beginning in Fig. 6.3 can be explained by the azo trans-cis photoisomerization. For the decrease, we first considered that it could be attributed to the light scattering due to chromophore aggregation in domains, a phenomenon that often

accompanies light-induced azo-chromophore reorientation.<sup>7,8</sup> However, we were not able to detect any increase in scattering due to irradiation. A different explanation can be found considering that in the chemical structures of the four polymers, there are strongly electron-withdrawing cyano or nitro groups in **1** and **2**, respectively, inducing considerable permanent dipole moments, while in **3** and **4** strong molecular dipoles are not present. Given the fact that there was no transmission decrease in the single beam experiments for **3** and **4**, one reasonable explanation of the decrease shown in Fig. 6.3 can be an absorption increase due to the light-induced formation of dipolar aggregates,<sup>9</sup> which modifies absorption due to the shift of the electronic energy levels involved in the transition.

### 6.5 Light-induced absorption increase

In order to further investigate this point, the absorption coefficients of polymers **1** and **2** at different wavelengths were measured before and after irradiation.

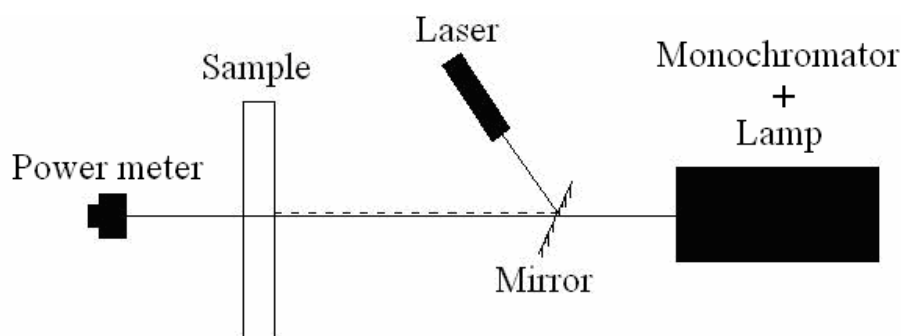


Fig. 6.4. Set-up for the measurement of absorption variation.

The set-up for the experiments is shown in Fig. 6.4 and the details of the measurements are described in the following. 1) The light intensity exiting the monochromator at different wavelengths ranging between 350 nm and 700 nm were measured by using a power meter. Such intensity, when compared to the intensity of the laser writing beam (see below) was low enough to ensure that its effects on the azo-polymer could be neglected. 2) Samples (with a thickness in the 20-30  $\mu\text{m}$  range) were placed perpendicularly to the monochromator beam. 3) The absorption coefficient of the sample was measured. 4) A He-Ne laser ( $\lambda = 632.8 \text{ nm}$  and  $I = 0.8 \text{ W cm}^{-2}$ ) was turned on and a mirror was used to reflect the laser beam. The laser beam was

perpendicular to the sample and it passed through the same spot illuminated by the monochromator. Samples were illuminated for hours, until the transmission of the laser beam decreased to about half of its initial value. 5) The laser was turned off, the mirror was removed and the absorption coefficient was measured again.

The absorption coefficients of polymer **1** at different wavelengths before and after the irradiation are shown in Fig. 6.5. It is clear that the absorption coefficients increased after irradiation at all wavelengths within the measurement range, and the decrease in Fig. 6.3 can be explained by the increase of absorption.

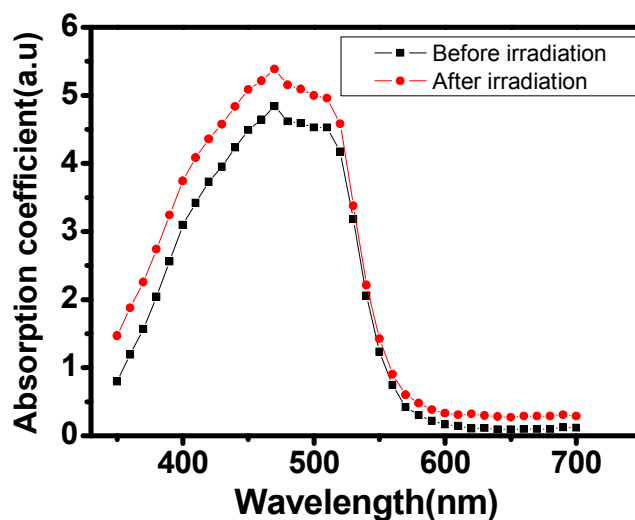


Fig. 6.5. Absorption variation of polymer **1** before and after irradiation.

The same experiment was also carried out on polymer **2** and the result is shown in Fig. 6.6.

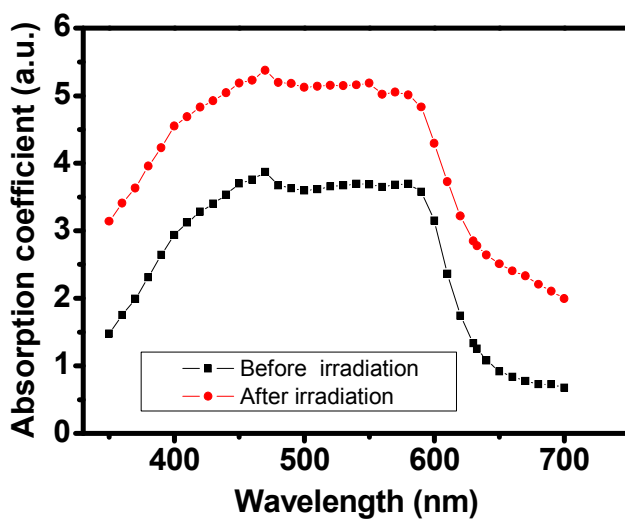


Fig. 6.6. Absorption variation of polymer **2** before and after irradiation.



## 6.6 Two-beam coupling (2BC) results

To this point, the photoconductivity and the light-induced chromophores reorientation at room temperature in our azo-polymers were demonstrated. These phenomena are prerequisites for the observation of the PR effect and experiments aiming at elucidating the PR properties of the materials under investigation will be described in the following. As already mentioned, the photorefractivity can be characterized by the observation an asymmetric energy exchange in 2BC experiments.

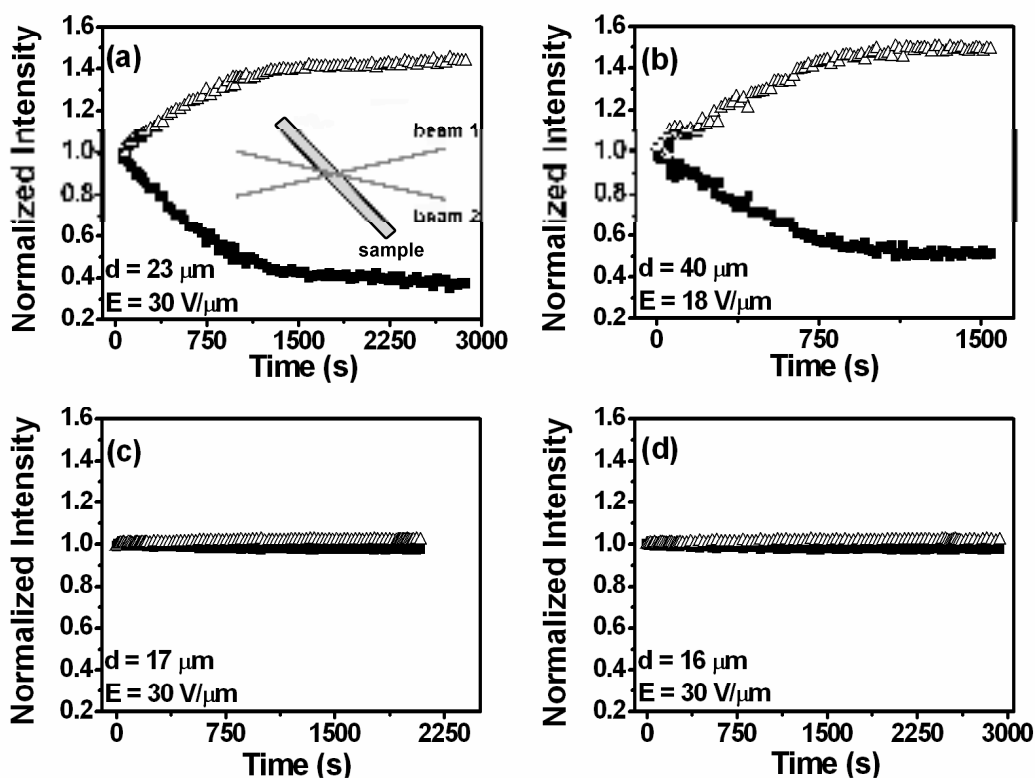


Fig. 6.7. Two-beam coupling experiment results at room temperature for polymers **1** (a), **2** (b), **3** (c) and **4** (d). Data for compound **2** have been obtained from a sample containing 20 % of the plasticizer DPP. In all cases, the grating period was  $\Lambda = 3 \mu\text{m}$ , light wavelength  $\lambda = 632.8 \text{ nm}$  and the light intensity was  $I = 0.8 \text{ W cm}^{-2}$ . The inset in (a) is a schematic illustration of the experimental set-up. All data were rescaled to eliminate the effect of the decreasing total transmission during irradiation.

2BC experiments were carried out at room temperature at  $\lambda = 632.8 \text{ nm}$  using the experimental set-up illustrated in Fig. 4.17. Considering the experimental geometry (see Fig. 4.14 (b)), in all experiments  $\Psi = 60^\circ$  and  $\theta = 10^\circ$ . According to Eq. (4.7), the grating

period was calculated as  $\Lambda = 3 \mu\text{m}$  ( $n \approx 1.6$ ). Given the sample thickness from  $16 \mu\text{m}$  to  $40 \mu\text{m}$ , the experiments were performed in the Bragg diffraction regime.<sup>10</sup> The 2BC results are shown in Fig. 6.7. The results for polymer **1** and **2** showed an obvious energy exchange between the two writing beams, which can be taken as a signature of the photorefractive nature of the photo-induced grating.<sup>11</sup> For polymer **1**,  $\Gamma = 480 \text{ cm}^{-1}$ , a very high value when compared both with absorption ( $\alpha = 168 \text{ cm}^{-1}$ ) and with literature data.<sup>12</sup> For polymer **2**,  $\Gamma = 230 \text{ cm}^{-1}$ . Compared with polymers **1** and **2**, the energy exchange in the case of polymers **3** and **4** was very small and the gain coefficient was  $\Gamma \sim 30 \text{ cm}^{-1}$  for both.

### 6.7 Inversion of energy exchange

According to Eq. (1.7), the sign of the phase shift depends on the direction of the external electric field, which means that the phase shift can be changed from a positive value to a negative value or vice versa, by inverting the direction of the electric field. Considering Eq. (4.25), the sign of the gain coefficient will also be inverted in this way, which means that the direction of energy exchange will be inverted. In order to prove this important feature, that can be considered as a confirmation of the PR nature of the obtained holograms, 2BC experiments at room temperature with different directions of external electric field were carried out. Polymer **1** was chosen to perform such experiments, and samples were prepared as described in section 4.1. In Fig. 6.8 (a), it is evident that the intensity of beam 1 increased. When the applied electric field was inverted, as shown in Fig. 6.8 (b), the intensity of beam 1 decreased, which means that the direction of energy exchange between the two beams depends on the polarity of the applied field.

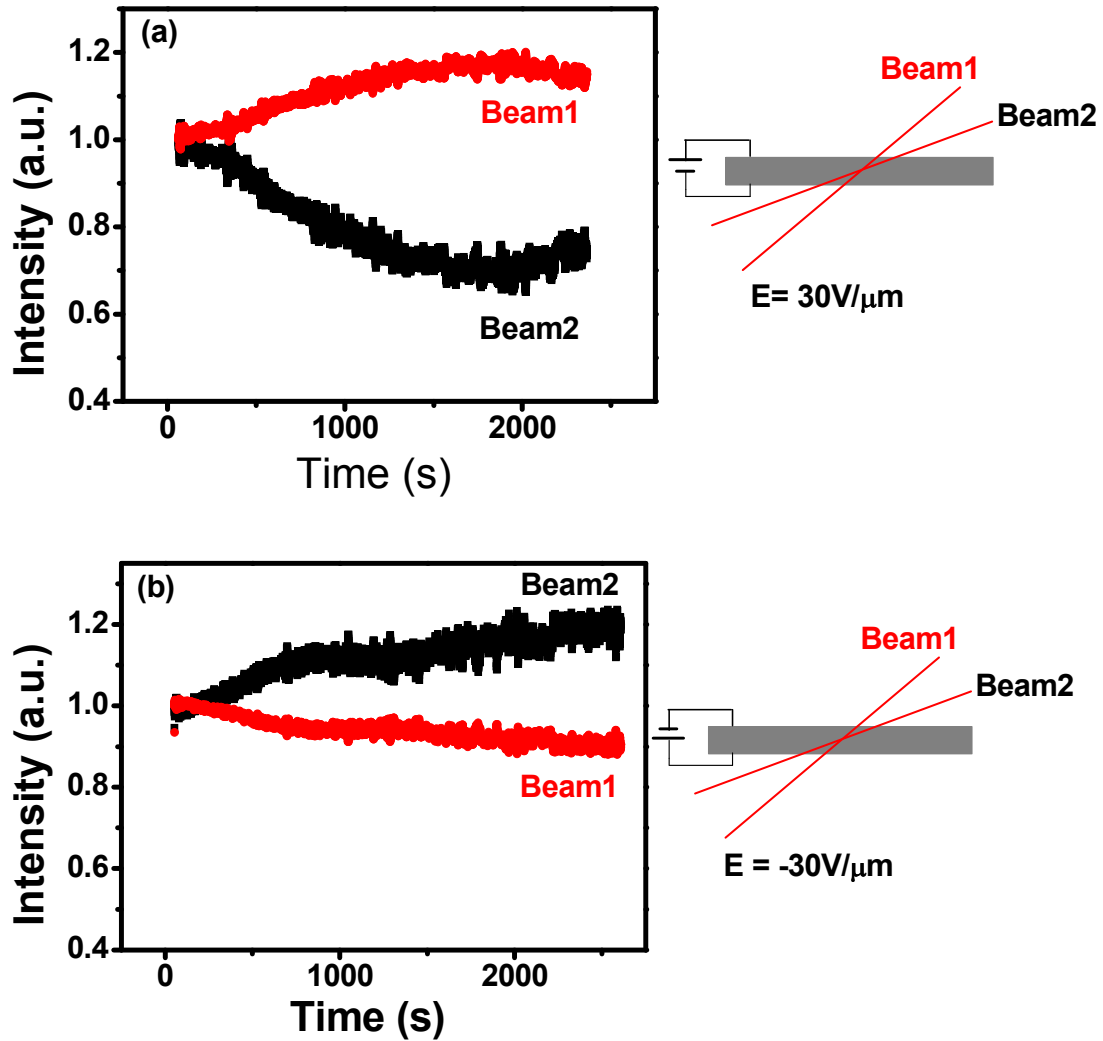


Fig. 6.8. Two-beam coupling experiment results at room temperature for polymer 1 with opposite directions of electric field. In all cases,  $\Psi = 60^\circ$ ,  $\theta = 10^\circ$  and the grating period was  $\Lambda = 3\ \mu\text{m}$ , the light wavelength was  $\lambda = 632.8\ \text{nm}$  and the light intensity was  $I = 0.8\ \text{W cm}^{-2}$ . All data were rescaled to eliminate the effect of the decreasing total transmission during irradiation.

## 6.8 Phase shift measurement

A further evidence of the PR nature of the obtained gratings can be derived from a direct measurement of the phase shift between refractive index grating and interference fringes using the moving grating technique described in section 4.9. The dependence of phase shift on electric field is shown in Fig. 6.9, according to Eq. (1.7). Charge transport is driven only by diffusion when the electric field is zero, hence the phase shift will be  $\pi/2$ , as already discussed in section 1.2. Along with the increase of the electric field, there will

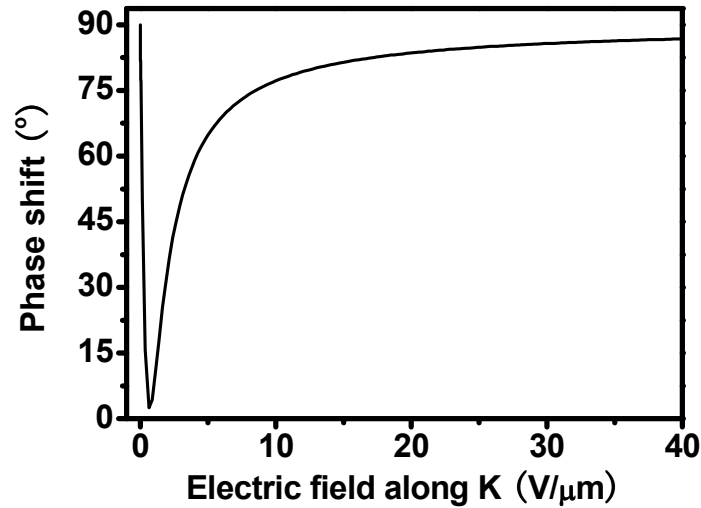


Fig. 6.9. Typical dependence of phase shift on electric field.

be first a sharp decrease of phase shift value, and then it will increase until saturation close to  $\pi/2$ . The decrease part is hard to see in the real measurement, because it happens only at very weak electric field. Usually we can only see the increasing part, as seen by some research groups.<sup>13-17</sup>

To measure the phase shift value, samples of polymer **1** (chosen again as a reference) were exposed to the two writing beams for a time long enough to reach a steady state grating, then they were translated along the grating vector with a speed  $V \sim 15 \mu\text{m/s}$ . The translation time was much shorter than the growth time of the refractive index grating, which was longer than 1000 s, as shown in Fig. 6.7 (a). During the translation, the light pattern was of course kept fixed. The resulting modulation of light intensity is shown in Fig. 6.10 (a). The sum and difference of the two beams are shown in Fig. 6.10 (b) and a positive phase shift value was extracted from the difference using Eq. (4.34). The sum gives evidence of a less intense grating induced by absorption, which is expected to be in phase with the interference fringes. However, due to the high noise level, the phase of the sum signal could not be measured.

A similar experiment was conducted with a field of opposite polarity. The result is shown in Fig. 6.11 and a negative phase shift was extracted from the difference.

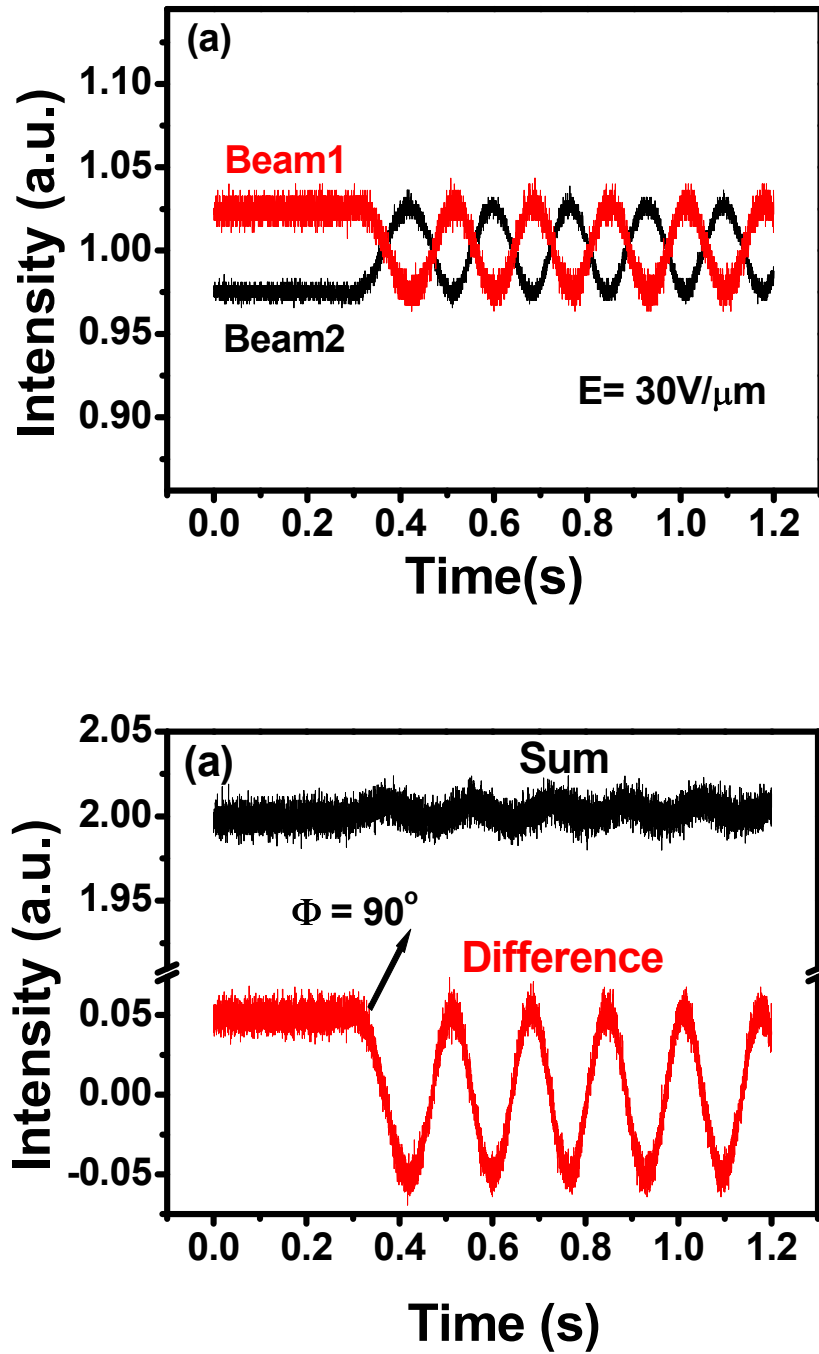


Fig. 6.10: (a) Dependence of the light intensity of the two writing beams as a function of time during the translation of the grating after 2BC experiment shown in Fig. 6.8 (a), starting at  $t = 0.3$  s, moving speed  $v = 15 \mu\text{m/s}$ . (b) Sum and difference of the two writing beams shown in (a).

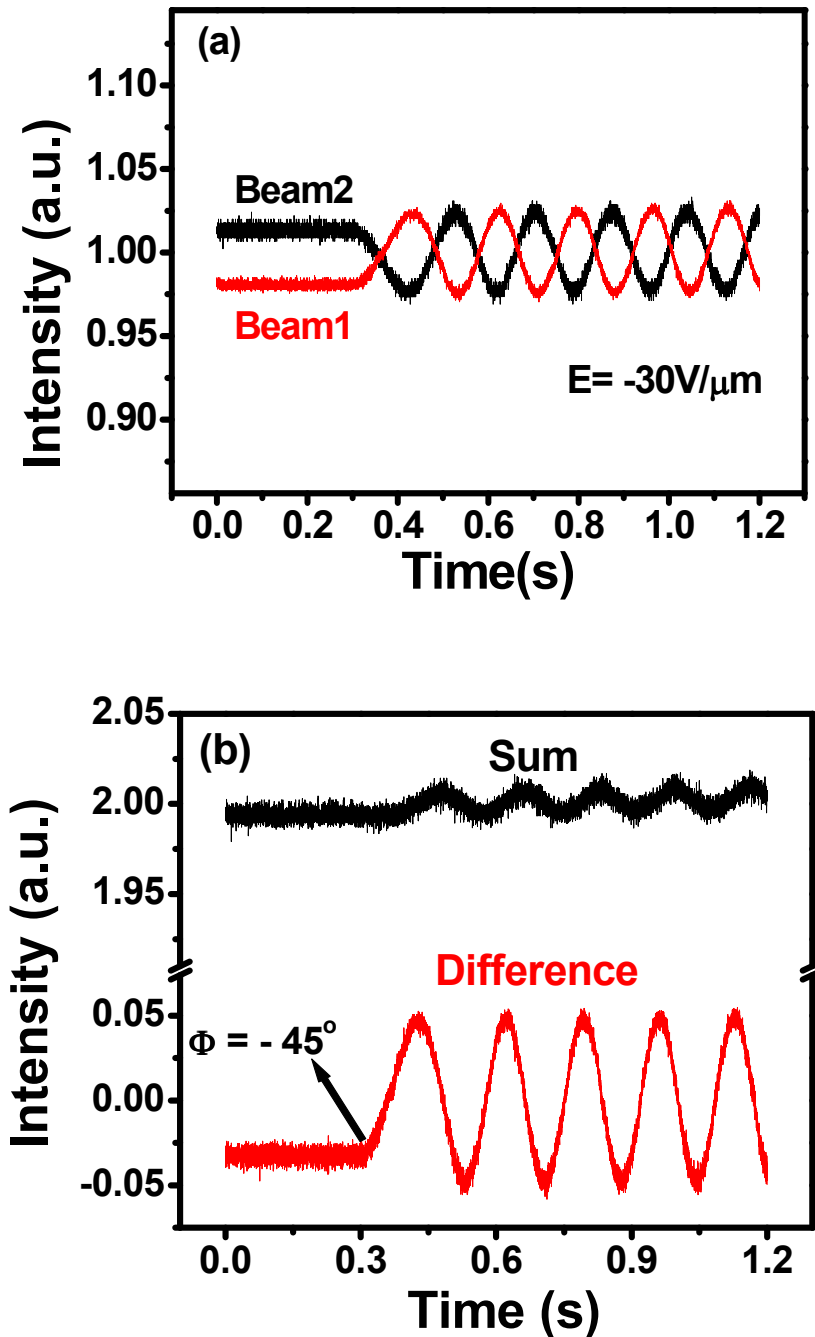


Fig. 6.11: (a) Dependence of the light intensity of the two writing beams as a function of time during the translation of the grating after 2BC experiment shown in Fig. 6.8 (b), starting at  $t = 0.3$  s, moving speed  $v = 15 \mu\text{m/s}$ . (b) Sum and difference of the two writing beams shown in (a).

### 6.9 Improvement of PR dynamics

Although polymers 1 and 2 show good PR performance, it takes more than 1000 s for the build-up of the refractive index modulation, as shown in Fig. 6.7 (a) and (b). Their

dynamics are slow, especially compared with some fast PR media with PR speed at the scale of milliseconds. There are some possible methods for improving such speed:

- 1) Increasing the intensity of light: stronger light intensity will generate more charges in an equal time, hence the formation of the space charge field will be faster. At the same time, the reorientation of azo moieties will be accelerated.
- 2) Using wavelengths closer to the absorption peak of azobenzene: as far as the effects are considered, this is equivalent to increasing light intensity.
- 3) Increasing the intensity of the external electric field to accelerate the formation of the space charge field.

Compared with some other PR polymers with faster response, the photoconductivity of polymer **1** and **2** is even higher. It is then reasonable to say that the limiting factor for PR speed in these azo-polymers is not the set up of the space charge field, but the chromophores reorientation.

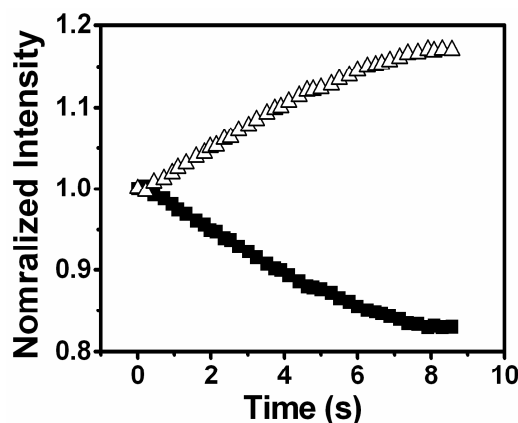


Fig. 6.12. Time evolution of energy exchange at  $\lambda = 532$  nm during two-beam coupling at room temperature for polymer **1**. The sample thickness was  $d = 32$   $\mu\text{m}$ , the grating period was  $\Lambda = 3$   $\mu\text{m}$ , the applied field was  $E = 22$  V/ $\mu\text{m}$  and the light intensity was  $I = 0.8$  W  $\text{cm}^{-2}$ .

The second method was carried out to accelerate the reorientation of azobenzene chromophores and then improve the PR speed of polymer **1**. As shown in Table 5.2, the absorption coefficient of polymer **1** at  $\lambda = 532$  nm is much higher than that at  $\lambda = 632.8$  nm. Two-beam coupling experiments were then carried out using the set-up as shown in Fig. 4.17, but the light was supplied by a DPSS (Diode-Pumped Solid-State) laser at

$\lambda = 532$  nm. As in other experiments, the same grating period  $\Lambda = 3$   $\mu\text{m}$  was obtained by setting  $\Psi = 60^\circ$  and  $\theta = 8.5^\circ$  in Fig. 4.14 (b). The same light intensity  $I = 0.8$   $\text{W cm}^{-2}$  as that in the experiments at  $\lambda = 632.8$  nm was used. Results, as shown in Fig. 6.12, show that at  $\lambda = 532$  nm the time constant of the build-up of the refractive index modulation is  $\tau \approx 5$  s, 2 orders of magnitude smaller than at  $\lambda = 632.8$  nm.

### 6.10 The roles of chromophore dipole moment and electric field

As already discussed, high  $T_g$ , non-poled polymers **1** and **2** exhibit light-induced conformational mobility, which can affect absorption and refractive index. However, these effects are local, in the sense that their extent is proportional to the local light intensity, and therefore they are not expected to contribute to the energy exchange in two-beam coupling. In order to be active within a PR medium, conformational mobility must be coupled to a non-local effect, and this is what can happen in photoconducting materials, such as the ones studied in this work. In fact, in this case the non-local entity is the photogenerated electric field, which is phase shifted with respect to the light pattern. The field itself would not reorient molecular dipoles so far below  $T_g$ , as confirmed by the birefringence measurements, but this is possible in the presence of light-induced conformational mobility.

The observation of energy exchange in the Bragg regime in a photoconducting material already constitutes sufficient experimental evidence in order to claim the role of an electric field in the orientation of chromophores. One further indication can be obtained by comparing the faster build-up of energy exchange with the slower time constant of light-induced birefringence, which was measured using the same light intensity. In the case of polymer **1**, these data are illustrated in Fig. 6.7 (a) and Fig. 6.1, respectively. During birefringence measurements no field is applied and birefringence originates from the fact that polarized light absorption (inducing the trans to cis isomerization) is higher for certain molecular orientations while the reverse process (cis to trans) yields random reorientations. In contrast, two-beam coupling is carried out in the presence of an electric field and this could not only make the cis-trans reverse process not random, but it could also induce the reorientation of non-excited chromophores, by using conformational mobility obtained via the rearrangements of neighbouring excited chromophores. Both effects can lead to faster orientation.



The importance of the electric field in the energy exchange experiments we describe may also be inferred by considering the data of Fig. 6.7 (c,d), obtained at  $\lambda = 632.8$  nm using polymers **3** and **4**, in which the high molecular dipoles associated with the cyano (polymer **1**) and nitro (polymer **2**) groups are not present. As a consequence, field-induced molecular reorientation is much less effective and energy exchange is greatly reduced. The same values of  $\Gamma$  as that at  $\lambda = 632.8$  nm were obtained for **3** and **4** in measurements at  $\lambda = 532$  nm, where their absorption is higher, ruling out the possibility that their lower PR performance at  $\lambda = 632.8$  nm is a consequence of their lower absorption (see Table 5.2).

All the experimental evidence illustrated above shows that, in our materials, conformational motions due to azo isomerization cannot account for PR behaviour if the coupling with a field is not present. In addition, given the similar optical gain measured for **3** and **4**, and comparing also with the results obtained for **1** and **2**, it is possible to conclude that both absorption and photoconductivity variations play a secondary role in determining the gain. In contrast, our data show that, at least in the materials we investigated, PR performance cannot be linked to the simple photoisomerization. The whole picture is instead consistent with a field-induced, light-assisted (via the isomerization) chromophore reorientation mechanism for the PR behaviour in high  $T_g$  azo-polymers, as shown in Fig. 6.13.

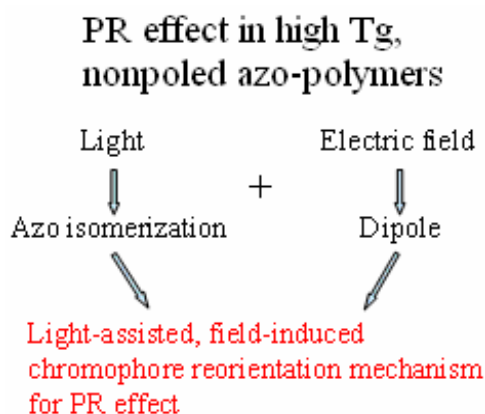


Fig. 6.13. The mechanism for the PR effect in high  $T_g$ , nonpoled azo-polymers at temperature well below  $T_g$ .

## 6.11 Photorefractivity with and without chiral groups

There are chiral groups in polymers **1** - **4**. Chirality is important when such materials are used as chiroptical switches. In this research, polymer **11** (chiral) and **12** (non-chiral) were chosen to check if chirality is a relevant property in the PR effect. The structures of these two polymers are shown in Table 5.1. These two polymers also have high T<sub>g</sub>, as shown in Table 6.3.

Table 6.3 Characterization data of the investigated polymeric derivatives.

Sample	Yield <sup>a)</sup>	$\bar{M}_n$ <sup>b)</sup>	$\bar{M}_w/\bar{M}_n$ <sup>b)</sup>	$T_d$ <sup>c)</sup>	$T_g$ <sup>d)</sup>
	%	g mol <sup>-1</sup>		°C	°C
11. Poly[(S)-MCAPP-C]	60	32900	1.5	345	195
12. Poly[MCAPE-C]	65	53800	1.5	322	163

a) Calculated as (g polymer/g monomer)·100, <sup>b)</sup> Determined by SEC in THF solution at 25°C, <sup>c)</sup> Initial decomposition temperature determined by TGA in air at 20°C/min heating rate, <sup>d)</sup> Glass transition temperature determined by DSC at 10°C/min heating rate under nitrogen flow.

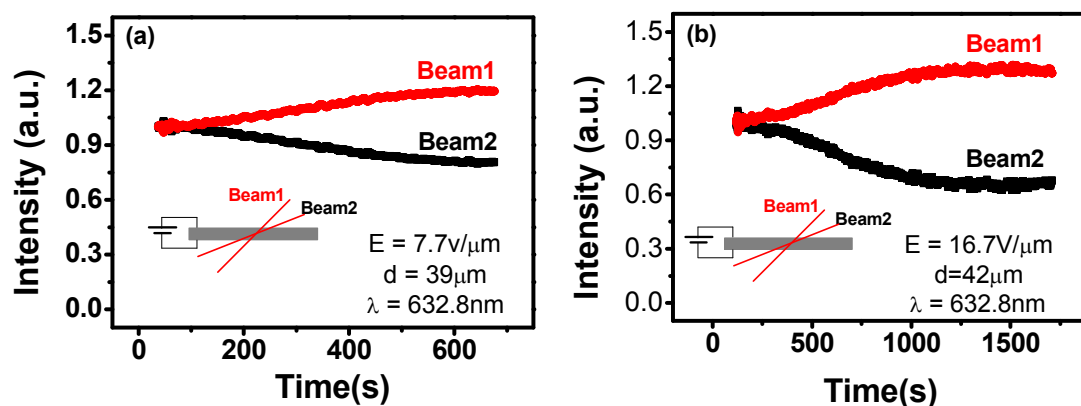


Fig. 6.14. Two-beam coupling experiment results at room temperature for polymers **11** (a) and **12** (b). Data for polymers **11** has been obtained from a sample containing 9.1 % of the plasticizer DPP. In both cases, the grating period was  $\Lambda = 3 \mu\text{m}$ , light wavelength  $\lambda = 632.8 \text{ nm}$  and the light intensity was  $I = 0.8 \text{ W cm}^{-2}$ . The inset in (a) and (b) are schematic illustrations of the experimental set-up. All data were rescaled to eliminate the effect of the decreasing total transmission during irradiation.

2BC experiments were carried out at room temperature on polymers **11** and **12** using the set-up illustrated in Fig. 4.17.  $\Psi = 60^\circ$  and  $\theta = 10^\circ$  (see Fig. 4.14 (b)). According to Eq. (4.7), the grating period was calculated to be  $\Lambda = 3 \mu\text{m}$  with  $n \approx 1.6$ . Given the samples thicknesses between  $39 \mu\text{m}$  and  $42 \mu\text{m}$ , the experiments were performed in the Bragg diffraction regime.<sup>1</sup> 2BC results are shown in Fig 6.13. The gain coefficient was  $\Gamma = 84 \text{ cm}^{-1}$  for polymer **11** and  $\Gamma = 139 \text{ cm}^{-1}$  for polymer **12**, of the same order of magnitude. The energy exchange in Fig 6.13 proves not only that both polymers exhibit PR properties, but also that the chirality is not a necessary requirement and has no substantial effect.

## 6.12 Photorefractivity in azo-polymers without carbazole groups

All the polymers showing PR behaviour illustrated above include a carbazole group in their structure, as shown in Table 5.1, and are photoconductors. However, although the carbazole group is not present in its chemical structure, polymer **15** is also photoconducting, as shown in Fig. 5.15. Because of its photoconductivity and of the presence of azobenzene groups, we tried to establish if polymer **15** might exhibit PR properties like the other polymers. Similar measurements were performed on polymer **16**, which is non-racemic version of polymer **15**.

2BC experiments were carried out at room temperature on polymers **15** and **16** using the set-up depicted in Fig. 4.17, with  $\Psi = 60^\circ$  and  $\theta = 10^\circ$ . Sample thicknesses for polymers **15** and **16** were both  $d = 33 \mu\text{m}$ . According to Eq. (4.7), the grating period was calculated to be  $\Lambda = 3 \mu\text{m}$  with  $n \approx 1.6$ . Given the sample thickness  $d = 33 \mu\text{m}$ , the experiments were performed in the Bragg diffraction regime. The 2BC results are shown in Fig 6.15. The gain coefficient is  $\Gamma = 135 \text{ cm}^{-1}$  for both **15** and **16**. The energy exchange proved that polymers **15** and **16** have PR properties. Hence, the carbazole group is not necessary for PR behaviour in azo-polymers. The photoconductivity and PR properties of **15** and **16** should be compared with a recent report<sup>18</sup> concerning a sol-gel material containing azo-moieties, in which a non-local holographic recording without photorefractive contribution is claimed, a conclusion based on the non-photoconductive properties of the material. As we have shown that photoconductivity can be exhibited by azo-compounds, such results might be considering differently, since even a very low photoconduction, below the detection limit of most measurement set-ups, might be

enough to trigger the onset of a photogenerated electric field, at least on long (tens or hundreds of seconds) time-scales.

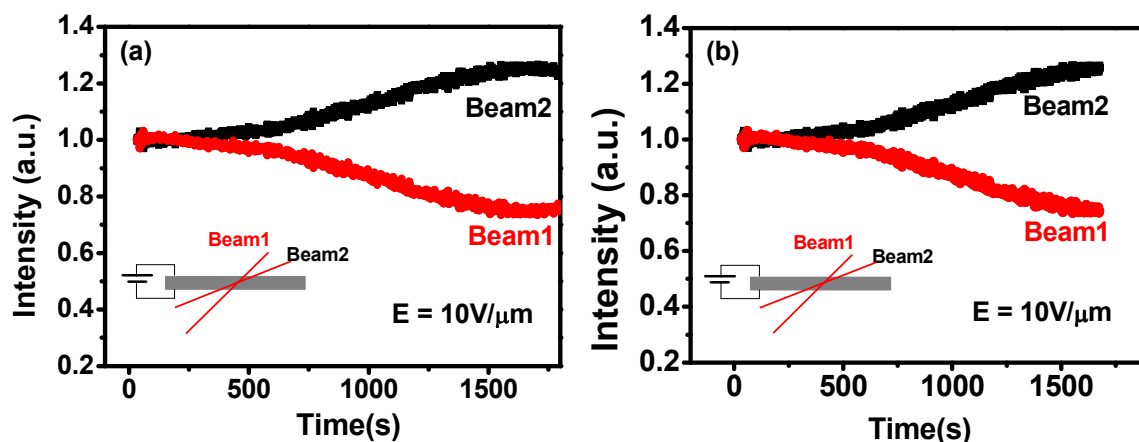


Fig. 6.15. Two-beam coupling experiment results at room temperature for polymers **15** (a) and **16** (b). In all cases, the grating period was  $\Lambda = 3 \mu\text{m}$ , light wavelength  $\lambda = 632.8 \text{ nm}$  and the light intensity was  $I = 0.8 \text{ W cm}^{-2}$ . The inset in (a) and (b) are schematic illustrations of the experimental set-up. All data were rescaled to eliminate the effect of the decreasing total transmission during irradiation.

For all the polymers containing the carbazole moiety, given the standard experimental conditions (a given sample tilt and a given electric field direction) beam 1 always gains energy from beam 2. However, using the same standard experimental conditions, for **15** and **16** the opposite energy exchange was observed in 2BC experiments, as shown in Fig. 6.15. Given the identical experimental conditions and the similar chemical structure, the only possible explanation of this behaviour is a different sign of the charge transporters, which is a fact known to affect the sign of energy exchange. As **1** - **12** are hole conductors, due to the presence of the carbazole moiety, these results seem to suggest that charge transport in **15** and **16** might be due to electrons rather than holes. Further studies are necessary in order to confirm this hypothesis.

### 6.13 Refractive index modulation mechanism

As discussed in section 1.3.4, two different effects can modulate the refractive index, the reorientational effect and the electro-optic effect. Transient ellipsometry experiments, described in section 4.8, were carried out using polymer **1** to distinguish

whether the refractive index modulation is due to the reorientational effect, to the electro-optic effect or to both. The result is shown in Fig. 6.16 and the sharp decrease of the phase modulation of light with frequency shows that the reorientational effect is the only contribution to the refractive index modulation in polymer 1.

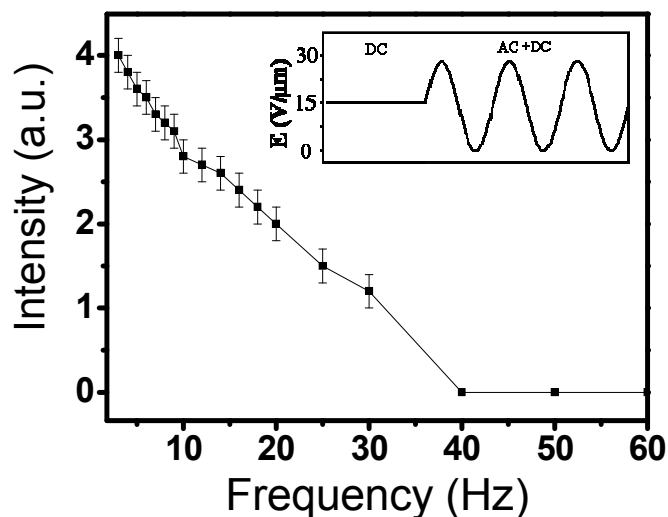


Fig. 6.16. Light intensity versus frequency in transient ellipsometry experiments: sample thickness  $d = 20 \mu\text{m}$ , AC + DC: 0-600 V.

#### 6.14 PR effect without external electric field

The unique characteristic of the PR effect is its non-local nature arising from charge migration, which leads to a phase shift between the incident light intensity pattern and the refractive index modulation. The driving forces for carrier migration are diffusion due to concentration gradients and drift when a static electric field is applied.<sup>19</sup> In addition, since in organics recombination can be the main final result after absorption, an external electric field is necessary to improve charge generation. Most polymeric materials are relatively good insulators, so that the ability of generated charges to move by diffusion alone is quite limited, and drift becomes the dominant mechanism,<sup>20</sup> which also requires external electric fields, leading to significant restrictions on practical applications.<sup>21</sup> Considering this, organic polymers which are low-cost, stable, easy to prepare and can exhibit the PR effect at low external fields are interesting.

We have illustrated above the PR behaviour in some azo-polymers in the presence of an external electric field. Usually, no PR effect can be observed without an applied field. However, 2BC gain has recently been reported in some PR polymeric materials

without an external field or prepoling.<sup>22-31</sup> Such an effect was called ‘all-optical photorefractivity’.<sup>30</sup> Considering the mechanism of all-optical photorefractivity, it is assumed that chromophores are oriented by a photoinduced electric field.<sup>23,24,26-29</sup> For azo-polymers, it is assumed in addition that the synergism of the photoassisted poling of azo dyes and the space-charge field induced by the light intensity gradient along the light path may be responsible for the PR effect.<sup>32</sup> Photoassisted poling effects in azo dyes have been studied by several groups.<sup>33-35</sup> It has been suggested that in the presence of polarized light, the repeated trans–cis–trans photoisomerization can enhance the rotational mobility of the azo groups and make them rotate easily at weak electric fields. When the sample is illuminated by the interference pattern, a periodic space-charge field can arise. At the same time, light absorption, due to the dye, produces intensity attenuation along the light path and induces a gradient of the photogenerated charge density. Then the charge displacement will be driven by the gradient and a space-charge field along the light path will be obtained.<sup>36</sup> These two kinds of space-charge fields may contribute to the local poling of the azo groups. While such an effect of symmetry breaking by space-charge field along the light path has been observed experimentally and explained theoretically in PR liquid crystal composites, the possibility of observing this effect in polymeric materials was also suggested.<sup>24,30</sup> In this section, the PR properties without external field of the azo-polymers studied in this work will be discussed.

The same set-up as shown in Fig. 4.17 was used to check the PR behaviour of these azo-polymers, but without external electric field. 2BC experiments were carried on polymers **1**, **2**, **11**, **12**, **15** and **16** at room temperature without external electric field. For all cases,  $\Psi = 60^\circ$  and  $\theta = 10^\circ$ . The results are shown in Fig. 6.17, and the energy exchange for each polymer clearly proved their PR property without external electric field. The energy exchange for each polymer was comparable to the result in 2BC with external electric field.

For 2BC experiments without external electric field, the direction of energy exchange was not fixed. Sometime the transmission intensity of beam 1 increased and sometime it decreased. The mechanism of the PR effect without an applied field in our materials is still an open question and further study should be performed in order to reach its full understanding.

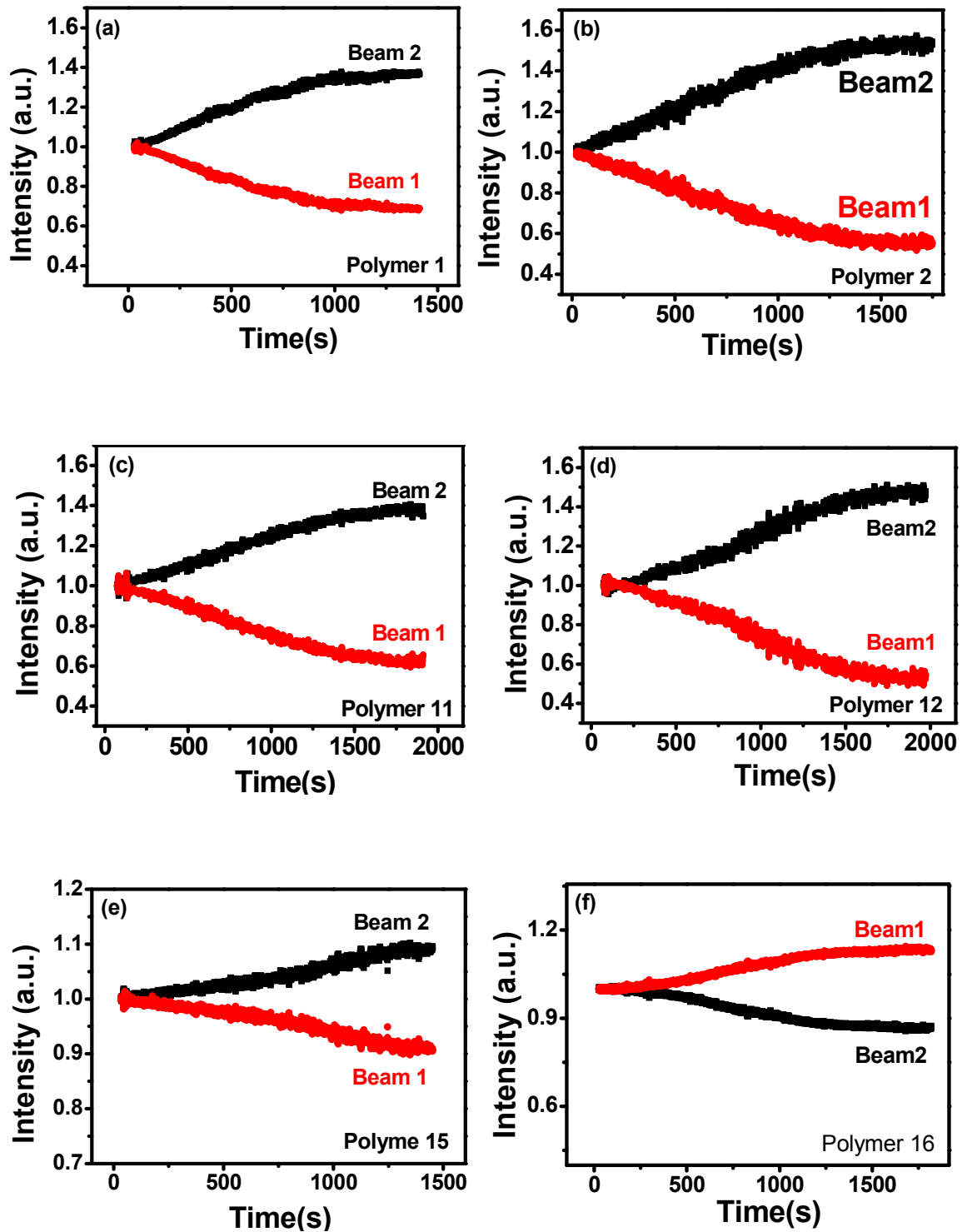


Fig. 6.17. 2BC without external electric field at room temperature for polymers (a) 1, (b) 2, (c) 11, (d) 12, (e) 15, (f) 16. The intensities of beam 1 and beam 2 were  $0.8 \text{ W cm}^{-2}$  for all cases. All data were rescaled to eliminate the effect of the decreasing total transmission during illumination.

## 6.15 Conclusions

In this chapter, we have shown that the PR behavior of nonpoled azo-polymers can be observed at temperatures more than 100 °C below their T<sub>g</sub>. Some conclusions related to such observation follow:

- 1) Light-induced chromophore reorientation can be obtained in these high T<sub>g</sub> azo-polymers at room temperature.
- 2) The absorption of the azo-polymers will increase after irradiation, as shown in Fig. 6.5 and 6.6.
- 3) In polymer **1**, the azobenzene and carbazole group were linked to each other on the same side-chain. In polymer **2**, the two groups are separated and they reside on different side-chains. The chiral spacer in polymer **2** is also different from that in polymer **1**. However, the energy exchange shown in Fig. 6.7 (b) indicates that polymer **2** also exhibits a gain of the same order as that of polymer **1**, which means that the PR performance depends neither on the fact that different functionalities reside on the same side-chain, nor on the nature of the chiral spacer.
- 4) The energy exchange can be inverted by inverting external electric field, as shown in Fig. 6.8.
- 5) The PR speed can be greatly improved by using wavelengths closer to the absorption peak of azobenzene. This is evident by comparing the results shown in Fig 6.7 (a) and Fig. 6.12.
- 6) The reorientational effect is the only contribution to the refractive index modulation in the PR effect of these high T<sub>g</sub>, nonpoled azo-polymers.
- 7) High T<sub>g</sub> azo-polymers without carbazole groups were found to be photoconducting for the first time. Because of their photoconductivity, they can also exhibit the PR effect at temperature well below T<sub>g</sub> without prepoling.
- 8) Although light activated conformational mobility of azo groups is a necessary requirement for the PR effect at temperatures below T<sub>g</sub>, the interaction between the strong dipole moment and electric field (external electric field + space charge field) is also necessary in order to encode a phase-shifted hologram, via the reorientation of polar chromophores. Our data indicate that the refractive index modulation is based not simply on the trans-cis isomerization of azo groups, but on a chromophore reorientation process induced by the electric field and assisted by the



photoisomerization, as shown in Fig. 6.13.

- 9) Comparable energy exchange can be obtained in 2BC at room temperature on the high T<sub>g</sub> azo-polymers with and without external electric field.

## BIBLIOGRAPHY

1. T. Ikeda. *J. Mater. Chem.*, **2003**, 13, 2037.
2. Y. L. Yu, T. Ikeda. *J. Photochem. Photobiol. C: Photochem. Rev.*, **2004**, 5, 247.
3. Y. Zhao, T. Ikeda. *Smart Light-Responsive Materials: Azobenzene Polymers for Photonic Application*. John Wiley & Sons: New York, USA **2009**.
4. C. Cojocariu, P. Rochon. *Pure Appl. Chem.*, **2004**, 7-8, 1479.
5. P. Rochon, E. Batalla, A. Natansohn. *Appl. Phys. Lett.*, **1995**, 66, 136.
6. T. Pedersen, P. Johansen, N. Holme, P. Ramanujam, S. Hvilsted. *Phys. Rev. Lett.*, **1998**, 80, 89.
7. J. G. Meier, R. Ruhmann, J. Stumpe. *Macromolecules*, **2000**, 33, 843.
8. I. Zebger, M. Rutloh, U. Hoffmann, J. Stumpe, H. W. Siesler, S. Hvilsted. *Macromolecules*, **2003**, 36, 9373.
9. A. Eisfeld, J. S. Briggs. *Chem. Phys.*, **2006**, 324, 376.
10. T. K. Gaylord, M. G. Moharam. *Appl. Opt.*, **1981**, 20, 3271.
11. P. Yeh. *Introduction to Photorefractive Nonlinear Optics*. John Wiley & Sons: New York, USA **1993**.
12. O. Ostroverkhova, W. E. Moerner. *Chem. Rev.*, **2004**, 104, 3267.
13. C. A. Walsh, W. E. Moerner. *J. Opt. Soc. Am. B*, **1992**, 9, 1642.
14. A. Grunnet-Jepsen, C. L. Thompson, W. E. Moerner. *Opt. Lett.*, 1997, 22, 874.
15. M. Liphardt, S. Ducharme. *J. Opt. Soc. Am. B*, **1998**, 15, 2154.
16. A. Grunnet-Jepsen, C. L. Thompson, W. E. Moerner. *J. Opt. Soc. Am. B*, **1998**, 15, 905.
17. H. Ono, T. Kawamura, N. M. Frias, K. Kitamura. *Appl. Phys. Lett.*, **1999**, 75, 3632.
18. F. Gallego-Gómez, F. D. Monte, K. Meerholz. *Nature Materials*, **2008**, 7, 490.
19. P. Günter. *Phys. Rep.*, **1993**, 93, 449.
20. W. E. Moerner, Scott M. Silence. *Chem. Rev.*, **1994**, 94(1), 127.
21. N. Tsutsumi, J. Eguchi, W. Sakai. *Optical Materials.*, **2006**, 29, 435.
22. C. J. Chang, H. C. Wang, G. Y. Liao, W. T. Whang, J. M. Liu, K. Y. Hsu. *Polymer*, **1997**, 38, 5063.
23. P. Cheben, F. Monte, D. J. Worsfold, D. J. Carlsson, C. P. Grover, J. D. Mackenzie. *Nature*, **2000**, 408, 64.
24. G. Gipparrone, A. Mazzulla, P. Pagliusi. *Opt. Commun.*, **2000**, 185, 171.
25. J. W. Lee, J. Mun, C. S. Yoon, K. S. Lee, J. K. Park. *Adv. Mater.*, **2002**, 14, 144.
26. W. E. Douglas et al. *Phys. Chem. Chem. Phys.*, **2002**, 4, 109.
27. R. Zheng, Y. Zhao, K. Min, C. Wang, F. Li. *Chin. Phys. Lett.*, **2002**, 19, 795.
28. L. Y. Li, Y. Y. Zhao, F. M. Li, J. Yang, G. R. Chen, C. C. Wang. *Chin. Phys. Lett.*, **2004**, 21, 1535.
29. M. M. Huang, Z. J. Chen, J. Zhang, Q. Wei, Y. H. Liu, Q. H. Gong et al. *Chin. Phys. Lett.*, **2004**, 21, 1969.
30. M. M. Huang, Z. J. Chen, J. Shi, S. K. Cao, Q. H. Gong. *Chin. Phys. Lett.*, **2006**, 23, 2468.
31. L. Y. Ding, D. S. Jiang, J. Huang. *Journal of Wuhan University of Technology-Mater. Sci. Ed.*, **2007**, 22, 638
32. L. Zhang, J. Shi, Z. Yang, M. M. Huang, Z. J. Chen, Q. H. Gong, S. K. Cao. *Polymer*, **2008**, 49, 2107.
33. Z. Sekkat, M. Dumont. *Appl. Phys. B*, **1992**, 54, 486.
34. Z. Sekkat, J. Wood, E. F. Aust, W. Knoll, W. Volksen, R. D. Miller. *J. Opt. Soc. Am. B*, **1996**, 13, 1713.

35. T. Enomoto, H. Hagiwara, D. A. Tryk, Z. F. Liu, K. Hashimoto, A. Fujishima. *J. Phys. Chem. B*, **1997**, 101, 7422.
36. F. Simoni, G. Cipparrone, A. Mazzulla, P. Pagliusi. *Chem. Phys.* **1999**, 245, 429.